A process-based stable isotope approach to carbon cycling in recently flooded upland boreal forest reservoirs

by

Jason James Venkiteswaran

A thesis

presented to the University of Waterloo

in fulfillment of the

thesis requirements for the degree of

Master of Science

in

Earth Sciences

Waterloo, Ontario, Canada, 2002

© Jason James Venkiteswaran, 2002.

AUTHOR'S DECLARATION FOR ELECTRONIC SUBMISSION OF A THESIS

I hereby declare that I am the sole author of this thesis. This is a true copy of the thesis, including any required final revisions, as accepted by my examiners.

I understand that my thesis may be made electronically available to the public.

Abstract

Reservoirs impound and store large volumes of water and flood land. The water is used for electricity generation, irrigation, industrial and municipal consumption, flood control and to improve navigation. The decomposition of flooded soil and vegetation creates greenhouse gases and thus reservoirs are a source of greenhouse gases. Reservoirs are not well studied for greenhouse gas flux from the water to the atmosphere. The FLooded Upland Dynamics EXperiment (FLUDEX) involves the creation of three experimental reservoirs in the upland boreal forest to study greenhouse gas and mercury dynamics.

The balance of biological processes, decomposition, primary production, methane oxidation and the nitrogen cycle in the reservoirs controls the greenhouse gas flux from the reservoir to the atmosphere. Understanding the importance and controlling factors of these processes is vital to understanding the sources and sinks of greenhouse gases within reservoirs.

The carbon and oxygen dynamics near the sediment-water interface are very important to the entire reservoir because many processes occur in this area. Light and dark benthic chambers were deployed, side-by-side, to determine the benthic flux of DIC and CH_4 across the sediment-water interface and to determine the role of benthic photoautotrophs in benthic DIC, CH_4 and O_2 cycling. Benthic chambers have shown photoautotrophs use the decomposing soil, rocks and exposed bedrock as a physical substrate to colonize and the carbon dioxide produced by the decomposing soil as a carbon source since the δ^{13}C-DIC value of the DIC added to light chambers is enriched relative to dark chambers and net photosynthesis rates are linked to community respiration. Benthic photoautotrophs consume 15-33% of the potential DIC flux into the water column. Methane produced by the decomposition of soils is partially oxidized by methanotrophs that use the photosynthetically produced oxygen. The δ^{13}C-CH_4 values of the CH_4 added to light chambers is enriched relative to dark chambers and 15-88% of the potential CH_4 flux into the water column is oxidized.

An isotope-mass budget for dissolved inorganic carbon and methane is presented for each reservoir to identify the importance of processes on a reservoir scale. Input of DIC to the reservoirs from overland flow can be important because concentration is greater and δ^{13}C-DIC values are depleted relative to inflow from Roddy Lake. Estimates of total reservoir primary production indicate that 3-19% of the total DIC production from decomposition is removed by photoautotrophs. The carbon cycling in biofilm and the importance of periphytic primary production needs to be better understood.

Dissolved $\delta^{13}C$-CH_4 values of CH_4 in reservoir outflow enriched 45-60‰, indicating that CH_4 oxidation was an important CH_4 sink within the reservoirs. Stable carbon isotope data indicates that the methane in the bubbles is partially oxidized so the site of bubble formation is the upper portion of the flooded soil. The fraction of methane converted to carbon dioxide in the FLUDEX reservoirs is similar to that of the wetland flooded for the Experimental Lakes Area Reservoir Project (ELARP). Approximately half of the dissolved CH_4 in the FLUDEX reservoirs was removed by CH_4 oxidation. The ebullitive flux of CH_4 from FLUDEX reservoirs is reduced 25-75% by CH_4 oxidation. The CH_4 flux to the atmosphere from peat surface of the ELARP reservoir became less oxidized after flooding: 91% to 85% oxidized. The floating peat islands of the ELARP reservoir were less oxidized than the peat surface. Similar to the CH_4 in the FLUDEX reservoirs, CH_4 in the ELARP peat islands was oxidized 56%. CH_4 oxidation is an important process because it reduces the global warming potential of the greenhouse gas flux since CO_2 is less radiatively active than CH_4.

Acknowledgements

I would like to acknowledge all those who have offered all forms of assistance. They include, but are not limited to:

my advisors, who have offered immense support and assistance; my laboratory-mates, in all the laboratories where I have worked, have been an endless source of advice and humour; the people of the Experimental Lakes Area, staff, researchers and students, generate an incredible environment for thought and fun; and my family, especially Terah and Helianthus, who have expressed depths of patience, understanding and love to which I aspire.

Dedication

Table of Contents

List of Figures

List of Tables

Chapter 1: Introduction

1.1 Carbon Cycling in Boreal Forests

The boreal zone is one of the Earth's larger biomes (~14.3 million km^2). The forests of the boreal zone are a mixed deciduous-coniferous forest between the tundra and temperate forest. The growing season is short. The role of fire in shaping the boreal forest and its carbon stores is important due to its frequency and effects on secondary succession on fire-disturbed landscapes (Kasischke et al. 1995). A considerable portion of the biomass burned and carbon released comes from the forest floor (Dyrness and Norum 1983). Large areas of mineral soil can be left exposed in severe fires (as reported by AuClair 1983 and Stocks 1987).

Recent studies indicate that approximately 714 Pg of carbon are stored within the boreal forest (summarized by Apps et al. 1993). Much of this large carbon pool (419 Pg) is stored in the approximately 2.6 million km^2 of peatland (Apps et al. 1993). An estimated 58 Pg of carbon are contained in the living biomass of the forested portion of the biome and 231 Pg in the litter and fungal-humic layers (Apps et al. 1993).

Upland ecosystems have a significantly greater carbon fixation potential than peatlands (Frockling & Crill 1994). The boreal peatlands have been net sinks since deglaciation (approx. 10 000 YBP) and are, thus, significant components of the boreal biome because they contain 25-37% of the global pool of soil carbon (Gorham 1991; Kasischke et al. 1995). Therefore the balance of the processes of uptake and release of carbon within the boreal forest is key to determining the net effects of reservoir creation in the boreal forest.

There are four processes that control the storage and release of carbon in boreal forests: (i) the rate of plant, lichen and fungus growth; (ii) the rate of decomposition of dead organic matter; (iii) the rate of formation of permafrost; and (iv) the frequency and severity of fires (cf. Kasischke et al. 1995). Since permafrost formation is not a factor at the study site, the carbon balance is the combination of growth-based carbon accumulation and carbon loss from decomposition and dramatic carbon loss of forest fires.

Future carbon flux from boreal reservoirs may need to be tempered against the increased decomposition resulting as a response to a warming climate. Apps et al. (1993) predict a net loss of high carbon store areas in the boreal forest as a warmer, drier mid-continent favours prairie (grassland) encroachment into the present boreal region more than the boreal forest migrating northward. Further, a change in the disturbance regime, such as the fire induced 86% reduction in net carbon sink from 1986-1989, may need to be considered.

1.2 Reservoirs

Dam structures are built to store water to compensate for river level fluctuation. The storage of water can be used to generate electricity, supply water for agriculture, industry, and municipal consumption, control flooding, and improve navigation. How well dam structures deliver these uses is strongly contested (Rosenberg et al. 2000; Roy 1999). Cumulative effects of impoundment have reduced sea levels (Chao 1993, 1995) and have caused global-scale ecological changes in riparian ecosystems (Nilsson & Berggren 2000).

Several studies have shown that the intra-wetland variability of GHG (greenhouse gas) flux can be as large as the inter-wetland variability (Crill et al. 1988; Moore & Knowles. 1989; Roulet et al. 1992). Extrapolating these large ranges to the global scale is tenuous. Additionally, estimates on global wetland coverage are difficult to obtain, especially for small temporal/ephemeral wetland systems since they are often neglected on aerial maps (cf. Weyhenmeyer 1999). This problem exists for reservoirs. St. Louis et al. (2000) discuss the difficulty estimating total reservoir coverage at length. Briefly, the International Commission on Large Dams' (ICOLD) database (ICOLD 1998) is incomplete, e.g. some countries only report dams greater than a certain size, others report only hydroelectric dams, and surface area is not included for all dams; Canada is one of fourteen countries that do not list surface area. St. Louis et al. (2000) note that independent data for four provinces total 73 000 km^2. The surface area of natural lakes in the four provinces is 219 000 km^2 (Natural Resources Canada 2001). Additionally, the number of small dams and the flooded area behind small dams, worldwide, is unaccounted for. The most recent global estimate for reservoir surface area is similar to that for natural lakes: 1.5 million km^2 (St. Louis et al. 2000; Shiklomanov 1993).

Hydroelectric power is often portrayed as a clean source of renewable energy with little environmental damage and socio-economic effects (Bourassa 1985; Rosenberg et al. 1977). Various papers and books identify the variety of environmental and socio-economic problems associated with reservoir creation and operation (e.g. Rosenberg et al. 1995; Kelly et al. 1997; Bodaly et al. 1997; McCutcheon 1991; Richardson 1991). In the last decade, reservoirs created by flooding wetlands have been identified as source of GHG production and mercury methylation (summarized by Rosenberg et al. 1995 and St. Louis et al. 2000). The microbial processes involved in decomposing flooded vegetation and soil convert inorganic mercury to bioaccumulative methylmercury (Hecky et al. 1991) and stored carbon to carbon dioxide and methane (Rudd et al. 1993; Kelly et al. 1994; Duchemin et al. 1995). Additionally O_2 concentration decreases in the reservoir because of microbial respiration and a slowing of the water (Baxter and Glaude 1980). Further, the loss of O_2 can lead to fish kills. Siltation (from the loss of carrying capacity in the now slower river) destroys fish-spawning habitat (Rosenberg et al. 1995).

Rudd et al. (1993) calculate that boreal peatlands are sinks of CO_2 and small sources of CH_4 to the atmosphere and boreal forests are small CH_4 sinks and neutral with respect to CO_2. Microbial decomposition of the flooded carbon stores turns these approximately neutral GHG sites into large GHG sources to the atmosphere (Rudd et al. 1993; Kelly et al. 1997; Duchemin et al. 1995). Global annual estimated fluxes of carbon GHGs are 0.7×10^{14} $gC \cdot a^{-1}$ CH_4 and 1.0×10^{14} $gC \cdot a^{-1}$ CO_2, 70 and 90% of which are estimated to be from tropical reservoirs (St. Louis et al. 2000).

Geomorphological changes take place along newly created ‘shoreline’ of reservoirs. For example erosion along former rivers leads to channel simplification (Nilsson & Berggren 2000). Duration of flooding and fluctuation in water levels also causes changes to landscapes. Temporal reservoirs, where water levels are seasonally drawn down, reduce biodiversity along shorelines that, during low water levels, are entirely above water. Lake-like and biodiverse shorelines can develop in reservoirs that have little fluctuating shore water levels. In northern and boreal reservoirs, the shoreline is entirely above water only during late winter when covered by ice and snow (Nilsson et al. 1997). Vegetation has been modelled along large impoundment and run-of-the-river (a series of small dam structures that resembles a series of

rapids instead of a monolithic dam) reservoirs in Sweden (Nilsson et al. 1997). Species diversity decreased upon impoundment flooding, recovered to below pre-flood levels after three decades and thereafter declined. Run-of the-river reservoirs reduced species diversity to a lesser extent and reduced riparian area; both types of reservoirs reduced plant densities along new shorelines (Nilsson et al. 1997).

Decomposition of newly flooded soils releases nitrogen and phosphorus, temporarily increasing aquatic production. Some plant species will produce aerenchyma and adventitious roots as a response to permanently flooded soils (Junk and Piedade 1997), some will elongate shoots to reach the open air (Blom and Voesenek 1996) and other species will immediately stop growth and die.

The scope of reservoir studies is large and continued research in many areas will continue to improve the understanding of reservoir dynamics. A better understanding of soil nutrient cycling and decomposition is needed particularly in the sensitivity of floodplains and forests to inundation (e.g. Poff et al. 1997). Net effect measurements that not only consider carbon flux before and after flooding, but improvements in understanding change in biodiversity and ecosystem function need to be made to better understand all the effects of reservoir development.

1.3 Reservoir Research at the ELA

The Experimental Lakes Area Reservoir Project (ELARP) started in 1992 and was established to quantify the net change in GHG flux to the atmosphere and to better understand the processes causing elevated methylmercury levels in biota after flooding (Kelly et al. 1994). Site selection for ELARP was to mimic a worst-case-scenario because of the tremendous decomposable carbon stores in lowland peatlands. Three main factors were involved in selection of a wetland site for ELARP: many reservoirs in northern countries include wetlands since narrow and deep reservoir locations have mostly been developed; methylmercury production has been identified and related to a source organic matter; and the large store or organic carbon in peatlands can act as the source of long–term GHG flux to the atmosphere.

The 16.66 ha experimental site included 2.39 ha of open water (Lake 979) and 14.4 ha of peatland. Water level in the pond was raised 1.3 m for an approximately 100 d flood season with drawdown to mimic flood levels in northern hydroelectric reservoirs. During the second and third year of flooding gas accumulation within the peat caused peat islands to form (Poschadel 1997). ELARP results, as reported by Kelly et al. (1997), indicate that the flooded lowland peatland (with a central pond) shifted from being a small long-term sink of CH_4 and CO_2 (-7 to -16 $gC \cdot m^{-2} \cdot a^{-1}$) to a large source (+130 $gC \cdot m^{-2} \cdot a^{-1}$). Additionally, methane oxidation became less important after flooding in mediating GHG flux.

The follow-up project to ELARP, the Flooded Upland Dynamics Experiment (FLUDEX), is designed to represent the other end of the continuum of carbon storage in the boreal forest. Whereas ELARP included a peatland with tremendous stores of organic carbon in the form of peat, FLUDEX is based on jack pine (*Pinus banskiana* Lamb.) dominated forest that underwent near complete burning in 1980 (Boudreau 2000). Similar to ELARP, FLUDEX is designed to study GHG production and mercury dynamics resulting from flooding upland forests. Due to the variety of forest and forest soil combinations present in the boreal forest, three reservoirs were created, in the Roddy Lake (L468) watershed, to represent this variety: a moist forest; a dry forest; and a dry forest with bedrock outcrops.

1.4 Research Approach and Research Objectives

Reservoir CO_2 and CH_4 cycling in boreal reservoirs is part of the boreal carbon cycle (Figure 1). Reservoir processes have limnological analogues but the carbon stores in flooded wetlands (not shown) or flooded forests are different.

Decomposition, primary production, methanogenesis and methane oxidation affect carbon GHGs in the reservoirs and are not separated by concentration analyses. Two papers are presented to identify and characterize carbon greenhouse gas cycling in boreal reservoirs and assess a new isotope technique in determining gross primary production. The net effects of reservoir processes are studied by constructing mass budgets; however, individual processes cannot be separated. To characterize and quantify the processes that drive the GHG flux from boreal reservoirs to the atmosphere, a stable carbon isotope mass balance is presented. Process can be separated from one another by coupling reservoir water, concentration and isotope

budgets. Also, benthic and near-benthic (so-called bottom water) processes are separated using carbon and oxygen stable isotopes.

1.5 Thesis Layout

This thesis is comprised of a general introduction, description of research objectives, sampling protocol and general analytical methods, followed by two chapters in the form of articles ready for submission to peer-reviewed journals.

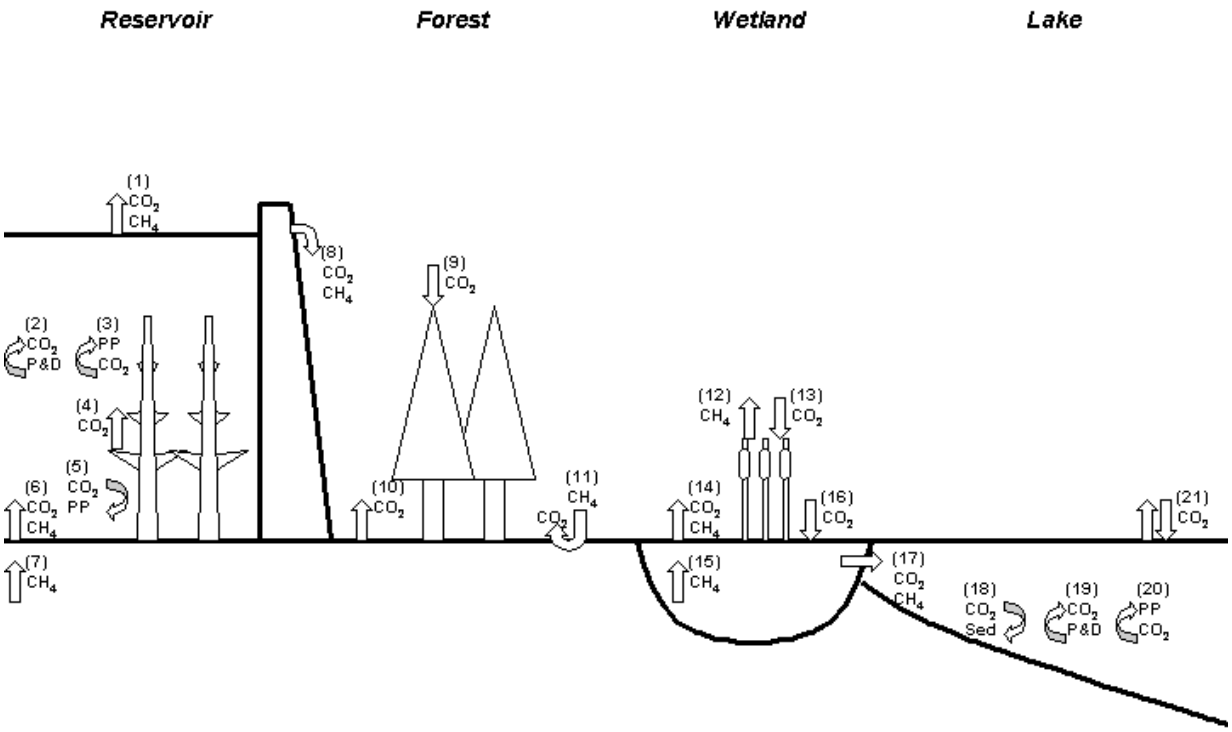

Figure 1 Conceptual model of CO_2 and CH_4 cycling in the boreal forest.

Twenty-one processes or fluxes affecting CO_2 and/or CH_4 are show for reservoir, forest, wetland lake systems: (1) gas exchange between reservoir surfaces and atmosphere; (2) particulate and dissolved carbon mineralization; (3) phytoplankton and epixylic primary production; (4) mineralization of dead vegetation; (5) benthic primary production; (6) net flux from soil to water column from soil mineralization, methane oxidation and methanogenesis; (7) methanogenesis; (8) flux from reservoir to downstream; (9) net photosynthesis; (10) soil mineralization; (11) methane oxidation by soils; (12) methane flux to the atmosphere through some vascular plants; (13) photosynthesis; (14) net flux from wetland surface to atmosphere; (15) methanogenesis; (16) photosynthesis at wetland surface and water column; (17) flux from wetlands to (18) sedimentation of photosynthetic organisms; (19) particulate and dissolved carbon mineralization; (20) phytoplankton and attached algal primary production; and (21) gas exchange between lake surface and atmosphere.

Chapter 2: xSite description and methods

2.1 Experimental Lakes Area

The Experimental Lakes Area (ELA), established in 1968, is located (see Figure 2) east of the Lake of the Woods in north-western Ontario. Winnipeg is approximately 250 km to the west and Kenora is approximately 50 km west-northwest. The watersheds of 58 lakes plus 3 stream segments set aside for research lie between 49°34' and 49°47' N and between 93°36' and 93°52' W. ELA was established as a place to perform whole ecosystem experiments, initially to study eutrophication in the St. Lawrence–Great Lakes, particularly Lake Erie. Historically research has focused on eutrophication, acidification, trace metal dynamics and limnological processes. In the last ten years, the focus has switched to reservoir effects (GHGs and mercury), hormonal mimicry, climate change effects, and mercury dynamics.

ELA is situated on the south lobe of a massive pink granodiorite batholith (Davies & Pryslak 1967), near the south-western edge of the Canadian Shield and is characterized by exposed outcrops of this bedrock with a uniform consistency and a pinkish colour. The granite is strongly sheared, jointed and faulted (Nicolson 1975). Overburden is generally thin to non-existent, particularly on the ridges. Sandy loam with highly variable gravel and cobbles typifies valley deposits. Profiles indicate typically humo-ferric podzols on the well-drained uplands and humic gleysols in the basins (Nicolson 1975; Department of Agriculture 1978); soils are thin and rapidly leached. Brunskill and Schindler (1971) address the geology and soils of ELA in more detail.

Meteorological records from Kenora and Emo indicate a cold continental climate with local modification by larger lakes and other geographic features (Brunskill and Schindler 1971). A meteorological station (49°40'55" N, 93°44'50" W, 435 masl) has been continuously collecting data from its establishment at ELA in June 1969 (K Beaty, pers. comm.). Annual precipitation is 691 mm (1970-1996); annual mean temperature is 2.4ºC (1970-1996); January mean monthly temperature ranged from –21.8ºC (1972) to –12.4ºC (1987); and July mean monthly temperature ranged from 16.5ºC (1975) to 21.2ºC (1974). Beaty and Lyng (1989) provide extensive detail on hydrometeorological records of ELA. More in-depth site and lake

descriptions can be found in volume 28 (1971) of the Journal of the Fisheries Research Board of Canada, now Can. J. Fish. Aquat. Sci., and Schindler (1980).

2.2 Flooded Upland Dynamics Experiment

Each FLUDEX reservoir is approximately 0.7 ha in surface area with a mean depth of approximately 1.0 m. Maximum depth is no greater than 2.5 m. The reservoirs are built against a slope such that water is contained on three sides by wooden and gravel dykes and the fourth side is a 'shore'. Where the water level is 1 m or greater a wooden dyke, with a polypropylene barrier in the middle, anchored and sealed directly to bedrock was constructed. Where the water level is less than 1 m, a gravel dyke with a polypropylene barrier was constructed. Several paths were cut through the forest to allow researched to access most parts of the reservoirs by foot or boat. Studies of carbon stores in each reservoir were undertaken, prior to flooding, by Huebert (1999) and Boudreau (2000).

GHG fluxes to the atmosphere were measured before and during flooding in all reservoirs. Flooding began in June 1999 by pumping water low in total Hg, DOC, DIC and CH_4 from Roddy Lake to each reservoir. In late September water was removed from the reservoirs by stopping inflow and opening valves in the reservoirs to simulate the fall–winter drawdown that takes place in boreal hydroelectric reservoirs.

Reservoir 1 contains two easily identifiable community types, likely controlled by the hydrologic regime over the low slope of the land. Slow water movement over bedrock and small pools standing water persisted in the upslope area of the flooded land. Prior to flooding much of the western half of the reservoir soil was moist. The entire reservoir is dominated by a dense, even-aged stand of *P. banksiana*. The dominant ground shrub in the wet area was *Ledum groenlandicum* (Labrador tea); associated with large patches of *Sphagnum spp*.. The drier area, mainly the eastern half of the reservoir, were colonized by tall shrubs of *Alnus viridis* ssp. *crispa* (Ait.) Pursh (green alder) [syn. *Alnus crispa* (Ait). Turrill], *Betula papyrifera* Marsh. (white birch), and *Prunus pensylvanica* L. f. (pin cherry). Groundcover in the drier area was dominated by *Polytrichum spp.* *Picea mariana* (Mill.) BSP (black spruce) saplings were present throughout the reservoir, but were less than 1.5 m in height (Huebert 1999). Farrar (1995) notes that *P. mariana* is often an understory species in *P. banksiana* dominated

forests since the saplings of the latter are shade intolerant. This suggests that the communities in Reservoir 1 are in transition from first succession growth after a devastating fire to a more complex and diverse forest.

Reservoir 2, more homogeneous than reservoir 1 or 3, is dominated by a dense, even-aged stand of *P. banksiana*. Tall shrubs of *A. viridis* ssp. *crispa* and *B. papyrifera* dominate most of the reservoir. Several large *B. papyrifera* trees, which likely lived through the 1980 fire, are inside the reservoir. Few low shrubs of *Vaccinium spp.* were present. Groundcover of mosses, lichens, and herbs *Cornus canadensis* L. (bunchberry) and *Maianthemum canadense* Desf. (Canada mayapple) exists throughout the reservoir (Huebert 1999).

Reservoir 3 is characterized by extensive bedrock outcrops and shallow soils allowing the reservoir to be easily divided into two dominant communities. Soil drainage was very rapid and soils were very dry. The overstory, where it exists, is dominated by a "sometimes dense", even-aged stand of *P. banksiana*. One *Pinus resinosa* Ait (red pine) tree, a species that also colonizes after a forest fire, is present. *B. papyrifera* and *Vaccinium spp.* are the dominant tall shrub and low shrub, respectively. The bedrock outcrops, lacking trees, contained large areas of *Cladina spp.* and *Polytrichum spp.* (Huebert 1999).

In 1999, prior to flooding, each reservoir had five carbon sampling sites, each containing three collars for gas flux chamber measurements. Collars, 10 cm length of 30 cm diameter pipe (PVC), were inserted approximately 5 cm into the ground. At two of the five sites per reservoir a device (sippers) for sampling the water column and pore water was installed. Each sipper was constructed of Tygon tubing ($^1/_4$ x $^1/_8$ x $^1/_{16}$, R-3603), with a screen, fixed to a pipe (PVC) anchored into the soil and supported by guy-wires.

Table 1 FLUDEX reservoir characteristics such as area, volume, forest type and dominant vegetation types.

	Reservoir 1	Reservoir 2	Reservoir 3
Water Surface Area (m^2)	6900	5000	6600
Ungauged Direct Runoff Area (m^2)	48300	7300	600
Reservoir Volume (m^3)	6940	4159	7647
Mean Depth (m)[1]	1.0	0.8	1.2
Length of wooden wall (m)	132	92	237
Length of gravel dyke (m)	102	41	94
Renewal Time (d)	8	6	7
Dominant vegetation type	*Pinus/Ledum/Sphagnum* *Pinus/Polytrichum*	*Pinus/Betula*/litter	*Pinus/Vaccinium*/litter *Polytrichum/Cladina*/bedrock
Forest Type Relative Carbon Content	Moist forest High carbon	Dry forest Medium carbon	Very dry forest Low carbon
Boudreau (2000) & Joyce (2001) naming scheme	L for *Ledum*	P for *Pinus*	G for granite

[1] calculated as (Reservoir Volume) ÷ (Water Surface Area)
data from Beaty (2001)

Table 2 Total above-ground biomass (kg dry wt·ha^{-1}) and carbon (kg C·ha^{-1}) for FLUDEX reservoirs.

	Reservoir 1		Reservoir 2	Reservoir 3	
	Pinus/Ledum/ Sphagnum	*Pinus/Polytrichum*	*Pinus/Betula*	*Pinus/Vaccinium*	*Polytrichum/ Cladina*
Tree[1] biomass	34600±13600[3]	70500±23500	55800±53500	52800±34900	0
Tree[1] carbon	17400±7700	36200±11700	27600±28300	26800±18100	0
Shrub[2] biomass	5490±3200	263±86	250±316	446±318	279±391
Shrub[2] carbon	2450±1330	116±48	132±183	229±169	126±123
Litter biomass	4230±2710	1220±561	1230±456	1310±797	118±79
Litter carbon	1980±1270	570±263	574±214	612±373	55±37
Total biomass	44300±14200	72000±2350	5730±5350	54600±34900	397±399
Total carbon	21800±7920	36900±11700	28300±28300	27600±1810	181±128

[1] includes trees, saplings and tall shrub over 1.5 m in height.
[2] includes low shrubs less than 1.5 m in height, herbs, mosses and lichens.
[3] mean ± standard deviation
data from Huebert (1999)

Table 3 Position of sipper sampling ports used to vertically characterize the reservoirs.

Reservoir	Sampling Site[1]	Site names according to Boudreau (2000) & Joyce (2001)	Location of Sampling Port (relative to sediment-water interface, cm)
1	1	L1	120, 100, 80, 60, 40, 20, 2, -2, -25
1	3	L3	80, 60, 40, 20, 2, -3, -10
2	3	P3	80, 60, 40, 20, 2, -2, -15
2	5	P5	80, 60, 40, 20, 2, -5
3	1	G1	140, 120, 100, 80, 60, 40, 20, -3, -12
3	3	G3	140, 120, 100, 80, 60, 40, 20, 2, -3

[1] Sample Site refers to the carbon sampling sites identified on Figure 4, Figure 5 and Figure 6.

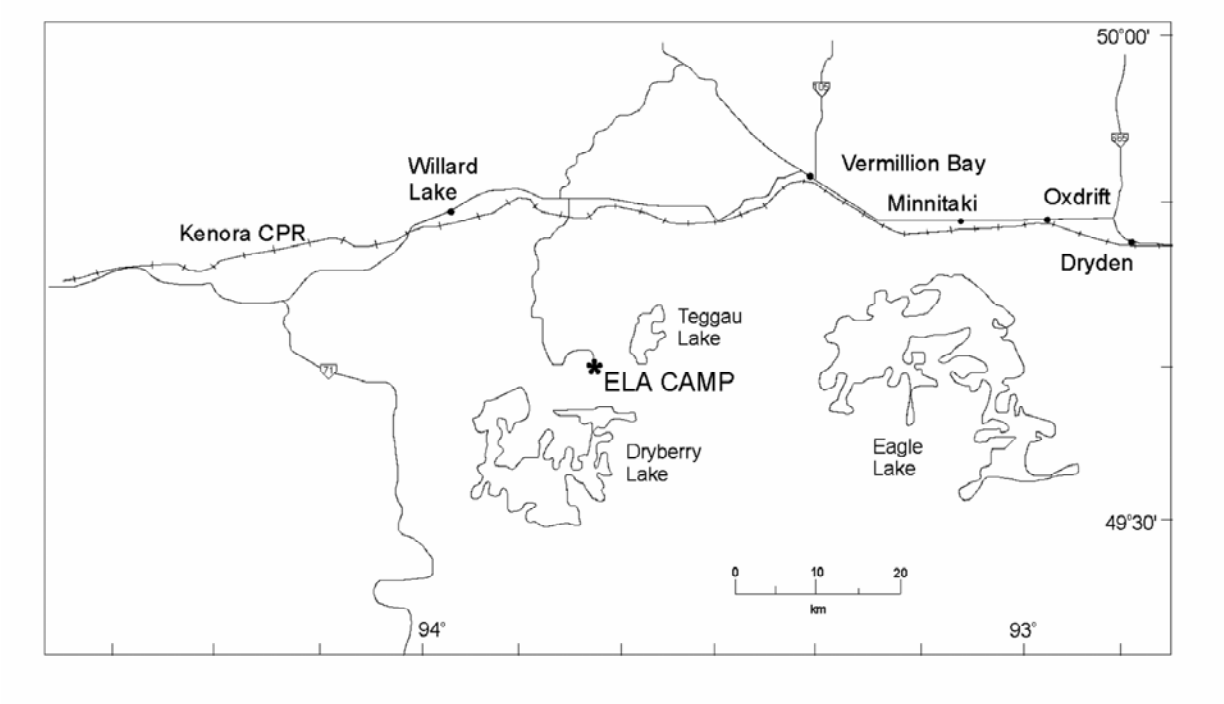

Figure 2 The Experimental Lakes Area (ELA) is approximately 50 km east-southeast of Kenora, Ontario.

Established in 1968, ELA is the research station where the Flooded Upland Dynamics Experiment (FLUDEX) is occurring. Map is modified from Boudreau (2000) and Mewhinney (1996).

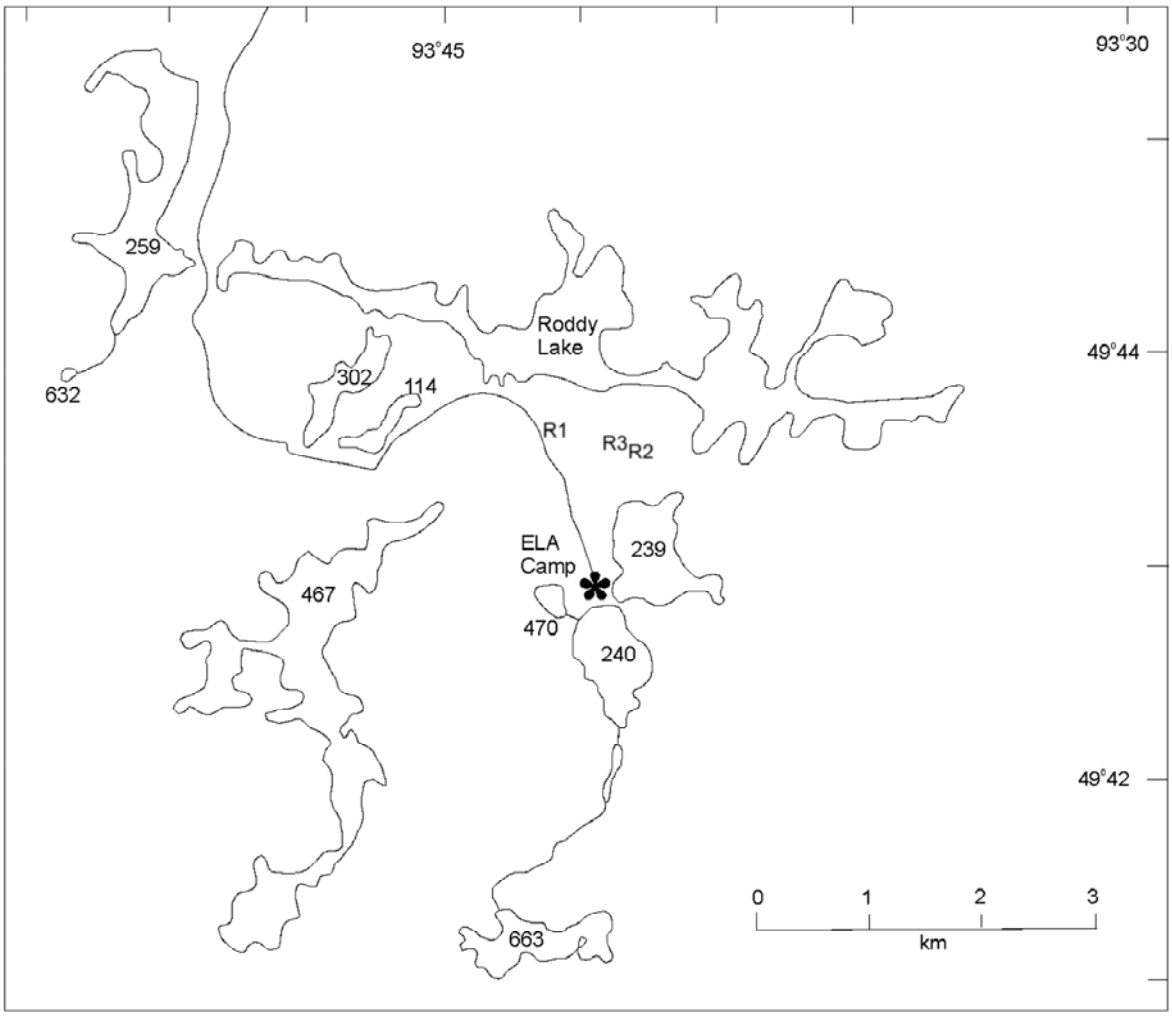

Figure 3 The three FLUDEX reservoirs (R1, R2 and R3) are located several kilometers north of the ELA camp and reference L239.

Water is pumped from Roddy Lake (L468) into the reservoirs. L114 inflow enters the north-east arm of L114. Northwest inflow to L239 enters the middle of the shore of the northwest bay of L239. Map is modified from Boudreau (2000) and Mewhinney (1996).

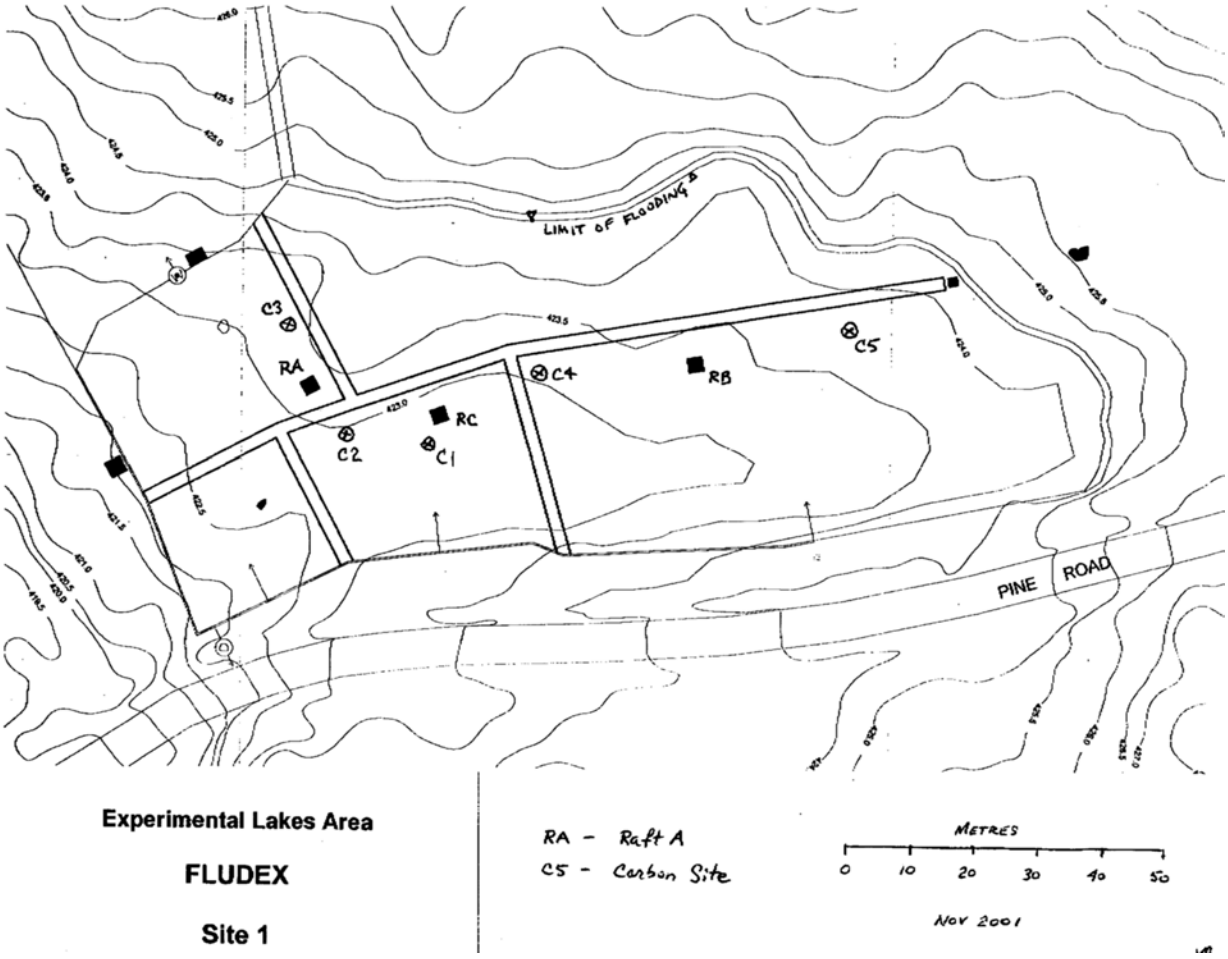

Figure 4 Topographic map of FLUDEX reservoir 1 showing sampling locations (Carbon Site), inflows (I, with arrow pointing into reservoir), outflow (W) and drains (D).

Each reservoir is contained by wooden and gravel dykes on three sides and flooded against a slope as the fourth side (Limit of Flooding). Countour lines of the ground surface have a 0.5 m interval. North is to the left of the figure. K. Beaty (unpubl. data) provides this map.

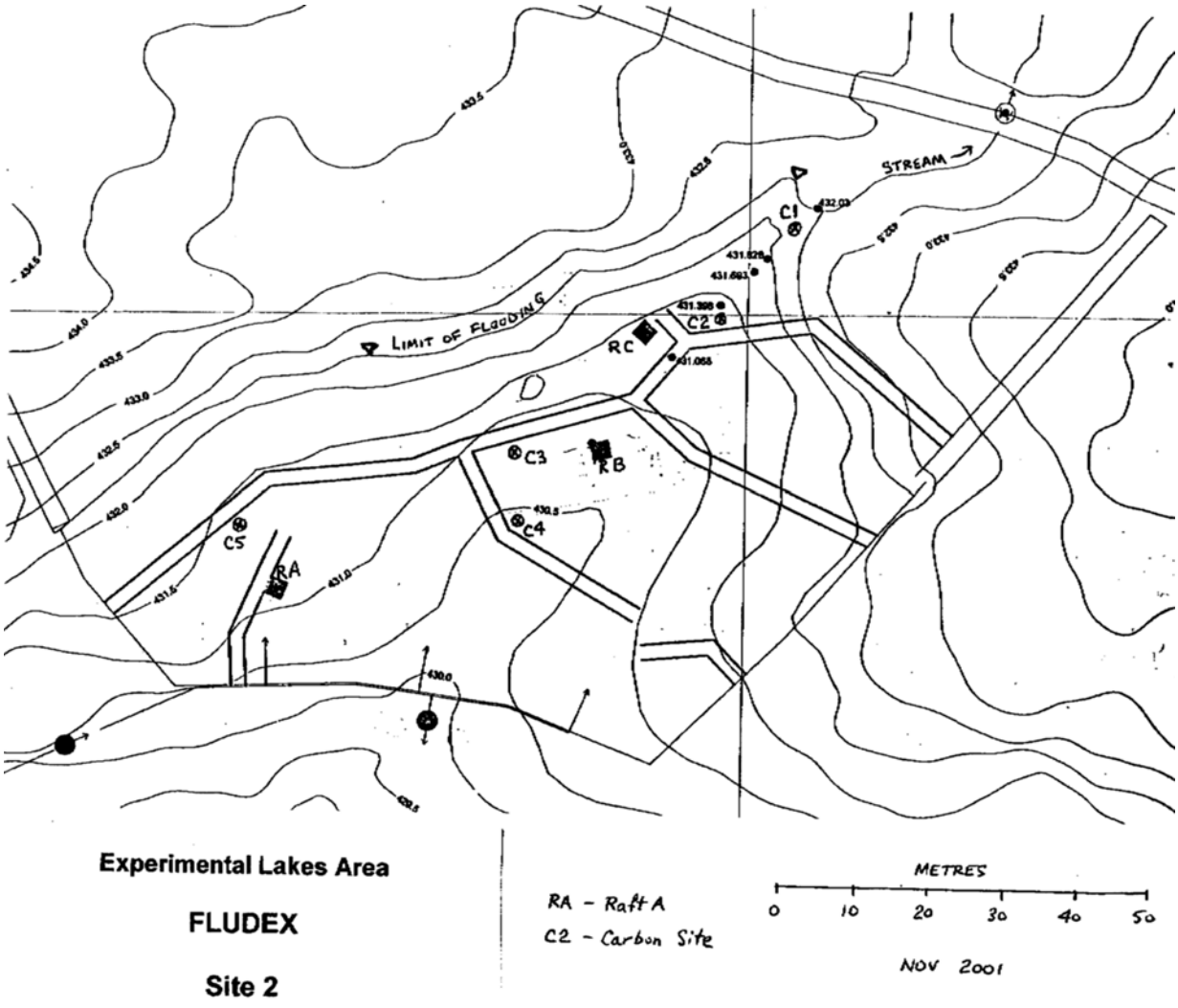

Figure 5 Topographic map of FLUDEX reservoir 2 showing sampling locations (Carbon Site), inflows (I, with arrow pointing into reservoir), outflow (W) and drains (D).

Each reservoir is contained by wooden and gravel dykes on three sides and flooded against a slope as the fourth side (Limit of Flooding). Countour lines of the ground surface have a 0.5 m interval. North is to the top of the figure. K. Beaty (unpubl. data) provides this map.

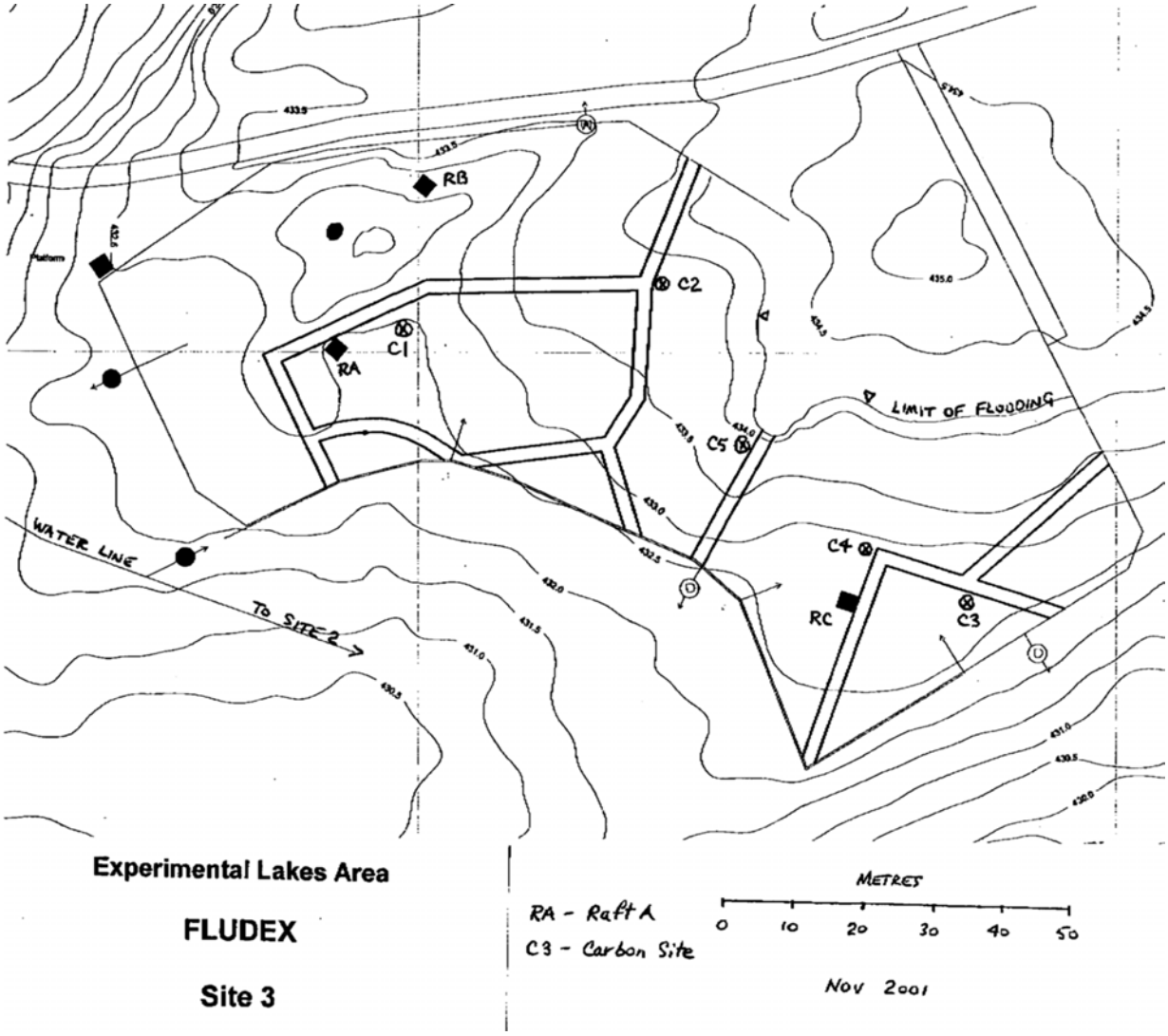

Figure 6 Topographic map of FLUDEX reservoir 3 showing sampling locations (Carbon Site), inflows (I, with arrow pointing into reservoir), outflow (W) and drains (D).

Each reservoir is contained by wooden and gravel dykes on three sides and flooded against a slope as the fourth side (Limit of Flooding). Countour lines of the ground surface have a 0.5 m interval. North is to the top of the figure. K. Beaty (unpubl. data) provides this map.

Chapter 3: Methods

3.1 Stable isotopes

Stable isotopic compositions are measured with mass spectrometers. Compositions (or signatures) are reported in delta notation (δ), as values permil (‰, parts per thousand), relative to an international standard: Vienna Pee Dee Belemnite (VPDB), a carbonate for ^{13}C and ^{18}O; and Vienna Standard Mean Oceanic Water (VSMOW), for ^{2}H and ^{18}O. All ^{13}C values will be reported relative to VPDB and all ^{18}O–O_2 values relative to VSMOW. Direct measurement of the absolute number of each isotope is avoided by measuring the ratio of the two isotopes (e.g. ^{13}C:^{12}C). Delta values are calculated via the following equation:

$$\delta_{sam} = \left(\frac{R_{sam}}{R_{std}} - 1 \right) \times 1000‰$$

where *R* represents the ratio of heavy isotope to light isotope of the sample and the standard.

Many biological processes exhibit a preference for, or discrimination against, light or heavy stable isotopes. Most often the preference is for the light stable isotopes (e.g. ^{12}C and ^{16}O). Urey (1947) and Craig (1954) defined the *fractionation factor*, α, as the isotope ratio of the product divided by that of the source:

$$\alpha_{b-a} = \frac{R_b}{R_a},$$

where R_a is the ratio of the source and R_b is the ratio of the product and, since α is a quantity close to unity, the *enrichment factor*, ε, as the deviation of α from unity and reported in permil: $\varepsilon = (\alpha - 1) \times 1000‰.$

Enrichment can be calculated directly from delta notation,

$$\varepsilon_{b-a} = \left(\frac{\delta_b + 1000}{\delta_b + 1000} - 1 \right) \times 1000‰$$

where δ_a is the δ ‰ value of the source and δ_b is the δ ‰ value of the product. The sign associated with values for α and ε is controlled by defining the reactant as *a* and the product as *b*. For example photosynthesis via the C_3 pathway is associated with a -19‰ fractionation (i.e. $\varepsilon_{\text{-plant-CO2}}$=-19‰).

3.2 Sampling Regimen

Many reservoir processes or fluxes in Figure 1 were characterized directly. Surface gas exchange (1), net benthic flux from the sediment to the water column (5 and 6) and outflow (8) samples were collected and analyzed for stable isotopes of carbon and oxygen. Periphytic algal growth (3 and 5) was estimated by algal growth experiments and subsamples analyzed for stable isotopes. Water column mineralization of particulate and dissolved carbon (2) and mineralization of dead vegetation were not characterized directly. Additionally, other inputs and outputs of water were characterized (see Chapter 5:).

3.3 Analysis protocols

δ^{13}C-DIC , δ^{13}C-CH_4

Liquid samples for δ^{13}C-DIC and δ^{13}C–CH_4 analyses were collected in 50, 60 and 125 mL serum bottles (Wheaton 223745, 223746, 223748). All were sealed with prepared rubber septa (Vacutainer septa, baked at 60ºC for no less than 12 hours). The bottles were filled to overflowing and a filled septum was inverted on the bottle. An 18 gauge needle was inserted just through the septum to allow any trapped atmospheric gas to escape while the septum was seated in the mouth of the bottle.

To preserve samples, 0.2 mL of saturated (41.7 g·(100 mL H_2O)$^{-1}$) sodium azide solution was used in 50 and 60 mL serum bottles, 0.4 mL into 125 mL serum bottles, within two hours of collecting the sample (Vandergrant pers. comm.)

Gas samples were collected by probing reservoir sediments and trapping the bubbles in an inverted funnel. Samples were then transferred to pre-evacuated 11 mL tubes (Vacutainer 366431). Blood tubes were over-pressurized with 13 mL of gas sample to prevent intrusion of atmospheric gas into the sample. Preservation was not required.

The analyses δ^{13}C of CH_4 and DIC were done using a gas chromatograph–combustion–isotope ratio mass spectrometer (GC–C–IRMS) at the Environmental Isotope Laboratory (EIL). A headspace of helium (UHP, Praxair) was added to the sample by simultaneously

injecting the gas and withdrawing the corresponding volume of liquid. Four and 6 mL of helium were added to the 50 and 125 mL serum bottles, respectively. Since DIC analysis was to be performed on each sample, 1% of internal volume of 85% phosphoric acid was added. To equilibrate the gases between headspace and dissolved phases, the samples were shaken for at least two hours on a horizontal shaker at 60 revolutions per minute.

A gas sample (~4 nmol C) was extracted from the headspace of the bottle with a gas tight syringe (SGE) and injected into the gas chromatograph (HP 6890; injection port at 250°C). The GS GasPro column (30m x 0.32mm), at 5°C (cryogenically cooled) with a helium carrier gas (1.2 $mL \cdot min^{-1}$), separates CH_4 and CO_2. Importantly, the column separates N_2 from CH_4. Methane is completely combusted to CO_2 in Micromass combustion furnace (CuO catalyst, 850ºC) fitted to the GC. The two pulses of CO_2 flow into the mass spectrometer (MicroMass Isochrom) where masses 44, 45, and 46 are measured. Analysis of each sample is run in triplicate and is framed by two automated pulses of reference gas. Gas standards (30–300 µM C in helium) of an internal standard (EIL-8) are analyzed after no more than ten samples. Uncertainty of $\delta^{13}C$-CO_2 analysis is ±0.3‰ and of $\delta^{13}C$-CH_4 analysis is ±0.5‰. This method differs slightly from Boudreau (2000) since a lower oven temperature was required to resolve the CH_4 peak (now masses 44 and 45 as CO_2) from N_2O (masses 44, 45, and 46) and NO_2 (mass 46).

$\delta^{18}O$-O_2

Samples for $\delta^{18}O$ analysis were collected in pre-evacuated 125 mL serum bottles (Wheaton 223784) with 0.24 mg sodium azide (equivalent of 0.4 mL of saturated ($41.7\ g \cdot (100\ mL\ H_2O)^{-1}$) solution, Vandergrant pers. comm.) as a bacteriostatic agent. Blue butyl septa (Bellco Glass 2048-11800) and aluminium crimp seals were used to seal the bottles (Wassennar and Koehler 1999). A new 21 gauge needle was used each time a septum was to be punctured since repeated use dulls the needles and can tear the septum. Simultaneous O_2 concentration and temperature measurements were made with a probe (YSI 54). O_2 concentration measurements were confirmed by Winkler titration (Stainton et al. 1977) of 60 mL (60 mL BOD bottle) of water with reagents from ELA Chemlab.

The $\delta^{18}O\text{-}O_2$ analysis is a relatively new procedure because it was done via headspace analysis with a gas chromatograph–isotope ratio mass spectrometer (GC–IRMS) at the EIL. A headspace of helium (UHP, Praxair) was added to the sample by simultaneously injecting the gas and withdrawing the corresponding volume of liquid—to 125 mL serum bottles (160 mL internal volume) 6 mL of helium was added. The reference gas line of a Gilson autosampler fitted to a Micromass Isochrom isotope ratio mass spectrometer was modified to accommodate the simple $\delta^{18}O\text{-}O_2$ analysis equipment (after Wassenaar and Koehler 1999; see Figure 7). A 0.25" tee fitting (UltraTorr) with a septum (Supelco Thermolite 8x4 mm) in the third port is the injection port. Following the inline, splitless injection port, is a CO_2 trap (10 cm x 1 cm o.d., ascarite granules) and H_2O trap (20 cm x 1 cm o.d., 50:50 mixtures of magnesium perchlorate and quartz chips). A 5 Å molecular sieve (1 m, 80°C) resolves $O_2$from N_2. The mass spectrometer is empirically tuned to measure masses 32, 33 and 34. Precision on $\delta^{18}O\text{-}O_2$ measurements is ±0.3‰.

DIC and CH_4 concentration

DIC and CH_4 concentrations were measured by equilibrated headspace (5:55 mL gas:water) gas chromatography (Varian 3800, ruthenium [VIII] oxide catalyst, H_2 and Ar gases, FID detector). Samples were collected in pre-evacuated 50 mL serum bottles (Wheaton 223745) and acidified with 0.1 mL of concentrated H_3PO_4. Samples were kept cool and dark and analyzed within two weeks. Uncertainty of DIC and CH_4 analyses is ±3.5%.

O_2 Concentration

O_2 concentrations were measured by Winkler titration (Stainton et al. 1977) of 60 mL water. Samples were collected in 60 mL BOD bottles (Wheaton 223746). Samples were kept cool and dark until fixed with $MnCl_2$ and KI-NaN_3 alkaline solution. Thereafter, samples were analyzed within 3 days. Uncertainty of O_2 concentration analysis is ±0.2 ppm.

Dissolved organic matter

Samples for analysis of dissolved organic matter (DOM) were collected in 1 L bottles with cone-lined (Poly-Seal) caps. Samples were filtered through precombusted (550°C, 6

hours) GF/F filters (Whatman 0.7 μm nominal pore size) and acidified to pH 3 with 10% hydrochloric acid for preservation. Filters were frozen and retained.

Routine measurement of DOC (dissolved organic carbon) and TDN (total dissolved nitrogen) concentrations in reservoir outflow was performed by ELA Chemlab on an O I Total Organic Carbon Analyzer (Model 700) and a Technicon AutoAnalyzer II, segmented flow/colourimetric analyzer, respectively. DOC concentration analyses of L114 inflow creek was performed on a Rosemount Analytical Dohrmann (DC190) total carbon analyser at the Environmental Geochemistry Laboratory. δ^{13}C-DOC, δ^{15}N-DON and C:N (DOM) analyses were performed via EA-IRMS on a Carlo Erba EA1108 elemental analyser coupled to a MicroMass Isochrom mass spectrometer at the EIL. Liquid samples were prepared by freeze-drying to dryness. Uncertainty of δ^{13}C-DOC analysis is ±0.2‰ and of δ^{15}N-DON is ±0.3‰.

Biofilm

Samples for isotope ratios and C:N ratio were collected by scraping from pine dowels in each reservoir and filtered onto precombusted (550°C, 6 hours) GF/F filters (Whatman 0.7 μm nominal pore size). Filters were kept frozen until sample preparation and analysis was performed using the protocol for DOM.

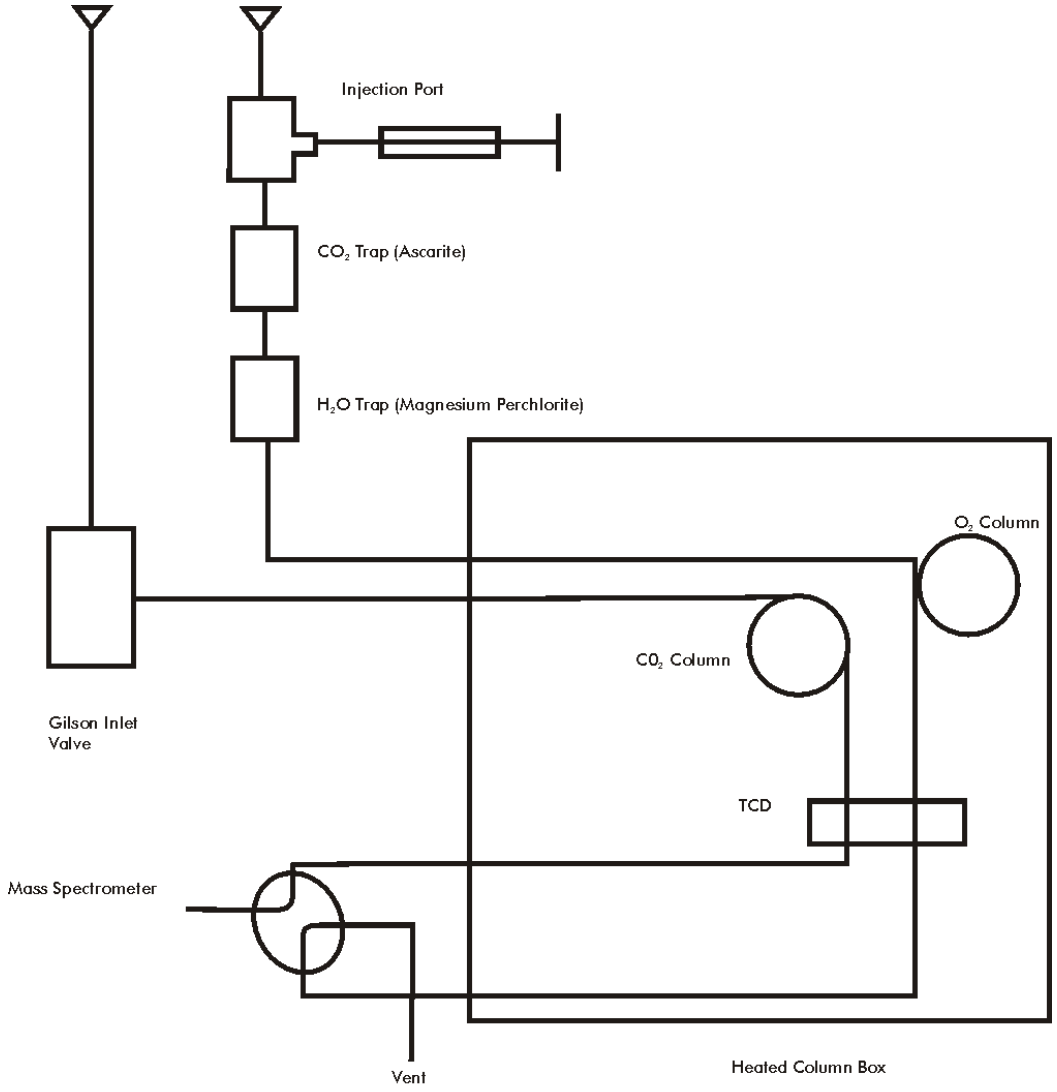

Figure 7 Schematic diagram of Gilson µGas modifications for $\delta^{18}O$-O_2 analysis.

The line not used by the Gilson auto-sampler was modified to include a three-way as a injection port, CO_2 trap and H_2O trap.

Chapter 4: Carbon and oxygen cycling at or near the sediment-water interface in flooded upland forests.

4.1 Introduction

Flooding forested systems for reservoir development shifts the ecosystem carbon balance towards decomposition (St. Louis et al. 2000; Kelly et al. 1994, Rudd et al. 1993). Previously, the forest ecosystem was either a net carbon sink, accumulating organic soils and standing vegetation, or the forest ecosystem was in equilibrium and there was no net change in the amount of carbon stored (Rapalee et al. 1998; Nalder & Wein 1999. Recent studies in Canada (Kelly et al. 1997; Duchemin et al. 1995; cf. St. Louis et al. 2000) have confirmed that boreal landscapes contain significant stores of carbon that, when flooded, cause reservoirs to be large sources of greenhouse gases (GHG) to the atmosphere.

To research GHG and mercury dynamics of flooding upland areas, the FLooded Upland Dynamics EXperiment (FLUDEX) at the Experimental Lakes Area (ELA) began in 1999. FLUDEX is the companion project of the Experimental Lakes Area Reservoir Project (ELARP), where a 17 ha wetland complex was flooded to study GHG and mercury cycling. Fluxes of CO_2, CH_4 and N_2O to and from the atmosphere were measured to determine the potential GHG contribution of reservoirs.

Benthic processes of decomposition, photosynthesis and CH_4 oxidation directly affect the magnitude of GHG flux from the reservoir surface to the atmosphere so understanding the sources of decomposable carbon and the rates of decomposition are very important to predicting future GHG fluxes (Figure 8). Primary production by benthic algae, water column algae and attached algae, and CO_2 reduction remove CO_2. Heterotrophic respiration, photorespiration and CH_4 oxidation add CO_2. Methyl-type fermentation and CO_2 reduction add CH_4. Thus, understanding the balance between decomposition, photosynthesis and CH_4 oxidation is important because the balance determines the magnitude and isotopic signature of the GHG flux to the atmosphere. Stable isotope analyses have been widely used to determine the sources of decomposing carbon and carbon cycling in wetlands (e.g. Happell et al. 1993),

rice paddies (e.g. Chanton et al. 1997) and reservoirs (Poschadel 1997; Scott et al. 1999; Kelly et al. 1997).

The sediment-water interface (SWI) is an important zone in the reservoirs because decomposition of organic carbon fuels the GHG flux from the surface of the reservoirs. There is more carbon in the forest floor (litter and FH layers) that becomes the SWI in flooded forests, than in the foliage of standing vegetation (Boudreau 2001; Huebert 1999). The SWI is a unique and important niche because there are concentration gradients and a surface on which a biofilm can grow. Benthic chambers are deployed to study the balance of these processes (decomposition, photosynthesis and CH_4 oxidation; see Figure 8) at the SWI. Light and dark chambers are used to separate out the light-dependent processes, i.e. photosynthesis and methane oxidation encouraged by photosynthetically derived O_2. Figure 9 shows the differences between the processes inside light and dark benthic chambers. In both chambers, there is a flux of DIC and CH_4 from the sediments to the water column, CH_4 is oxidized and O_2 is removed by respiration. However, in light chambers there are three other processes that occur: primary production removes DIC from the chamber; primary production adds O_2 to the chamber; CH_4 oxidation encouraged by photosynthetically derived O_2 decreases the CH_4 flux across the SWI; and CH_4 oxidation removes CH_4 from the water column. Though CH_4 oxidation occurs in both light and dark chambers King (1990) proposes that CH_4 oxidation occurs to a greater extent in the light because of photosynthetically derived O_2.

Several assumptions are implicit in deploying light and dark benthic chambers. First, changing the benthic conditions by deploying the chamber does not change the benthic processes or the rates at which they occur. Second, to separate light-dependent processes by comparing the light and dark chambers, the non-light dependent processes are assumed to occur at the same rate and location in both chambers, affected by the same thickness of boundary layer, and that the dissolved constituents, the benthic biofilm and the soil below both the light and dark chambers are the same.

Benthic Processes: definition and stable isotope systematics

In an aquatic system, several processes occur contemporaneously. Three important processes are photosynthesis, decomposition, which is part of community respiration, and CH_4 oxidation. The processes are observed within a system.

a. Photosynthesis

Gross photosynthesis (P_g) is the light-dependent rate of electron flow from water to terminal electron acceptors such as CO_2. During this process, carbon is fixed through the conversion of CO_2 to biomass and production of O_2. P_g is measured on the basis of O_2 production rather than carbon fixation because of photorespiration (R_p). R_p is the rate of electron flow from organic carbon to CO_2 with the associated production of CO_2 (Falkowski & Raven 1997). P_g includes all carbon fixed whether or not the fixed carbon becomes part of the organism or is expelled or secreted. Community respiration (R_c) is the respiratory loss from a system that includes R_p and heterotrophic decomposition (Falkowski & Raven 1997). R_c includes the respiratory production of CO_2 by heterotrophs and the CO_2 lost by photoautotrophs during R_p. Thus R_c is not a direct measure of decomposition. The difference can be as much as 25% (Falkowski & Raven 1997).

Net photosynthesis (P_n) is the difference between P_g and R_p. It is most often measured by the change in O_2 in light chambers as a proxy for net organic production, i.e. $P_g = P_n - R_c$. However, P_n and net primary production (NPP, the organic carbon produced by photosynthetic processes) can, and usually does, include a dark period with an associated respiratory loss of carbon. Additionally, gross primary production (GPP) is the total electron equivalents originating from the photochemical oxidation of water. So, adding dark respiratory losses to light-dependent O_2 evolution gives a measure of P_g and thus gross primary production (GPP) can be calculated from the measurement of apparent net primary production (NPP) and community respiration (R_c); i.e. $GPP = NPP + R_c$ (Falkowski & Raven 1997).

The net result of all isotope discrimination during photosynthesis via the Calvin-Benson pathway (i.e. C_3 plants) is an overall enrichment of approximately -20‰ ($\varepsilon_{bulk\text{-}CO2} \approx$-20‰) relative to the source CO_2 (Vogel 1993). This fractionation has a greater magnitude than that

which the Hatch-Slack (i.e. C_4 plants) and Crassulacean acid metabolism (CAM) cycle exhibit. Hatch-Slack and CAM systems are both β-carboxylation reactions. In terrestrial systems, the pathways are clearly demarked by their δ^{13}C-bulk values. In aquatic systems, however, the isotope fractionation is more complicated. In the Calvin-Benson system the variations in δ^{13}C-bulk values are related to the availability of DIC as $CO_{2(aq)}$, the boundary layer thickness and the rate of photosynthesis (Osmond et al. 1987). As DIC becomes limiting, the magnitude of the enrichment decreases and the δ^{13}C-bulk value of photoautotrophs becomes enriched relative a non-DIC limited system (Hecky & Hesslein 1995).

Recent advancements in stable O_2 isotope analyses (Wassenaar and Koehler 1999) provide an efficient analytical technique (δ^{18}O-O_2) that can be used to determine P_g and R_c rates in a light chamber. This advancement removes the necessity of using two chambers to determine photosynthetic rate by difference and provides a direct measurement of gross photosynthesis.

The net reaction of oxygenic photoautotrophs is:
$2H_2O + CO_2 + Light \rightarrow (CH_2O) + H_2O + O_2$. However, this does not elucidate the source of the O_2. Writing the equation as a pair of reduction-oxidation reactions (the 'light' and 'dark' reactions) identifies the source of O_2 as H_2O:

$$\begin{aligned} 2H_2O + Light &\rightarrow 4H^+ + 4e^- + O_2 \\ CO_2 + 4H^+ + 4e^- &\rightarrow (CH_2O) + H_2O \end{aligned}.$$

Figure 10 shows the O_2 concentration and δ^{18}O-O_2 trends resulting from respiration and photosynthesis relative to atmospheric equilibrium. The δ^{18}O-O_2 value at atmospheric equilibrium is +24.2‰ in water, 0.7‰ enriched relative to the atmosphere (Kroopnick & Craig 1972). Respiration decreases the O_2 concentration in the water and preferentially consumes $^{16}O_2$ leaving the remaining O_2 isotopically enriched. Quay et al. (1995) experimentally determined this fractionation factor (α_R) to be 0.986. Dark chamber experiments can determine the isotope fractionation associated with community respiration. Photosynthesis increases the O_2 concentration and O_2 produced by photosynthesis will have the same δ^{18}O value as the H_2O (generally <-7‰ in Canada and <0‰ globally; Rozanski et al. 1993) since the photolysis of water is not associated with any isotopic fractionation (Guy et al. 1993).

The ^{18}O method described by Bender et al. (1987) uses spiked $H_2{}^{18}O$ to trace photosynthetically produced O_2. However, photosynthetically derived O_2 has a very different $\delta^{18}O$-O_2 value than that of atmospheric O_2 and dissolved O_2. Natural H_2O can be used as the isotope tracer if the photosynthetic rates are sufficiently high and thus and isotope spike is not needed.

b. Decomposition

Decomposition of soils releases dissolved organic matter, nutrients, contaminants, chemical species and ultimately CO_2 and/or CH_4. Litter and soil decomposition mechanisms are complex and not well understood (e.g. Ågren et al. 1996; Balesdent et al. 1987; Benner et al. 1987; Nadelhoffer & Fry 1988). Flux of CO_2 from the ground surface to the atmosphere in a forest is similar to the flux of DIC and CH_4 from the flooded soil to the water column in that the products and by-products of soil decomposition are moving from the soil to the overlying medium.

Oxic decomposition of soils involves heterotrophic respiration during the mineralization of soil organic carbon. O_2 consumption during this process, which enriches the $\delta^{18}O$-O_2 value of the remaining O_2, is included in R_c.

During decomposition different groups of compounds are modified and mineralized at different rates, e.g. sugars vs. lignin. The recalcitrant components tend to accumulate relative to more easily decomposed components. Carbon isotope enrichment of soil profiles is well documented but recalcitrant soil components (e.g. lignin) are isotopically depleted relative to bulk litter (Nadelhoffer & Fry 1988). Recent studies indicate that the stable carbon isotope dynamics of the initial stages of decomposition produced CO_2 enriched relative to bulk carbon (Šantrůčková et al. 2000a, 2000b; Baril 2001; Boudreau 2000; Schweizer et al. 1999). Therefore, the $\delta^{13}C$-DIC value of decomposition (^{13}C-DIC_{decomp}) and flux across the sediment-water interface (SWI) relative to the substrate may not be constant.

Anoxic decomposition of organic matter may produce CH_4. Fermentation of acetate produces CH_4; other methylated substrates that are potential methyl-sources have a short residence time due to an effective combination of production and consumption (Whiticar

1999). In highly reducing environments, where other methanogenic substrates are in low concentration, methanogens reduce CO_2, which enriches the δ^{13}C-DIC value of the residual DIC pool. Using δ^{13}C values from 1999 (Boudreau 2000), the δ^{13}C-CH_4 values of CH_4 produced via acetate fermentation (-60 and -50‰) differ from CH_4 produced via CO_2 reduction (<-74‰) because the δ^{13}C values of the substrate and the enrichment factors of each pathway differ (Whitticar 1999).

c. Methane oxidation

Methanotrophs at the oxic-anoxic interface oxidize CH_4 to CO_2 (Whittenbury et al. 1970). Forest soils generally oxidize CH_4 at rates several orders of magnitude lower than the CO_2 flux from the soil to the atmosphere. Crill (1991) identifies the FH-mineral soil interface as the site of CH_4 oxidation in mixed-forest soils. Isotopic fractionation during CH_4 oxidation (α_{mo}) can be used to quantity this process. Whiticar (1999) summarizes CH_4 oxidation isotope fractionation factors as 0.969 to 0.995 in laboratory experiments; a similar range has been found in natural systems. Fractionation factors evaluated as part of FLUDEX and ELARP ranged from 0.978 to 0.987 (mean=0.984, n=14) (Venkiteswaran, unpubl. data).

4.2 Methods

Field sampling and equipment

Prior to the first season of flooding in 1999, fifteen plastic collars, in groups of three, were inserted approximately 5 cm into the soil at five locations in each reservoir. Each 25 cm diameter collar extends above the soil approximately 10 cm. A grove on the top of the collar allows a clear plastic (HDPE) chamber to be seated and sealed, creating a chamber of water (approximately 9 L) over the soil. After flooding, chambers were deployed from boat onto the collars. Each chamber was fitted with a motor and propeller, turning at 12 rpm, to ensure mixing of the trapped water. Tubing attached to a sampling port held afloat by a buoy allowed sampling of the trapped water during the experiments. Chambers, darkened to prevent light from entering, were deployed approximately 15 cm from clear chambers. Each pair of chambers was deployed for 4-5 hours. Initial and final samples for concentration (one bottle for DIC and CH_4 and one bottle O_2) and table isotopes (one bottle for δ^{13}C-DIC and δ^{13}C-CH_4

and one bottle $\delta^{18}O\text{-}O_2$) were taken (see Section 3.2). Analytical protocols are outlined in Section 3.3. C. Matthews (unpubl. data) provides carbon concentration data.

Calculations

Rates of change in DIC and O_2 concentrations in the benthic chambers with time were calculated to assess $R_{c\ DIC}$ and $R_{C\ O}$ (dark chamber), $R_{n\ DIC}$ and $P_{n\ O}$ (light chamber) and $P_{n\ DIC}$ and $P_{g\ O}$ (by difference) (see Table 4). Stable carbon isotope analyses can determine the source of decomposed material and provide evidence for the importance of primary production and CH_4 oxidation. Using the change in DIC and CH_4 in benthic chambers and the change in carbon isotopes, the $\delta\ ^{13}C\text{-}DIC$ and $\delta\ ^{13}C\text{-}CH_4$ added to the chamber can be calculated. In the dark chamber, this yields the $\delta\ ^{13}C\text{-}DIC_{decomp}$ (Equation 2; Table 5), which is the $\delta^{13}C$ of the DIC released from all decomposition and respiration activities from the sediment to the water column; in the light chamber this yields the net daytime carbon isotope flux from the sediment. In a similar fashion, $\delta^{13}C\text{-}DIC_{added}$ (Equation 3; Table 5) can be calculated for light chambers. The difference of the $\delta^{13}C$-DIC values of DIC added to dark and light chambers yields $\delta^{13}C\text{-}DIC_{photo}$ (Equation 4; Table 5); this is the $\delta^{13}C$ of $P_{n\ DIC}$. Table 5 summarizes the calculations.

Gross photosynthetic rates are determined by the DIC difference between dark and light chambers under the assumption that respiration rates and substrates are the same in both light and dark chambers. P_g is also calculated by $\delta\ ^{18}O\text{-}O_2$ in light chambers with O_2 concentration and stable isotope data from only a light chamber (Equation 5; Table 5). This technique is relatively new and there are few studies that have employed it. So, there are few comparable studies and no studies have been done of these assumptions.

O_2 fractionation during respiration (α_R) (Equation 6; Table 5) is determined by the change in O_2 concentration and O_2 isotope ratio in dark chambers via a rearrangement of the Rayleigh equation. Finally, a benthic respiration to photosynthesis ratio (Equation 7 Table 5) is calculated without O_2 concentration data from only the change in $\delta^{18}O\text{-}O_2$ with respect to time.

4.3 Results

Carbon

Benthic DIC and CH_4 fluxes across the SWI are a result of microbial decomposition of soil, DOC and other organic matter both from within the soil and at the SWI, CH_4 oxidation, reduction of CO_2, hydrologic flow and photosynthesis of benthic photoautotrophs. The hydrologic flow dynamics of the flooded soil will affect diffusive and advective transport in the soils based on soil properties. Changes in the relative importance of these processes will affect the magnitude of the flux with time.

In dark chambers the DIC flux from the sediment to the water column (R_c) exhibited a large range, -90-1600 $mgC \cdot m^{-2} \cdot d^{-1}$. The DIC flux in light chambers was smaller in value and range than that of dark chambers, 0-900 $mgC \cdot m^{-2} \cdot d^{-1}$. P_n, calculated as the difference between dark and light chambers, also varies greatly, -760-2900 $mgC \cdot m^{-2} \cdot d^{-1}$. P_n, is greatest in locations where R_c is greatest (r^2=0.79) (see Figure 11). All points but one lay below the 1:1 line where P_n equals R_c. The majority of points (13) points lay within a 500 $mgC \cdot m^{-2} \cdot d^{-1}$ offset from the 1:1 line. This indicates that benthic photoautotrophic consumption of DIC maintains a narrow offset from community respiration. Further, the slope of the best-fit line is less than 1 (*m*=0.87) and thus photoautotrophs are not able to maintain a constant offset as R_c increases. At very high values of R_c benthic photoautotrophs may asymptotically approach a theoretical maximum P_n. The linear relationship between R_c and P_n indicates a strong relationship between decomposers and photoautotrophs at the SWI. The DIC flux across the SWI is a large carbon source for benthic photoautotrophs and the cycling of carbon at the SWI may be the cause of the constant offset exhibited in Figure 11.

The δ^{13}C-DIC accumulating in the benthic chambers is a result of all processes affecting DIC flux. In dark chambers the $\delta^{13}C\text{-}DIC_{decomp}$ enriches with greater flux (r^2=0.42) and ranges from -34 to -17‰ (Figure 12, Table 6).

In light chambers, the δ^{13}C-DIC added to the chamber is a result of all process affecting DIC flux and removal by benthic photoautotrophs. The δ^{13}C-DIC values vary from -39 to +3‰. The δ^{13}C-DIC added to the chamber exhibits bifurcation where nine points fall along

the δ^{13}C-DIC$_{resp}$ line of best fit for the dark chambers and five points fall along a line with a much greater slope (Figure 12). A separation between light and dark chambers occurs when photosynthesis has enriched δ^{13}C-DIC added to light chambers. However, the days when δ^{13}C-DIC added to light chambers was much more enriched than average were days of full, direct sun. The nine light chambers that plot parallel to and above the dark chamber in Figure 12 were cloudy and/or rainy days. The site-specific δ^{13}C-DIC$_{decomp}$ shows a small, ~3‰ enrichment from early-June to mid-August (Figure 15). The δ^{13}C-DIC added to the light chamber shows no single trend with time.

Calculated δ^{13}C-DIC$_{photo}$ values are affected by small differences in chamber flux values when $P_{n\ DIC}$ (denominator of Equation 4; Table 5) is small. Above P_n DIC values of 300 mgC·m^{-2}·d^{-1} the δ^{13}C-DIC$_{photo}$ values range from –32 to –13‰ (Figure 14). This is smaller than expected since applying a photosynthetic enrichment factor ($\varepsilon_{biomass\text{-}CO2}$) of –19‰ to δ^{13}-CO$_{2\ init}$ values produces a range of –41 to –34‰. If δ^{13}C-DIC$_{photo}$ values are related to δ^{13}-CO$_{2\ init}$ values then enrichment factor is smaller than expected, $-14<\varepsilon<+6$. Since there is not a linear relationship between the δ^{13}C-DIC$_{added}$ to light chambers or the δ^{13}C-DIC$_{photo}$ values and $P_{n\ DIC}$ (Figure 13 and Figure 14) this indicates that there is a coupling of the DIC flux from the soil and the benthic photoautotrophs. The water column DIC trapped in the benthic chamber is not used as a primary source of DIC by the photoautotrophs instead the rate of DIC flux from the soil has a controlling effect on $P_{n\ DIC}$.

Light and dark chambers exhibit different ranges in the CH_4 flux from the sediment to the water column, -60-130 and 0-50 mgC·m^{-2}·d^{-1}. The dark CH_4 flux was equal to or greater than the light CH_4 flux in fourteen of nineteen chamber pairs. Concentration analysis quantifies the magnitude of the flux, but isotopic analysis identifies the importance of CH_4 oxidation in the chambers.

Both CH_4 oxidation and methanogenic pathways affect the δ^{13}C-CH_4 values of the CH_4 flux. The δ^{13}C-CH_4 added to the dark chambers (Figure 16) exhibits a large variability (-64 to -89‰) at low (5-15 mgC·m^{-2}·d^{-1}) CH_4 flux from the sediment to the water column, but generally more enriched values (-63 to -70‰) at higher CH_4 flux from the sediment to the

water column (15-40 $mgC \cdot m^{-2} \cdot d^{-1}$). The $\delta^{13}C\text{-}CH_4$ added to dark chambers is never more enriched than -63‰.

CH_4 flux in light chambers exhibits an enriched $\delta^{13}C\text{-}CH_4$ value added to the chambers with greater CH_4 flux. The $\delta^{13}C\text{-}CH_4$ added to chambers becomes more enriched as the flooded season progresses in dark and light chambers (Figure 16; r^2=0.64, 0.62). CH_4 added to light chambers is enriched relative to CH_4 added to dark chambers (Figure 16). This indicates that a greater fraction of the potential CH_4 flux across the SWI has been oxidized. Two processes can cause the seasonal enrichment of the CH_4 flux in light and dark chambers: CH_4 oxidation relative to the source CH_4 and acetate fermentation relative to CO_2 reduction. One or both of these processes can cause the seasonal enrichment in $\delta^{13}C\text{-}CH_4$ values added to benthic chambers.

Oxygen

Initial O_2 concentrations in the benthic chambers were 2-6 $mg \cdot L^{-1}$. In all but six pairs of chambers, O_2 concentration change in light and dark chambers was greater than analytical uncertainty. The analytical uncertainty of O_2 concentration measurements translates to 63 $mgO_2 \cdot m^{-2} \cdot d^{-1}$ over the shortest time a chamber was deployed and 47 $mgO_2 \cdot m^{-2} \cdot d^{-1}$ over the longest time a chamber was deployed.

O_2 concentration decreased in all dark chambers. In light chambers O_2 concentration both increased and decreased. In dark chambers O_2 concentration decrease is a measure of community respiration ($R_{c\,O}$). The range of $R_{c\,O}$ values is 0-1680 $mgO_2 \cdot m^{-2} \cdot d^{-1}$ and exhibited no seasonal trend (Table 8). Light chamber O_2 concentration change is net photosynthesis ($P_{n\,O}$) and shift from net loss of O_2 in June and early-July to a mixture of increases and decreases in early August (-90 to 570 $mgO_2 \cdot m^{-2} \cdot d^{-1}$) and mid-September (-140 to 1330 $mgO_2 \cdot m^{-2} \cdot d^{-1}$). Gross photosynthesis, the sum of dark and light chambers ($P_{g\,O}$), exhibits a similar trend

Calculated benthic $P_{g\,18O}$ increased as the flood season progressed (r^2=0.50, 0.23 and 0.96 for reservoirs 1, 2 and 3). Benthic photosynthesis became relatively more important

(determined by R_c:P_g) in reservoirs 2 and 3 as the flood season progressed. Benthic reservoir 1 R:P remained around 2.2:1 (Figure 18).

Normalizing O_2 concentration and $\delta^{18}O$-O_2 data to initial values (i.e. change in O_2 concentration and change in $\delta^{18}O$-O_2) (Figure 19) reveals a separation between light and dark chambers. There are three scenarios that can exist: respiration dominates; photosynthesis dominates; and respiration and photosynthesis approximately balance. In chambers where respiration dominates, the O_2 concentration decreases and there is a concomitant enrichment of the $\delta^{18}O$-O_2 value due to the isotope fractionation of respiration (α_R). In chambers where photosynthesis dominates, the O_2 concentration increases and there is a concomitant depletion of the $\delta^{18}O$-O_2 value due to photosynthetic input of depleted O_2. In chambers where photosynthesis and respiration approximately balance (i.e. little or no net change in O_2 concentration), the $\delta^{18}O$-O_2 value should deplete because photosynthetically derived O_2 is more depleted relative to the initial $\delta^{18}O$-O_2 value than the enrichment expected by respiration. In broad terms, these three scenarios are quadrants 2 (respiration dominates), 4 (photosynthesis dominates) and 3 (respiration and photosynthesis approximately balance) of Figure 19. Quadrant 1 represents an impossible scenario where O_2 saturation increases and $\delta^{18}O$-O_2 values enrich. Quadrant 1 is the top-right quadrant; quadrant 2 is the top-left quadrant, and so forth counter-clockwise. Figure 10 indicates the direction in which O_2 saturation and $\delta^{18}O$-O_2 will change under the three scenarios. Some light chamber points fall with the majority of dark chamber points indicating that benthic processes in some light chambers were very similar to those in dark chambers. The points that fall into the quadrant where photosynthesis dominates (quadrant 4) indicate that a rapid depletion of $\delta^{18}O$-O_2 occurs with photosynthetic input dominating. There are a few points falling in the area where respiration and photosynthesis approximately balance (quadrant 3). This may suggest tight O_2 coupling between benthic photoautotrophs and oxic decomposers where photosynthetic O_2 is rapidly consumed by decomposers on and in the soil, and does not enter the water column of the benthic chamber. So, the water sampled from the chamber may not show any signs, concentration or isotope, of benthic processes.

Analyses of $\delta^{18}O$-O_2 and O_2 concentration in dark benthic chambers are used to determine the $\delta^{18}O$-O_2 fractionation factor (α_R) during respiration (Equation 3). The mean of

the fractionation factors is α_R=0.987±0.010 (mean ± standard deviation, n=19). Fifteen of eighteen α_R values were between 0.980 and 1.000 (Table 9).

4.4 Discussion

The δ^{13}C-DIC value of DIC from decomposition

Reservoirs accumulate and transfer to the atmosphere DIC from decomposition. Community respiration (the rate of DIC added to dark benthic chambers, $R_{c\ DIC}$) is controlled by the carbon feeding respiration and the diffusive flux of DIC species through the water-logged soil profile into the water column. The δ^{13}C-DIC value of the DIC produced from decomposition (δ^{13}C-DIC$_{decomp}$) is controlled by microbial processes that isotopically fractionate during respiration, isotopic effects from the diffusive flux of DIC and isotopic and compositional variability of source material. The δ^{13}C-DIC$_{decomp}$ (-33‰ to –17‰) values are not the same as the δ^{13}C-bulk values of the underlying soils (-28‰ to –26‰ (litter to FH layers) and –30‰ to -26‰ (*Sphagnum* to peat) (Boudreau 2000)) because several processes isotopically fractionate the DIC.

Soil carbon is not isotopically homogeneous within a soil horizon or with depth. There are two main soil types in the FLUDEX reservoirs. Both soil types show a characteristic enrichment in the δ^{13}C of bulk material with depth: -28‰ (litter) to –26‰ (FH layer) and –30‰ (*Sphagnum*, groundcover, not a true soil layer) to -26‰ (peat) (Boudreau 2000). There are several steps along the mineralization of soil and some that must isotopically fractionate. Laboratory incubation of reservoir soil layers shows a +3 to +6‰ enrichment ($\varepsilon_{CO2\text{-}soil}$=+3 to +6‰) in CO_2 relative to the corresponding soil layer when litter, FH layers and *Sphagnum spp.* are decomposed. A -2 to +1‰ enrichment ($\varepsilon_{CO2\text{-}soil}$=-2 to +1‰) is observed when S-layer (O_f; Dept. of Agriculture 1978) and peat are decomposed in the short-term (Baril 2001; Boudreau 2000). This indicates that the early decomposition of litter-FH soil should produce DIC with a δ^{13}C-DIC value in the range of –22 to –26‰. *Sphagnum* and peat based soils would produce DIC with a δ^{13}C-DIC value of -24 to -27‰. Isotopic fractionation during diffusion of DIC through the soil is described by Graham's Law as the ratio of diffusive velocities to the ratio of the masses taking into consideration the mass of the medium, water (Clark & Fritz 1997). For

DIC species in water, this is a fractionation of –1.9‰ at steady state. The combination of isotopic fractionations associated with decomposition, CH_4 oxidation, diffusion and benthic photoautotrophs could account for the enriched $\delta^{13}C\text{-}DIC_{decomp}$ values added to dark chambers compared to soil values.

The $\delta^{13}C$-DIC effects of primary production

The removal of DIC from reservoirs by primary production reduces the potential DIC flux from the surface of the reservoir to the atmosphere and enriches the $\delta^{13}C$-DIC value of the residual DIC. The $\delta^{13}C$-DIC value of the DIC flux across the SWI into light chambers shows enrichment relative to $\delta^{13}C\text{-}DIC_{decomp}$ added to dark chambers. The photosynthetic removal of DIC by photoautotrophs is associated with a -19‰ enrichment ($\varepsilon_{\text{-plant-}CO2}$=-19‰) such that the algal biomass is significantly depleted relative to the carbon source in systems where carbon is not limiting (Hecky & Hesslein 1995). Where carbon is limiting, the enrichment is smaller; at the SWI water movement may be slow enough that boundary layers develop around the algae and so the algae would be carbon limited if not light and nitrogen limited. Thus the calculated $\delta^{13}C\text{-}DIC_{added}$ in light chambers is enriched due to the preferential removal of $^{12}CO_2$. Benthic biofilm, an amalgam of algae, diatoms, bacteria, etc., was visually present in all collars.

The thickness and development of the benthic biofilm, and water movement will affect the DIC flux across the SWI and the $\delta^{13}C$-DIC value of the DIC flux across the SWI. That the daytime benthic flux is reduced 71%±27% by benthic primary production is very important for the DIC cycling in the reservoirs. This translates to a 15-33% potential reduction in DIC flux across the SWI when weighted for daylight hours during the flooded season.

CH_4 production and oxidation

CH_4 oxidizers have discrete requirements for growth including strong gradients of O_2 and CH_4 (Whittenbuy et al. 1970; Wake et al. 1993; Rudd et al. 1974). However, if dissolved inorganic nitrogen (DIN) is greater than 15 μM the CH_4 oxidizers are no longer inhibited by O_2 concentrations greater than 1 $mg \cdot L^{-1}$ (Rudd et al. 1976; Sansone and Martens 1978). The SWI meets these requirements (Figure 20).

CH_4 production pathways depend on the substrate and group of methanogens. It is unlikely that methanogenic processes differ between side-by-side light and dark chambers. The isotopically heavier $\delta^{13}C\text{-}CH_4$ values of CH_4 flux in light chambers than in dark chambers (Figure 16) is a strong indication that methanotrophs are oxidizing CH_4. King (1990) shows that rapid and stable changes in CH_4 flux are a result of 'photostimulation' of CH_4 oxidation and not changes in CH_4 production. Further, he suggests the oxidation is not the result of photosynthetic organisms but due to the light-mediated changes in O_2 distribution within and on illuminated sediments. Similarly, Frenzel and Karofeld (2000) observe O_2 from aerenchymatic plants supporting CH_4 oxidation in a wetland. The benthic chamber data obtained in FLUDEX also supports King's hypothesis.

The degree of oxidation is related to two things: growth of the methanotophic community; and productivity and composition of benthic photoautotrophs. First, the soil porewater concentration of CH_4 increases several fold to several orders of magnitude during the first month of flooding and remains elevated thereafter (Venkiteswaran, unpubl. data). The methanotrophic population likely increases in response to the seasonal increase in CH_4 concentration. Though DIN concentration (RA Bodaly, unpubl. data) shows no seasonal trend and stays within 1-5 µM. Second, benthic photoautotrophic communities develop during the flood season (R_c:P_g Figure 18; $P_{g\ 18O}$ Table 8) and the net result is that the $\delta^{13}C\text{-}CH_4$ value of the CH_4 flux from the sediment to the water column becomes progressively more enriched indicating that a greater fraction of the potential CH_4 flux across the SWI is oxidized. The fraction of CH_4 oxidized is estimated by using the $\delta^{13}C\text{-}CH_4$ value of the CH_4 added to the dark chambers as the source CH_4, the $\delta^{13}C\text{-}CH_4$ value added to the light chamber as the remaining CH_4 pool and an experimentally derived fractionation factor of 0.987±0.001 (mean ± standard deviation, n=8) (Venkiteswaran, unpubl. data) for FLUDEX reservoirs. These values are applied to a rearrangement of Equation 6. Light and dark benthic chamber data yields an estimate of 15-88% of the potential CH_4 flux across the SWI is reduced by oxidation.

Oxygen isotope fractionation during respiration (α_R)

Few values exist for the oxygen isotopic fractionation during microbial respiration (α_R). The published values are for oceanic water and tropical river water. The values of α_R is

required to calculate R_c:P_g and $P_{g\ 18O}$ from $\delta^{18}O$-O_2 values. The mean of the α_R values determined in dark benthic chambers α_R=0.987±0.010 (mean ± standard deviation, n=19) encompassed the range of values determined by Quay et al. (1995) in Amazonia. They reported α_R=0.982±0.003 for flask incubations of river water. Oceanic values of similar magnitude have been reported from 0.982-0.990 (Kroopnick & Craig 1976; Bender & Grande 1987; Bender 1990; Kiddon et al. 1993). Quay et al. (1993; 1995) summarized α_R for bottle incubations. Calculated *in situ* and incubation α_R values may differ because plant, animal and bacterial respiration may fractionate differently and the α_R in the chambers is the accumulated effect of all processes. The higher α_R values (i.e. closer to 1.000) may indicate conditions where O_2 availability was limited. There is no linear correlation between α_R and O_2 concentration. However, O_2 availability is not necessarily limited by O_2 concentration in the water column trapped by the benthic chamber but limited by O_2 availability where the heterotrophs are located—at and below the SWI.

A comparison of estimates of gross photosynthesis

Benthic gross photosynthesis has been calculated via two methods: difference in the change in O_2 concentration between light and dark benthic chambers; and via $\delta^{18}O$-O_2 analysis in light benthic chambers. Figure 17 indicates that at as $P_{g\ O}$ increases, so does $P_{g\ 18O}$. This is expected because both are estimates of gross O_2 evolution and both P_g values rely on the change in O_2 concentration in light chambers (see Table 4 and Table 5). The $P_{g\ O}$ estimates are greater than the $P_{g\ 18O}$ estimates.

The concentration based data suffer from assuming that processes in light and dark chambers differ only by photosynthesis. DIC, CH_4 and O_2 concentration data indicate that the SWI within a reservoir is heterogeneous with respect to carbon flux across the SWI and O_2 consumption and production at the SWI. There has been little published research that uses this $\delta^{18}O$-O_2 approach to estimate gross photosynthesis and none has focussed on the SWI. More research needs to be done to determine why the $P_{g\ 18O}$ values are less than $P_{g\ O}$ values and which better estimates true gross photosynthesis.

Importance of respiration versus photosynthesis

The benthic balance of respiration to photosynthesis (R:P) is an important summary of benthic processes since the benthic fluxes are a balance between microbial decomposition of organic carbon that consumes O_2 and primary production that consumes carbon and produces O_2. In the broadest sense R:P is a measure of a systemic heterotrophy or autotrophy. In these reservoirs, heterotrophic decomposition of freshly flooded soil organic matter was predicted to dominate the system leading to water column anoxia in portions of the reservoirs. In carbon terms R:P is the balance between CO_2 production and CO_2 consumption (fixation). Because of photorespiration (R_p) measurements of photosynthesis are net measurements ($P_{n\ DIC}$). In oxygen terms R:P is the balance between O_2 consumption and O_2 production. The gross production of O_2 can be determined with $\delta^{18}O$-O_2 and O_2 concentration and this affords a measure not influenced by R_p.

The main assumption made in O_2 concentration calculations is that the light and dark chambers behave identically with the exception of photosynthesis. O_2 concentration data indicates that $P_{n\ O}$ increases generally during the flooded season but some sites indicate that $P_{n\ O}$ decreases.

While it is true that decomposition of the dominate carbon and O_2 cycles in the reservoirs, analysis of $\delta^{18}O$-O_2 in light chambers shows a general increase in $P_{g\ 18O}$ and $R_{c\ O}$ during the flooding season; but $P_{g\ 18O}$ increases at a greater rate. This indicates that at the process level, photosynthesis becomes more important relative to respiration. Benthic R_c:P_g declines in reservoirs 2 and 3 as the flooding season (Figure 18). In reservoir 1, R_c:P_g remains, on average, constant.

4.5 Summary

The benthic chamber experiments confirm that photosynthesis plays an important role in carbon and O_2 cycling in the FLUDEX reservoirs after two years of flooding. Benthic photoautotrophs reduce the daytime DIC flux from the sediment to the water column by, on average, 71% and consume 15-33% of the potential DIC flux into the water column. Benthic photoautotrophs isotopically enrich the $\delta^{13}C$-DIC added to the water column; the magnitude of

the enrichment depends upon the quantity of primary production. The O_2 produced by photosynthesis is implicated in reducing the CH_4 flux from the sediment to the water column by encouraging CH_4 oxidation and prevents the reservoirs from becoming anoxic; the partially oxidized CH_4 is isotopically enriched relative to the unoxidized source. An estimated 15-88% of the potential CH_4flux across the SWI is removed by CH_4 oxidation. This reduces the potential GWP of the GHG flux from the reservoir water since CH_4 has a GWP twenty-one times that of CO_2 (IPCC 1996). The decline in R_c:P_g during the flooding season indicates improving O_2 conditions in the bottom water of the reservoirs. This is important to prevent hypoxia or anoxia that harms fish and can encourage CH_4 oxidation. Since benthic photoautotrophs perform an important role in the GHG cycling in the FLUDEX reservoirs, separate fluxes and isotope values must be used for daytime and nighttime fluxes when calculating mass budgets and balances.

Table 4 Summary of abbreviations, the chambers in which the processes are measured, the equations to calculate the rate of the process and assumptions associated with calculating the processes. SWI is the sediment-water interface.

Process		Chamber	Equation	Assumptions
Abbreviation	**Name**			
$P_{g\ 18O}$	Gross photosynthesis	Light	^{18}O-O_2 (Equation 5)	Isotope fractionation is precisely known
$P_{g\ O2}$		Dark, Light	$\Delta O_{2\ light} + \Delta O_{2\ dark}$	Light and dark systems are identical
$P_{g\ DIC}$	Gross photosynthesis	Dark, Light	$P_{n\ DIC} + R_{c\ DIC}$	Light and dark systems are identical
$P_{n\ O}$	Net photosynthesis	Light	$\Delta O_{2\ light}$	
$P_{n\ DIC}$	Net photosynthesis	Dark, Light	$\Delta DIC_{dark} - \Delta DIC_{light}$	CO_2 reduction is negligible; CH_4 oxidation is negligible; Light and dark systems are identical
R_p	Photorespiration	Dark, Light	Included in $R_{c\ DIC}$	Light and dark systems are identical
$R_{c\ O}$	Community respiration, nighttime DIC flux across SWI	Dark	$\Delta O_{2\ dark}$	
		Light	^{18}O-O_2 (Equation 5)	Isotope fractionation is precisely known
$R_{c\ DIC}$	Community respiration	Dark	ΔDIC_{dark}	Benthic photoautotrophs do not affect below SWI DIC flux; $R_{p\ DIC}$ is fully included; CO_2 reduction is negligible
$R_{n\ DIC}$	Net community respiration; daytime DIC flux across SWI	Light	ΔDIC_{light}	
^{13}C-DIC_{decomp}	^{13}C of flux across SWI	Dark	Equation 2	Benthic photoautotrophs do not affect below SWI DIC flux in the dark
^{13}C-DIC_{photo}	^{13}C of photosynthesis at SWI	Dark, Light	Equation 4	$P_{n\ DIC}$ is sufficiently large enough
α_R	^{18}O-O_2 isotope fractionation of respiration	Dark	Equation 6	
α_{mo}	^{13}C-CH_4 isotope fractionation of CH_4 oxidation		Equation 4, but with $\delta^{13}C$-CH_4 and CH_4 concentration	

Table 5 Summary of abbreviations, the chambers in which the processes are measured and the equations to calculate isotope-based values.

Process		Chamber	Equation	Equation number
Abbre-viation	Name			
$\delta^{13}C_{decomp}$	^{13}C of flux across SWI	Dark	$\delta^{13}C_{decomp} = \frac{C_{final} \times \delta^{13}C_{final} - C_{init} \times \delta^{13}C_{init}}{C_{final} - C_{init}}$	(2)
$\delta^{13}C_{added}$	^{13}C of flux across SWI	Light	$\delta^{13}C_{added} = \frac{C_{final} \times \delta^{13}C_{final} - C_{init} \times \delta^{13}C_{init}}{C_{final} - C_{init}}$	(3)
$\delta^{13}C_{photo}$	^{13}C of photosynthesis at SWI	Dark, Light	$\delta^{13}C_{photo} = \frac{R_c \times \delta^{13}C_{decomp} - DIC_{light} \times \delta^{13}C_{added}}{P_n}$	(4)
P_g	Gross photosynthesis	Light	$P_g = \frac{\frac{\delta^{18}O_{final} - \delta^{18}O_{init}}{\Delta t} - \frac{O_{2\,final} - O_{2\,init}}{\Delta t}\left(\delta^{18}O_{init} \times \alpha_R\right)}{\delta^{18}O_w \times \alpha_P - \delta^{18}O_{init} \times \alpha_R}$	(5)
α_R	^{18}O-O_2 isotope fractionation of respiration	Dark	$\alpha_R = \frac{ln\left(\frac{\delta^{18}O_{init} + 1000}{\delta^{18}O_{final} + 1000}\right)}{ln\left(\frac{O_{2\,init}}{O_{2\,final}}\right)} + 1$	(6)
R_c:P_g	respiration: photosynthesis	Light	$\frac{R_c}{P_g} = \frac{\frac{\delta^{18}O_{final} - \delta^{18}O_{init}}{\Delta t} + \delta^{18}O_w \times \alpha_P}{\frac{\delta^{18}O_{final} - \delta^{18}O_{init}}{\Delta t} - \delta^{18}O_{init} \times \alpha_R}$	(7)

Abbreviation	Item	Notes
$\delta^{13}C$	$\delta^{13}C$-DIC $\delta^{13}C$-CH_4	
C	DIC concentration CH_4 concentration	
O_2	O_2 concentration	
$\delta^{18}O$	$\delta^{18}O$-O_2	
$\delta^{18}O_w$	$\delta^{18}O$-H_2O	
α_P	$\delta^{18}O$-O_2 isotope fractionation of photosynthesis	α_P=1.000±0.003 (Guy et al. 1993)
final	final conditions	
initial	initial conditions	

Table 6 Summary of rates of DIC-based processes and δ^{13}C-DIC added to dark and light chambers in FLUDEX reservoirs. Concentration data from C. Matthews (unpubl. data).

Location	Date	Dark		Light		Dark-Light		Dark: Dark-Light
		R_c ($mgC \cdot m^{-2} \cdot d^{-1}$)	$\delta^{13}C$- DIC_{added} (‰)	DIC ($mgC \cdot m^{-2} \cdot d^{-1}$)	$\delta^{13}C$-DIC_{added} (‰)	P_n ($mgC \cdot m^{-2} \cdot d^{-1}$)	$\delta^{13}C$-DIC_{photo} (‰)	R_C:P_n
Reservoir 1-1	03-Jul-00	790	-23.2	250	-2.2	550	-32	1.4:1
Reservoir 1-1	31-Jul-00	1200	-20.3	20	-50.8	1100	-21	1.0:1
Reservoir 1-1	14-Aug-00	790	-24.9	250	-38.8	550	-32	1.4:1
Reservoir 1-3	23-Jun-00	1100	-26.6	20	-25.2	1100	-19	1.0:1
Reservoir 1-3	03-Jul-00	750	-24.6	190	-27.2	570	-25	1.3:1
Reservoir 1-3	31-Jul-00	90		110	-26.8	80	5	1.2:1
Reservoir 1-3	14-Aug-00	510	-26.8	430	-25.5	80	-41	6.8:1
Reservoir 1-3	12-Sep-00	610	-33.6	370		240	41	2.5:1
Reservoir 2-3	23-Jun-00	750	-17.0	190	3.0	570	-20	1.3:1
Reservoir 2-3	01-Aug-00	170	-18.0	130	-15.9	40	79	4.6:1
Reservoir 2-3	15-Aug-00	780	-24.2	210	-11.8	570	-24	1.4:1
Reservoir 2-5	23-Jun-00	1600	-20.0	220	-22.8	1400	-18	1.2:1
Reservoir 2-5	04-Jul-00	990	-31.0	230	-72.0	760	-28	1.3:1
Reservoir 2-5	15-Aug-00	1200	27.4	859	-22.3	370	-12	3.4:1
Reservoir 2-5	13-Sep-00	630		96	-17.4	530	-24	1.2:1
Reservoir 3-1	24-Jun-00	-90	-19.1	320	-24.4	-410	-19	0.2:1
Reservoir 3-1	14-Sep-00		-22.7	850				
Reservoir 3-4	24-Jun-00	390	-24.6	460	-20.8	-70	-54	-5.9:1
Reservoir 3-4	02-Aug-00	320	-24.4	0	-18.6	330	-24	1.0:1
Reservoir 3-4	16-Aug-00	2900	-32.5	860	-20.1	2900	-18	1.0:1

Concentration based DIC flux values <160 $mgC \cdot m^{-2} \cdot d^{-1}$ have initial and final DIC concentrations within analytical uncertainty. Thus $\delta^{13}C_{added}$ values calculated with flux values <160 $mgC \cdot m^{-2} \cdot d^{-1}$ are uncertain.
Concentration based CH_4 flux values <2 $mgC \cdot m^{-2} \cdot d^{-1}$ have initial and final DIC concentrations within analytical uncertainty. Thus $\delta^{13}C_{added}$ values calculated with flux values <2 $mgC \cdot m^{-2} \cdot d^{-1}$ are uncertain.

Table 7 Summary of rates of CH_4-based processes and $\delta^{13}C$-CH_4 added to dark and light chambers in FLUDEX reservoirs. Concentration data from C. Matthews (unpubl. data).

Location	Date	Dark		Light		Dark-Light
		CH_4 ($mgC \cdot m^{-2} \cdot d^{-1}$)	$\delta^{13}C$- CH_{4added} (‰)	CH_4 ($mgC \cdot m^{-2} \cdot d^{-1}$)	$\delta^{13}C$- CH_{4added} (‰)	CH_4 ($mgC \cdot m^{-2} \cdot d^{-1}$)
Reservoir 1-1	03-Jul-00	11	-71.8	6	-69.8	5
Reservoir 1-1	31-Jul-00	22	-63.5	-2		24
Reservoir 1-1	14-Aug-00	46		-23		70
Reservoir 1-3	23-Jun-00	11		6		5
Reservoir 1-3	03-Jul-00	10	-93.8	11	-78.4	-1
Reservoir 1-3	31-Jul-00	44		30	-77.1	14
Reservoir 1-3	14-Aug-00	19		15		4
Reservoir 1-3	12-Sep-00	1		-18		19
Reservoir 2-3	23-Jun-00	1		3		-2
Reservoir 2-3	01-Aug-00	38	-64.1	28	-54.2	11
Reservoir 2-3	15-Aug-00	9	-63.8	36	-37.5	-27
Reservoir 2-5	23-Jun-00	12		10		3
Reservoir 2-5	04-Jul-00	15	-88.9	6	-91.3	9
Reservoir 2-5	15-Aug-00	1		52		-51
Reservoir 2-5	13-Sep-00			130		
Reservoir 3-1	24-Jun-00	3		3		0
Reservoir 3-1	14-Sep-00	-7		-61		54
Reservoir 3-4	24-Jun-00	18		2		16
Reservoir 3-4	02-Aug-00	31	-70.7	73	-54.9	-43
Reservoir 3-4	16-Aug-00	6		120	-56.9	-120

Concentration based CH_4 flux values <1 $mgC \cdot m^{-2} \cdot d^{-1}$ have initial and final DIC concentrations within analytical uncertainty. Thus $\delta^{13}C_{added}$ values calculated with flux values <2 $mgC \cdot m^{-2} \cdot d^{-1}$ are uncertain.

Table 8 Summary of rates of O_2-based processes and $\delta^{18}O$-O_2–based processes in FLUDEX reservoirs.

Location	Date	Dark	Light	Light+Dark	Dark: Light+Dark	^{18}O-O_2	^{18}O-O_2
		R_c ($mgO_2 \cdot m^{-2} \cdot d^{-1}$)	P_n ($mgO_2 \cdot m^{-2} \cdot d^{-1}$)	P_g ($mgO_2 \cdot m^{-2} \cdot d^{-1}$)	R_g:R_c	R_c:P_g	P_g ($mgO_2 \cdot m^{-2} \cdot d^{-1}$)
Reservoir 1-1	03-Jul-00	500	11	610	4.4:1	2.0:1	77
Reservoir 1-1	31-Jul-00	220	140	360	0.6:1	2.1:1	97
Reservoir 1-1	14-Aug-00	43	-7	40	1.2:1	2.2:1	-34
Reservoir 1-3	23-Jun-00	550	-480	70	8.3:1	2.4:1	-2400
Reservoir 1-3	03-Jul-00	530	-290	240	2.2:1	2.5:1	-200
Reservoir 1-3	31-Jul-00	1680	420	2110	0.8:1	2.4:1	300
Reservoir 1-3	12-Sep-00	790	1330	2130	0.4:1	2.2:1	900
Reservoir 2-3	23-Jun-00	0	20	20	0:1	1.9:1	80
Reservoir 2-3	04-Jul-00	90	-30	60	1.5:1	2.5:1	-140
Reservoir 2-3	01-Aug-00	790	40	830	0.9:1	1.9:1	31
Reservoir 2-3	15-Aug-00	580	-130	440	1.3:1	1.8:1	-89
Reservoir 2-3	14-Sep-00		620			1.6:1	400
Reservoir 2-5	04-Jul-00	540	-410	130	4.3:1	2.8:1	-290
Reservoir 2-5	01-Aug-00	90	-90	4	22:01	2.1:1	-440
Reservoir 2-5	15-Aug-00	70	-10	70	1.1:1	2.2:1	-43
Reservoir 3-1	24-Jun-00			0			
Reservoir 3-1	05-Jul-00	590	-940	-350	-1.7:1	3.2:1	-680
Reservoir 3-1	02-Aug-00	260	32	580	0.4:1	1.9:1	220
Reservoir 3-1	16-Aug-00	20	30	50	0.3:1		
Reservoir 3-1	14-Sep-00	90	-140	-50	-1.8:1	1.8:1	1100
Reservoir 3-4	05-Jul-00	200	-810	-610	-0.3:1	2.6:1	-580
Reservoir 3-4	02-Aug-00	370	570	940	0.4:1	1.6:1	380

Concentration based R and P values <63 $mgO_2 \cdot m^{-2} \cdot d^{-1}$ have initial and final O_2 concentrations within analytical uncertainty.
$\delta^{18}O$-O_2 based P_g values are ±250 $mgO_2 \cdot m^{-2} \cdot d^{-1}$
$\delta^{18}O$-O_2 based R_c:P_g values are ±0.6:1

Table 9 Summary of $\delta^{18}O$-O_2 fractionation factors (α_R) of respiration in FLUDEX reservoirs.

Location	Date	Dark
		α_R
Reservoir 1-1	03-Jul-00	0.987
Reservoir 1-1	31-Jul-00	0.959
Reservoir 1-1	14-Aug-00	0.990
Reservoir 1-3	23-Jun-00	1.000
Reservoir 1-3	03-Jul-00	0.980
Reservoir 1-3	31-Jul-00	0.996
Reservoir 1-3	12-Sep-00	0.996
Reservoir 2-3	01-Aug-00	0.988
Reservoir 2-3	04-Jul-00	0.980
Reservoir 2-3	15-Aug-00	0.990
Reservoir 2-5	04-Jul-00	0.995
Reservoir 2-5	01-Aug-00	0.997
Reservoir 2-5	15-Aug-00	0.989
Reservoir 3-1	05-Jul-00	0.983
Reservoir 3-1	02-Aug-00	0.996
Reservoir 3-1	16-Aug-00	0.973
Reservoir 3-1	14-Sep-00	0.993
Reservoir 3-4	05-Jul-00	0.993
Reservoir 3-4	02-Aug-00	0.977
minimum		0.959
mean		**0.987**
standard deviation		0.010
maximum		1.000

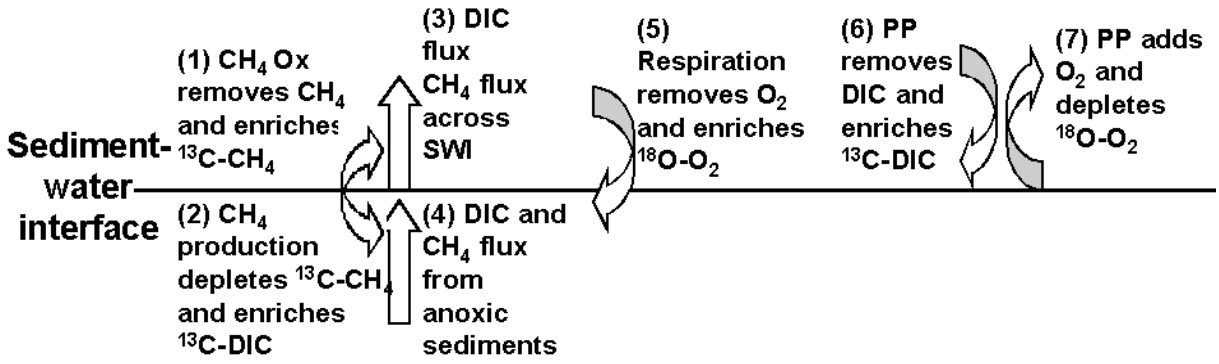

Figure 8 Conceptual model of DIC, CH_4 and O_2 cycling at or near the sediment-water interface in FLUDEX reservoirs.

The words *adds* and *removes* refer to concentration; *enriches* and *depletes* refer to stable isotopes. *CH_4 Ox* is CH_4 oxidation; *Respiration* is heterotrophic respiration and *PP* is primary production.

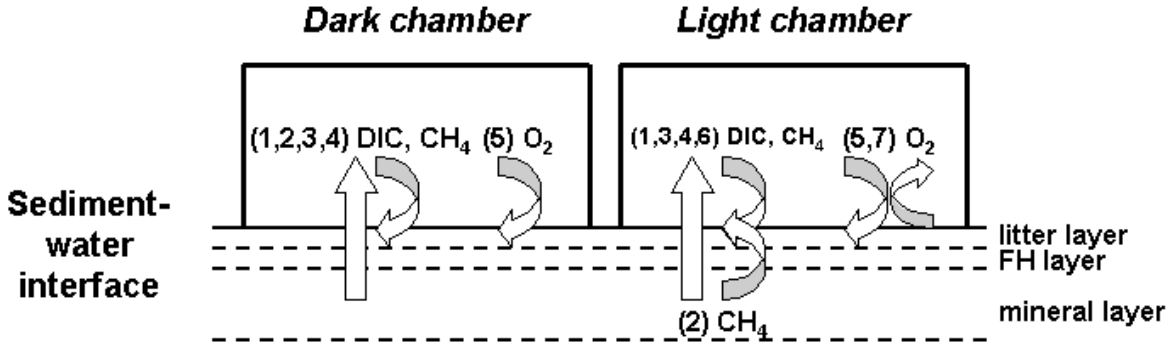

Figure 9 Conceptual model of DIC, CH_4 and O_2 cycling at or near the sediment-water interface of FLUDEX reservoirs inside light and dark chambers.

Numbers refer to processes identified in Figure 8.

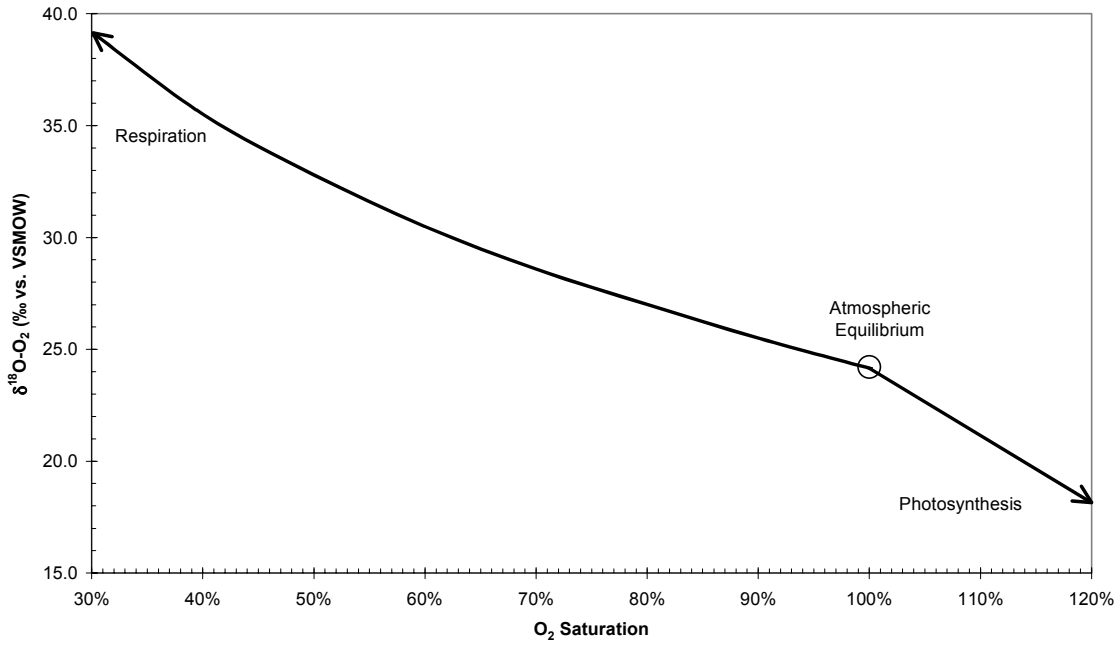

Figure 10 The level of O_2 saturation and $\delta^{18}O$-O_2 value of a sample is controlled by the balance of three processes: respiration, photosynthesis and gas exchange with the atmosphere.

At atmospheric equilibrium, the O_2 of saturated water would have a $\delta^{18}O$-O_2 value of +24.2‰ (Kroopnick & Craig 1972). Photosynthetically derived O_2 has the same $\delta^{18}O$-O_2 value as water (Guy et al. 1993), -10‰ in this figure. The $\delta^{18}O$-H_2O value remains unchanged during photosynthesis and respiration. The consumption and isotope fractionation of O_2 reduces the level of O_2 saturation and isotopically enriches the remaining O_2 (Quay et al. 1995).

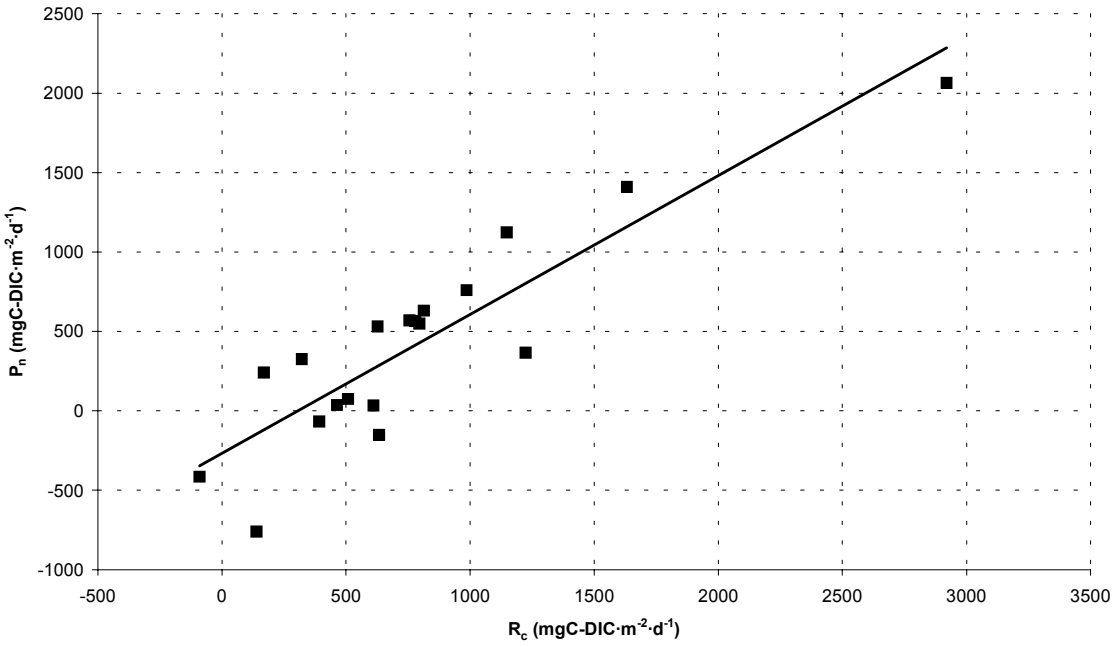

Figure 11 Community respiration ($R_{c\ DIC}$) and net photosynthesis ($P_{n\ DIC}$) (calculated by DIC concentration change difference between light and dark benthic chambers) rates in FLUDEX reservoirs, from 30-May to 22-September-2000.

Data from all sampling locations and date are shown. Concentration data from C. Matthews (unpubl. data).

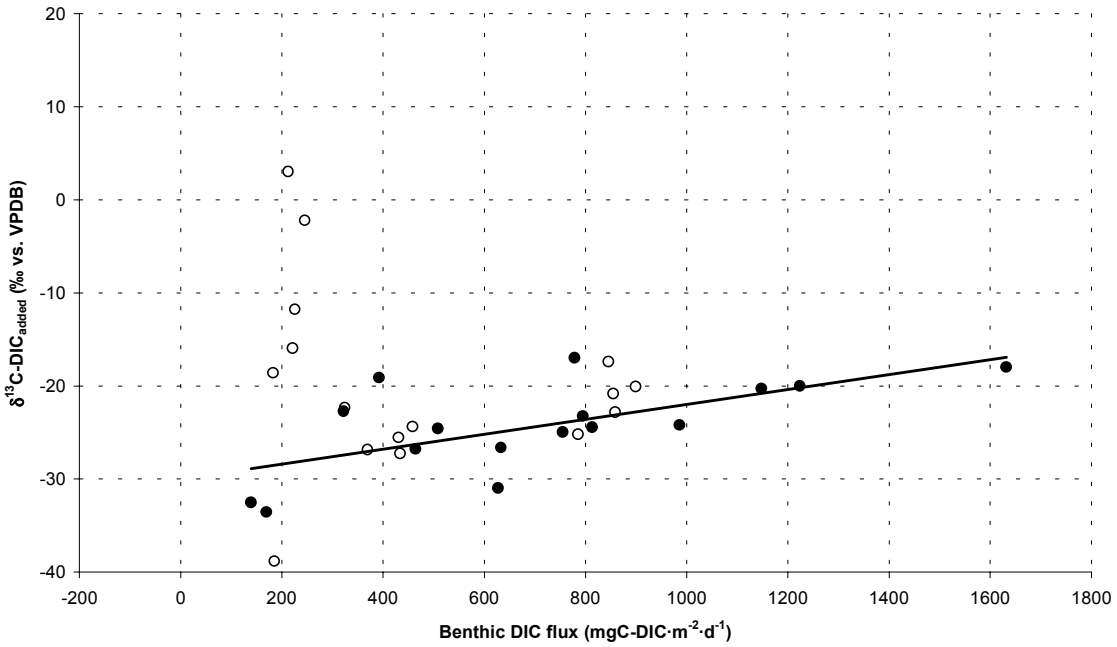

Figure 12 Benthic DIC flux (calculated by DIC concentration change) and δ^{13}C-DIC$_{added}$ (calculated with Equation 2) in light (open circles) and dark (closed circles) chambers in FLUDEX reservoirs from 30-May to 22-September-2000.

Line of best fit (r^2=0.42) for dark chambers is shown. Concentration data from C. Matthews (unpubl. data).

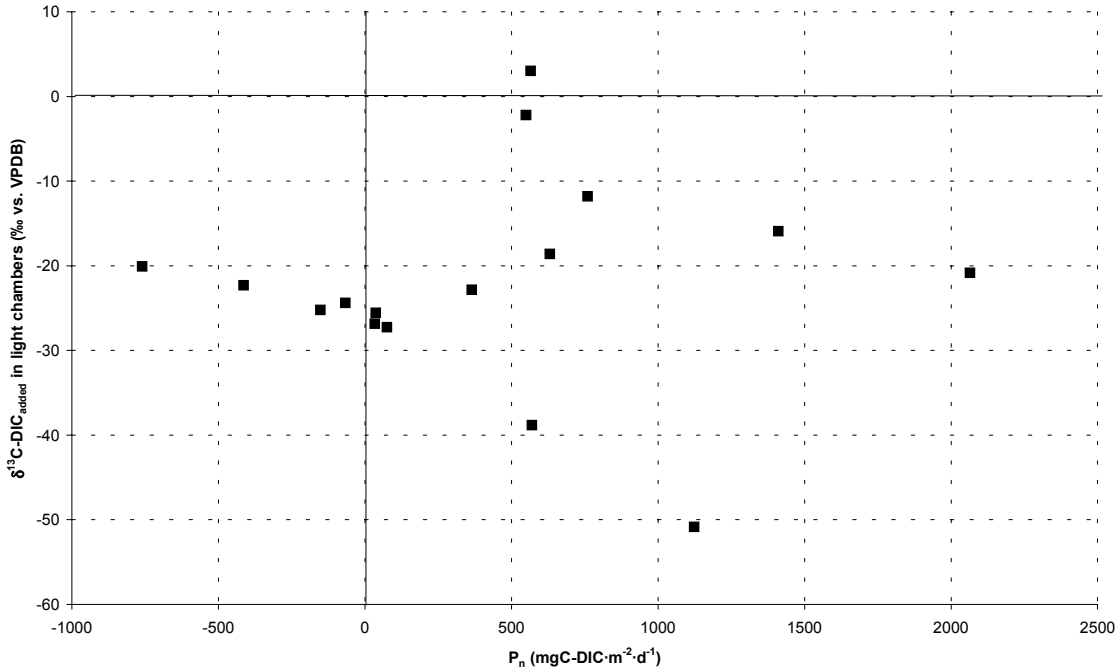

Figure 13 Benthic net photosynthesis (P_n) and the $\delta^{13}C\text{-}DIC_{added}$ to light chambers in FLUDEX reservoirs from 30-May to 22-September-2000.

Concentration data from C. Matthews (unpubl. data). One point (530, -72‰) is not shown so that the $\delta^{13}C\text{-}DIC_{photo}$ scale is not dominated by that point.

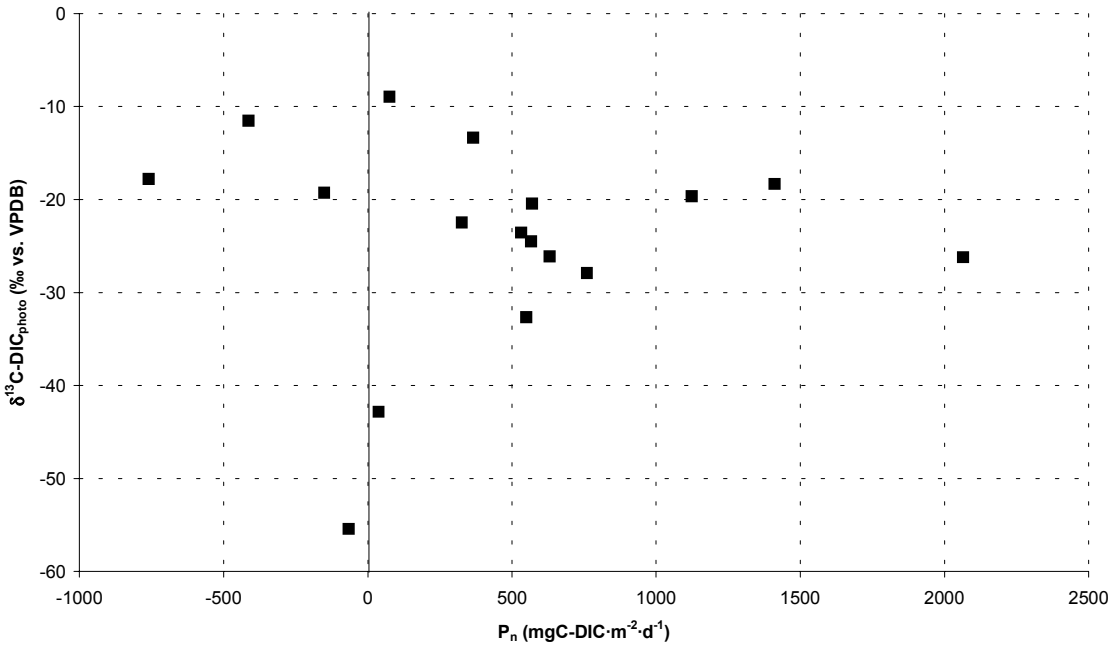

Figure 14 Benthic net photosynthesis (P_n) and the δ^{13}C-DIC_{photo} in light chambers in FLUDEX reservoirs from 30-May to 22-September-2000.

Concentration data from C. Matthews (unpubl. data). Two points (240, -152‰; 30, +41‰) are not shown so that the δ^{13}C-DIC_{photo} scale is not dominated by those points.

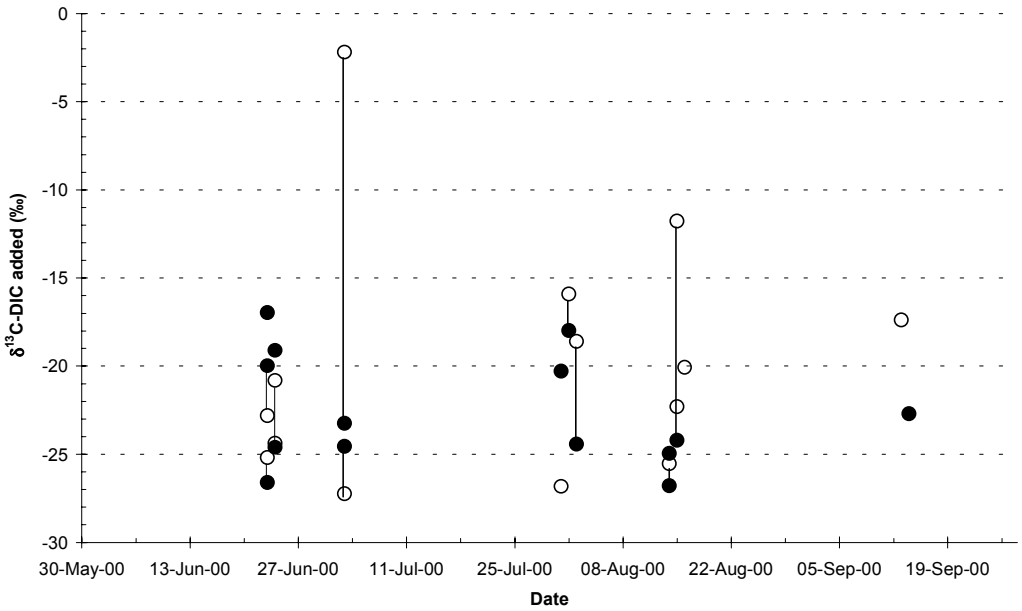

Figure 15 Benthic δ^{13}C-DIC values of the DIC flux from the soil to the water column from light (open circles) and dark (closed circles) benthic chambers in FLUDEX reservoirs from 30-May to 22-September-2000.

Data from side-by-side light and dark chambers are paired by a vertical line.

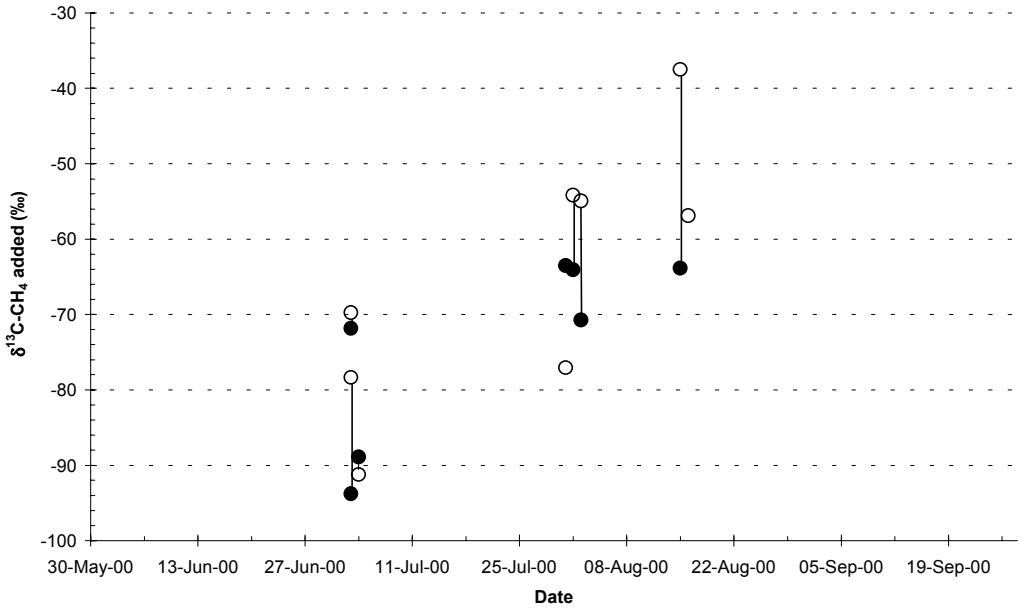

Figure 16 Benthic $\delta^{13}C$-CH_4 values of the CH_4 flux from the soil to the water column from light (open circles) and dark (closed circles) benthic chambers in FLUDEX reservoirs from 30-May to 22-September-2000.

Data from side-by-side light and dark chambers are paired by a vertical line.

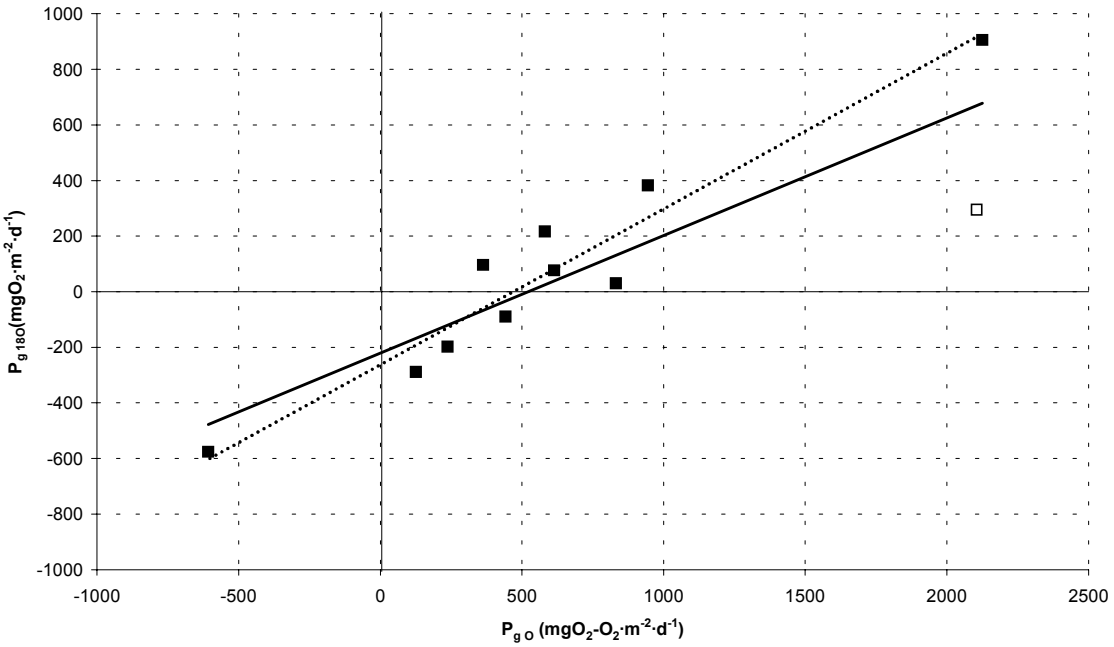

Figure 17 Benthic chamber gross productivity determined by O_2 concentration and $\delta^{18}O$-O_2 methods (see Table 4) from 30-May to 22-September-2000 in FLUDEX reservoirs.

Two lines of best fit are shown. The solid line (slope=0.42, r^2=0.77) includes all points on the graph. The dotted line (slope=0.55, r^2=0.92) does not include the point represented by the open square.

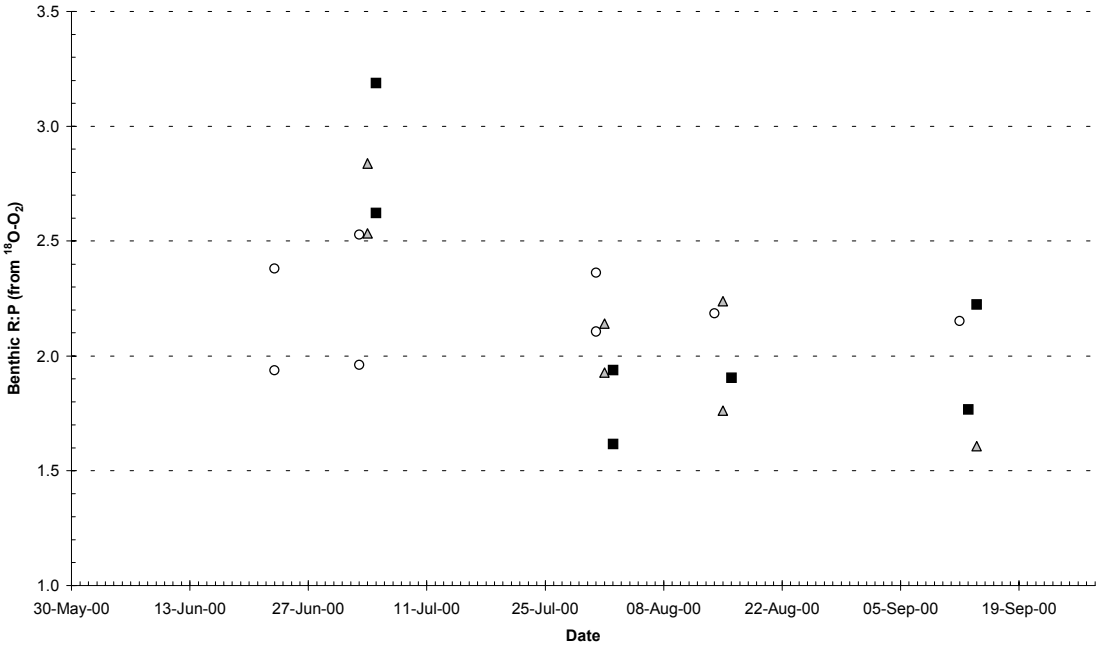

Figure 18 Benthic chamber R_c:P_g (calculated with Equation 5) from $\delta^{18}O$-O_2 for FLUDEX reservoir 1 (circle) 2 (triangle) and 3 (square) from 30-May to 22-September-2000.

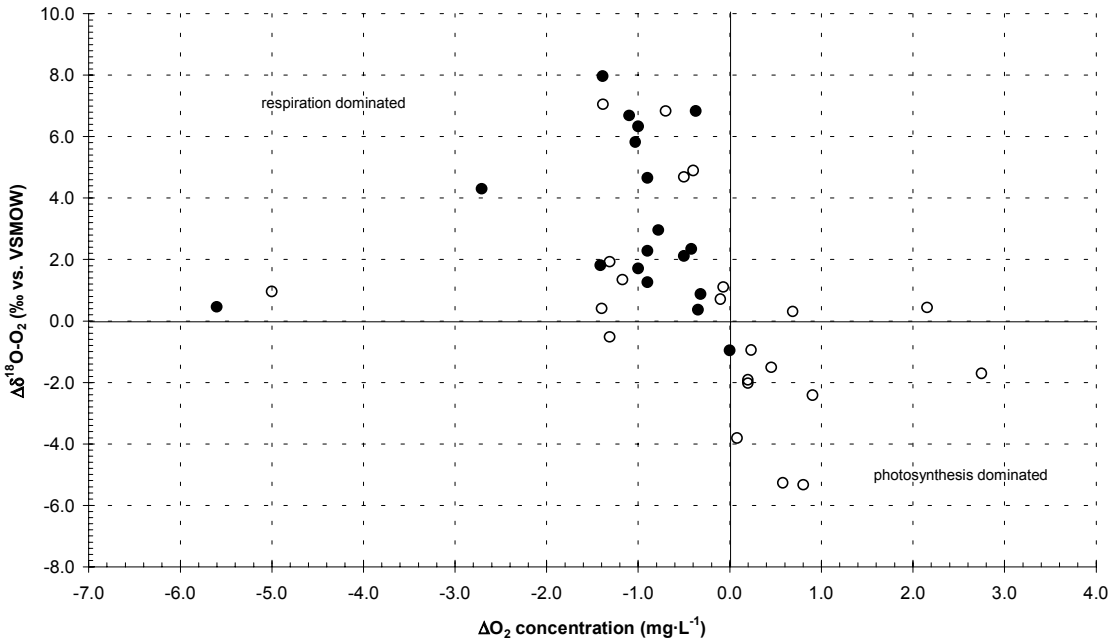

Figure 19 Benthic O_2 concentration and $\delta^{18}O$-O_2 dynamics for light (open) and dark (closed) benthic chambers in FLUDEX reservoirs from 30-May to 22-September-2000.

Note that axes are change in O_2 concentration and change in $\delta^{18}O$-O_2 during the 4-5 hours the chambers were deployed. Areas where respiration dominates and where photosynthesis dominates are shown; see Figure 10.

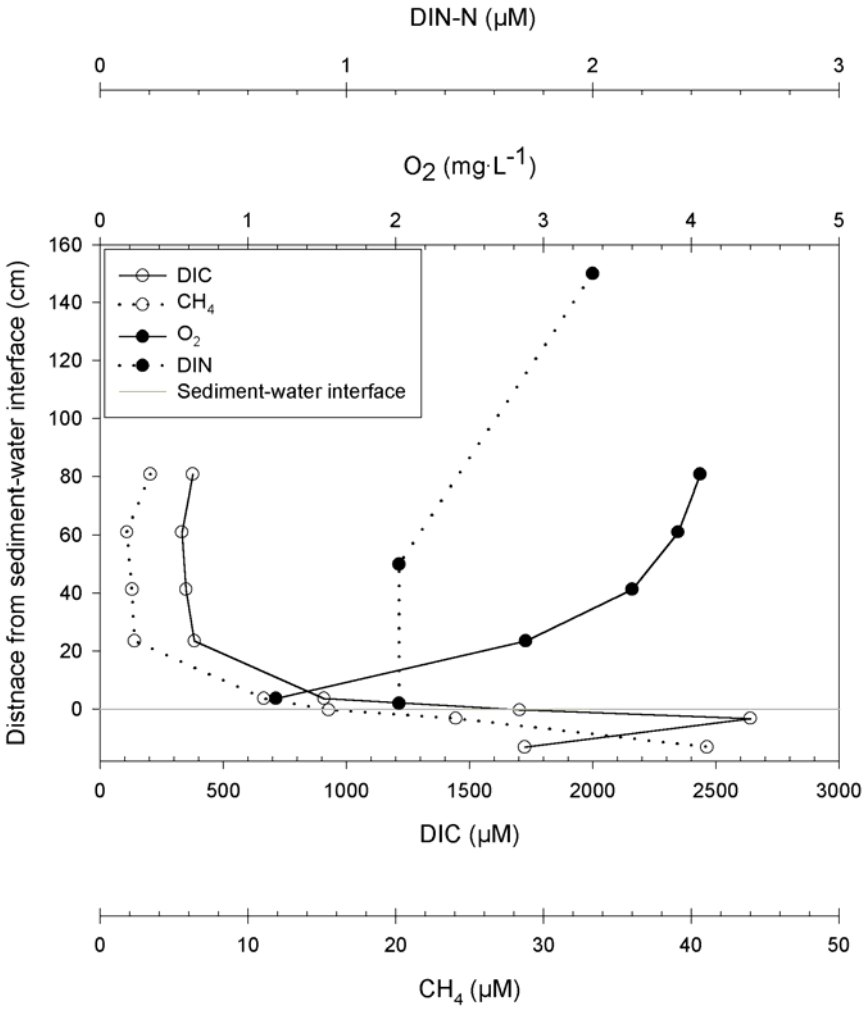

Figure 20 Water column and sediment concentration profile of DIC, CH_4 and O_2 in reservoir 2 at sampling site 5.

Water depth is 80 cm. DIC, CH_4 and O_2 samples were collected during the morning of 11-July-2000. DIN samples were collected at raft A, 10 m south of sampling site 5. Water depth at raft A is 1.5 m. DIN samples were collected during the morning of 16-July-2000 (RA Bodaly, unpubl. data).

Chapter 5: Processes affecting greenhouse gas production in three experimental boreal reservoirs: a stable carbon isotope mass balance approach

5.1 Introduction

Forested landscapes are carbon sinks or are carbon neutral relative to the atmosphere. Flooding of forested landscapes for reservoir development changes the ecosystem carbon cycle so that the newly constructed reservoir becomes a carbon source to the atmosphere. Flooding shifts the carbon balance so that the newly constructed reservoir is a carbon source to the atmosphere.

Two of the main dissolved carbon pools involved in the carbon cycle of reservoirs are DIC and CH_4. Construction of DIC and CH_4 mass budgets can aid in identifying important sources and sinks of carbon in the reservoirs. Performing a mass balance can identify missing or unsampled sources and sinks. However mass balances contain sources net measurements and thus do not identify the processes that contribute overall net values. For example, two competing process such as decomposition of organic matter producing CO_2 and primary production consuming CO_2 are not identified by a net measurement. Only the net change in CO_2 can be evaluated in benthic chamber experiments or on the reservoir level.

Stable carbon isotopes can separate the processes affecting DIC and CH_4 within the reservoirs. Competing processes can be separated by a stable carbon isotope mass budget where a mass budget only provides information about the net sum of many processes. Isotope fractionation during each process will alter the stable isotope value of the carbon pool. Further, stable carbon isotopes can be used to constrain certain processes by knowing isotope fractionation factors. Isotope-mass budgets of DIC and CH_4 for the three FLUDEX reservoirs are discussed in this chapter.

5.2 Conceptual model

A schematic diagram of the reservoirs (Figure 21) shows the inputs and outputs that need to be evaluated in a carbon cycling study in the reservoirs. Major inputs of DIC to the reservoirs are from inflow and overland flow. Water pumped from Roddy Lake (ultra-oligotrophic, low DOM, low Hg) is the majority of the inflow to the FLUDEX reservoirs. Overland flow enters the reservoirs from an upslope catchment, contributing 12%, 2% and 0.1% of the total water input to reservoirs 1, 2 and 3, respectively (Beaty 2001). Precipitation is ≤4% of total water inputs.

In the reservoirs DIC and CH_4 is generated by organic carbon decomposition that causes a flux of DIC and CH_4 across the SWI into the water column. When soil porewater concentrations of DIC and CH_4 are high, bubbles will be formed and trapped until their buoyancy is greater than the soil matrix that confines them. Some DIC will be fixed by photoautotrophs.

Outputs of DIC and CH_4 from the reservoirs are via gas exchange, outflow, wall seepage and fracture seepage. Gas exchange between the water column and atmosphere will cause a net flux of CO_2 and CH_4 from the reservoir. Wall seepage accounts for 16-19% of the water budget output from the reservoirs (Beaty 2001). Outflow via the V-notch weir accounts for 81% and 79% of the water budget outflow in reservoirs 1 and 2, respectively. In reservoir 3, V-notch weir outflow and fracture seepage each account for 40% of the water budget outflow. Water loss via evaporation is <2% in each reservoir.

Components of isotope-mass balance and expected values

Inflow from Roddy Lake is at atmospheric equilibrium concentration with respect to DIC (~125 μM) and CH_4 (~0.1 μM) (Joyce 2001). Boudreau (2000) found that the δ^{13}C-DIC of inflow from Roddy Lake was –7 to –5‰. Input from overland flow will exhibit characteristics of soil porewater such that the DIC concentration will be high because of decomposition of soil organic carbon and the δ^{13}C-DIC value should be similar to soil organic carbon (see below). Overland flow is expected to contain little CH_4 because there are no permanently water-logged soils in the catchments of the FLUDEX reservoirs.

Benthic chambers were deployed to determine the mass and stable carbon isotope flux of DIC and CH_4 across the SWI into the water column (Chapter 4:). Benthic processes measured by the chambers include decomposition of organic carbon to CO_2, CH_4 production and oxidation, and primary production consuming CO_2. All of these benthic processes isotopically fractionate carbon by different amounts. Laboratory incubations indicate that during the early part of dry forest soil decomposition the CO_2 produced is enriched relative to the source material ($\varepsilon_{CO2\text{-}soil}$=+2 to +5‰). Profiles of dry soils indicate an isotopic enrichment of soil carbon with depth approximately from–28 to –26‰ (Boudreau 2000). In moist, *Sphagnum* dominated soils little isotopic fractionation during the early part of soil decomposition has been observed. Soil profiles of *Sphagnum* dominated soils show bulk values of -27 to -25‰. The expected range of δ^{13}C-DIC flux values across the SWI into the water column is -26 to -21‰ if there is no fractionation by benthic photoautotrophs. The expected range of δ^{13}C-DIC flux values with benthic photoautotrophy is several permil enriched relative to without benthic photoautotrophy.

The CH_4 production pathways can be determined by the δ^{13}C-CH_4 values of the CH_4 flux across the SWI into the water column. The δ^{13}C-CH_4 values of CH_4 produced via acetate fermentation (-35‰>ε>-25‰) are different from CH_4 produced via CO_2 reduction (ε>-55‰) (Whiticar 1999). CH_4 produced via acetate fermentation should have δ^{13}C-CH_4 values between –60 and -50‰ since the source acetate should have a δ^{13}C-acetate value similar to δ^{13}C-DOC (-25‰; Boudreau 2000). Ferguson (2001) found that rapid leaching of dry forest soil produced δ^{13}C-DOC values enriched relative to the soil organic carbon ($\varepsilon_{DOC\text{-}SOC}$>0‰). The δ^{13}C-DOC values of DOC leached from dry forest soils after lengthy or repeated wetting is not known. CH_4 produced via CO_2 reduction will be more depleted relative to the CH_4 produced via acetate fermentation. Boudreau (2000) observed reservoir outflow δ^{13}C-DIC values no more enriched than -15‰. When corrected for DIC species fractionation and the enrichment factor is applied, expected δ^{13}C-CH_4 values are <-74‰ for CH_4 produced via CO_2 reduction.

CH_4 oxidation is not identified directly as a component of the mass balance; it is one of the components that affect the net CH_4 flux across the SWI into the water column. The δ^{13}C-CH_4 values of the CH_4 flux across the SWI into the water column are enriched when CH_4

oxidation occurs. The fraction of CH_4 that is oxidized and the initial $\delta^{13}C$-CH_4 values control the $\delta^{13}C$-CH_4 values of the CH_4 flux across the SWI into the water column, i.e. the greater the fraction that is oxidized the more enriched the $\delta^{13}C$-CH_4 values. If the initial $\delta^{13}C$-CH_4 values and the isotope fractionation factor are known, the fraction of CH_4 oxidized can be calculated.

Biofilm on trees and reservoir walls accumulates and cycles carbon with the water column. Periphytic algae in the biofilm isotopically fractionate carbon ($\varepsilon_{CO2\text{-}biomass} \approx -19‰$) during photosynthesis (Hecky & Hesslein 1995) when carbon is not limiting. When carbon is limiting, the net isotopic fractionation decreases ($-19‰ < \varepsilon_{CO2\text{-}biomass} < 0‰$). Using Boudreau's (2000) $\delta^{13}C$-DIC range and correcting for DIC species fractionation and applying the photosynthesis enrichment factor, expected $\delta^{13}C$-bulk values of periphytic algae are -43 to -38‰ when carbon is not limiting. When carbon is limiting the expected $\delta^{13}C$-bulk values of periphytic algae will be enriched relative to the -43 to -38‰ range.

Gas exchange with the atmosphere is an output of CO_2 and CH_4 from the reservoirs. CH_4 does not isotopically fractionate much when moving from a dissolved species to the atmosphere. The CO_2 flux to the atmosphere is isotopically different from the DIC; there are temperature-controlled fractionations between the species that comprise DIC and from dissolved to gaseous species. The relative quantity of each of the DIC species is controlled by pH. At pH values relevant to the FLUDEX reservoirs (pH<7) there are two important fractionation factors. First, $CO_{2(aq)}$ is depleted relative to HCO_3^- ($\varepsilon_{CO2\text{-}HCO3} = -8.5‰$ at 20ºC). Second, $CO_{2(g)}$ is enriched relative to $CO_{2(aq)}$ ($\varepsilon_{CO2(aq)\text{-}CO2(g)} = +1.1‰$ at 20ºC) (Clark & Fritz 1997).

Water is lost from the reservoirs via wall and fracture seepage, and outflow. Wall and fracture seepage water are expected to originate from the lower portion of the water column but likely short-circuits the soil because of the large volume of water lost. So wall and fracture seepage is expected to have DIC and CH_4 concentrations and $\delta^{13}C$-DIC and $\delta^{13}CH_4$ values similar to reservoir bottom water. The reservoir processes control the concentration and $\delta^{13}C$ values of DIC and CH_4 leaving via the outflow. Input of DIC and CH_4 from decomposition of organic matter will increase the DIC and CH_4 concentration in the water column and thus the outflow concentrations will be greater than the inflow concentration. Additionally, the

δ^{13}C-DIC of the outflow will be depleted relative to the inflow because the input of DIC from decomposition is depleted relative to the δ^{13}C-DIC of the inflow. Gas exchange will reduce the water column concentrations of DIC and CH_4 but Joyce (2001) and Boudreau (2000) found that outflow concentrations were greater than that of the inflow and δ^{13}C values were depleted relative to the inflow.

5.3 Methods

Field Methods

Inflow to the reservoirs was collected on three consecutive days per fortnight for DIC and CH_4 concentration and weekly for δ^{13}C-DIC and DOM analyses. DIC and CH_4 concentrations were measured by C. Matthews (unpubl. data). Inflow CH_4 concentrations were not sufficient for δ^{13}C-CH_4 analysis. Samples collected from each of the three inflow ports per reservoir indicated that dissolved gas concentrations were within analytical precision, so samples from the middle inflow to reservoir 3 were taken to represent the water inflow to all reservoirs.

Reservoir outflows were sampled on three consecutive days per fortnight for DIC and CH_4 concentration and weekly for δ^{13}C-DIC and δ^{13}C-CH_4 analyses from just inside the outflow V-notch weir in reservoirs 1 and 3, and for reservoir 2, 2 m upstream of the V-notch weir in the outflow creek. DIC and CH_4 concentrations were measured by C. Matthews (unpubl. data). Samples for DOM isotope analysis were taken every three weeks from these locations.

There are no defined inflow creeks or ephemeral overland flow channels into the reservoirs. The ephemeral L114 inflow creek was sampled as a proxy for overland flow into the reservoirs. The L114 inflow creek drains a forested and exposed bedrock catchment that was logged in the 1970s, a few years before the FLUDEX reservoir site was logged. Both sites were extensively burned in 1980. The catchment does not contain wetland soils (K. Beaty pers. comm.). Twice in July and once in August, when large rain events caused the L114 inflow creek to flow, samples for DIC, CH_4, δ^{13}C-DIC, δ^{13}C-CH_4 and DOM analyses were collected from the V-notch weir of the creek.

Inside each reservoir, water samples were taken fortnightly from the water column (see Table 3) via sippers. A sipper is a series of sampling tubes at approximately every 20 cm above the sediments and approximately every 5-10 cm within the sediments. Samples were collected for DIC, CH_4, $\delta^{13}C$-DIC and $\delta^{13}C$-CH_4 analyses.

Gas exchange between the reservoir surfaces and the atmosphere (or surface flux) depends on the gas flux coefficient and the concentration gradient between the dissolved CO_2 or CH_4 in the reservoir and the concentration in the atmosphere. Eight separate additions of SF_6 (e.g. Wanninkhof et al. 1985; Cole and Caraco 1998) indicate that the gas flux coefficients are similar over the flooding season (C. Matthews, unpubl. data). This coefficient can be converted to a coefficient for other gases (e.g. CO_2 and CH_4) via the ratio of the Schmidt numbers (Wanninkhof et al. 1985). The gas exchange between the reservoir surfaces and the atmosphere is then calculated with the gas-specific coefficients and the concentration gradient between the dissolved gases and the atmosphere.

Benthic flux was assessed fortnightly at each of five sampling sites within each reservoir by a fitting a 9 L polycarbonate chamber into a collar that was inserted into the soil prior to flooding. A small (approximately 10 cm across) propeller, driven by a 9 V motor (Efston Science, Toronto) at 12 revolutions per minute, ensured mixing of water trapped inside the chamber. The chamber was sampled via a length of Tygon ($^1/_8$ x $^1/_4$ x $^1/_{16}$, R-3603) tubing attached to the chamber and held afloat by a small buoy. Initial and final samples for DIC, CH_4, $\delta^{13}C$-DIC and $\delta^{13}C$-CH_4 analyses were taken initially and approximately six hours later. DIC and CH_4 concentrations were measured by C. Matthews (unpubl. data). At two sampling sites per reservoir a second submerged chamber, blackened to prevent light penetration, was deployed to determine flux not influenced by primary production.

Beaty (2001) estimated wall seepage by two different methods. First, all water flowing from the reservoirs is channelled and discharge is measured though a weir. Second, during maintenance to the inflow pump when there is no inflow, the outflow V-notch weirs are blocked and the decline in head is an estimate of wall seepage.

Water is lost from reservoir 3 via one or more bedrock fractures. An estimate of the rate of loss of water from the reservoir has been made by gauging the discharge of the known

egress of the fracture when it is at steady-state flow (Beaty 2001). The egress is outside of the reservoir and downslope approximately 30 m from the wall of reservoir 3.

At the end of the flooding season, 115 days from the start of inflow in 2000, the reservoirs were drained of water. The DIC and CH_4 contained in the standing water are estimated by the water column concentration and stable isotope profiles 2-4 days before the end of the flooding season. Combining the water level to water volume relationship (i.e. stage-discharge curve) with water column concentration and stable isotope profiles produces a mass and mass-weighted isotope value for each reservoir.

Biofilm is an agglomeration of algae, bacteria and associated organisms that covers most of the submerged surfaces in the reservoir. Biomass growth was estimated by biomass accumulation on vertical pine dowels. Ten dowels (pine, 0.25", 20 cm) were hung at each of five sites in each reservoir. Dowels were either harvested in 5 cm segments for productivity experiments using P_{CO2} or stripped of biofilm and redeployed. Biofilm from the stripped dowel was subsampled for nutrient, chlorophyll, species composition and biomass estimates (M. Paterson & D. Findlay, unpubl. data). Carbon accumulation was estimated based on standing stock and laboratory primary production incubations. Samples of biofilm grown for one month were analyzed for δ^{13}C-bulk values. The short time span (one month) samples were used to produce samples with reduced detritus and associated growth such as bacteria in order to give a better estimate of periphytic algae. The biofilm was concentrated by vacuum filtering the samples onto pre-combusted (550°C, 6 hours) GF/F filters (Whatman 0.7 μm nominal pore size) for δ^{13}C-bulk, δ^{15}N-bulk and C:N analyses.

Phytoplankton biomass estimates were performed weekly through June and July, then bi-weekly until the end of flooding. Samples from multiple locations were combined to produce an integrated sample. Phytoplankton samples were incubated for determination of productivity using P_{CO2} (D. Findlay, unpubl. data).

Bubble traps, inverted floating funnels (12" diameter), were sampled fortnightly to determine total ebullitive loss by volume from the reservoirs. One bubble trap was deployed at each of the five sampling sites within each reservoir. Samples of freshly disturbed bubbles

from the soil were collected for CO_2 and CH_4 concentration and $\delta^{13}C$-CO_2 and $\delta^{13}CH_4$ analyses. CO_2 and CH_4 concentrations were measured by C. Matthews (unpubl. data).

Analysis Methods

Analytical protocols are outlined in Section 3.3. DIC and CH_4 analyses were performed by gas chromatography (Varian 3800, ruthenium [VIII] oxide catalyst, H_2 and Ar gases, FID detector). Carbon concentration data for Roddy Lake inflow, V-notch weir outflow and gas exchange are provided by C. Matthews (unpubl. data). K. Beaty (2001) provides hydrological data. M. Patterson and D. Findlay (unpubl. data) provide periphyton data. D. Findlay (unpubl. data) provides phytoplankton data.

Evaluation of the isotope-mass budget

The mass budget is constructed by determining the mass of each component. In order to balance the budget, the sum of the inputs must equal the sum of the outputs. Combining daily inflow and outflow flow rates with concentration produces a daily mass transfer. The isotope-mass budget is constructed by determining the mass of each component and then mass weighting the isotope values. Inflow and outflow concentration and isotope values are linearly interpolated for days when a direct measurement was not made.

Mass loss through wall seepage is estimated by assuming a constant wall seepage flow rate and applying the average bottom water concentration of the reservoir. The average bottom water concentration was measured fortnightly and is defined as the average of the concentration of water 2 and 20 cm above the SWI. During flooding DIC concentrations at 2 cm above the SWI were 100-300% greater than those at 20 cm above the SWI. The difference between CH_4concentration at 2 cm and 20 cm above the SWI increases from 200% to 1400% during flooding. The same average bottom water concentration of reservoir 3 was applied to a constant flow of water lost to fracture seepage.

The benthic flux across the SWI to the water column is estimated by linear interpolation for the time between sampling. In reservoirs 1 and 3, where there are two soil community types, submerged chamber data is weighted by the area of each soil community

type; DIC and CH_4 flux ranges are different for the different soil types. Daytime and nighttime benthic fluxes across the SWI to the water column are estimated by time weighing the submerged chamber data of light and dark chambers, respectively.

The mass loss of gas exchange between the water column and the atmosphere is estimated by applying gas flux coefficients, determined fortnightly, with average of surface concentrations measured thrice daily for three days during the fortnight (C. Matthews, unpubl data).

Carbon accumulation by periphyton and phytoplankton is estimated by D. Findlay (unpubl. data). Periphyton is estimated by the accumulation of biomass on pine dowels several times over the flooded season. Phytoplankton is estimated by density estimates of phytoplankton in reservoir water.

Change in storage is estimated by volume weighting the water column concentration profile by the storage-discharge curve for each reservoir. Water column concentrations from 2-4 days before drawdown are used.

Mass of ebullitive flux from the soil to the atmosphere is estimated by the fortnightly flux measured in bubble traps.

The benthic flux portion of the isotope-mass budget can be broken down into two competing SWI processes: decomposition and photosynthesis. By rearranging the isotope-mass balance equation the mass and δ^{13}C-DIC values of decomposition and photosynthesis can be calculated (Equations 8 and 9). However, decomposition and photosynthesis also occur in the water column and within biofilm so their contribution must be removed from outputs and included in the total photosynthesis.

5.4 Results

Inflows and Outflow

DIC concentration in inflow (Roddy Lake) remains steady (124-140 μM) but δ^{13}C-DIC values shift from -13.5 to -5.5‰. Since inflow to all reservoirs was identical, only the inflow

rate differed, the mass of DIC in inflow is directly related to inflow rate; 143, 108 and 168 kgC-DIC with δ^{13}C-DIC values of –8.7, -8.7 and –8.8‰ (Table 11) were added to reservoirs 1, 2 and 3, respectively.

The L114 inflow creek was used to estimate the DIC concentration, δ^{13}C-DIC value and the northwest inflow to L239 was used to estimate the water volume yield of overland flow to all reservoirs. Inflow from ungauged runoff was sampled from L114 inflow following large (>20 mm) rain events. DIC concentration was similar on three events sampled (725-760 μM); δ^{13}C-DIC averaged -25.7‰. The volume of overland flow was estimated by Beaty (2001) and an isotope-mass estimate was calculated by using an average of three concentrations and two isotope values. L114 inflow creek DIC concentration was within 3% of reservoir 1 overland flow concentration measured on 24-July-2000. L114 inflow creek δ^{13}C-DIC values were within 2‰ on 07-July-2000 and 21-August-2000. Few samples from L114 inflow creek were collected because the creek only flows after large (>20 mm) rain events when antecedent conditions are favourable (approximately 10 mm of precipitation stored). The relative contribution of DIC from reservoir catchments varies because catchment size varies (Table 1). Overland flow contributed 15% (102 kgC-DIC), 3% (15 kgC-DIC) and <0.1% (1 kgC-DIC) to reservoirs 1, 2 and 3, respectively of the total inputs to the reservoirs (Table 11).

Outflow DIC concentrations peak in mid-July (Figure 22). Reservoir 2 outflow shows the greatest decline in concentration (398 to 188μM); reservoir 3 outflow concentration remains lowest (circa 200-300 μM); reservoir 1 outflow concentration remains higher (circa 300-400 μM) than that of the others. Outflow δ^{13}C-DIC values generally enrich during the flood season (Figure 22). The mass of DIC from reservoir outflow was markedly different in the reservoirs: 300, 183 and 123 kgC-DIC from reservoirs 1, 2 and 3, respectively (Table 11). The mass weighted δ^{13}C-DIC value of the DIC of reservoir outflow is more depleted where mass of DIC from outflow is greater; δ^{13}C-DIC of outflow is –17.9, -15.5 and –14.9‰ for reservoirs 1, 2 and 3, respectively (Table 11).

Outflow DIC concentrations are greater than that of the inflow indicating that DIC is produced in the reservoirs; the δ^{13}C-DIC value of outflows is depleted relative to that of the

inflow. This indicates that DIC is produced in the reservoirs and the source is isotopically depleted relative to inflow. The source is likely decomposition of soil organic matter.

Inflow CH_4 concentration from Roddy Lake was very low, <0.2 μM. L114 inflow creek CH_4 concentration was also very low, <0.1 μM. The contribution of inflow CH_4 to the mass budget is very small (<1%) relative to the input from the benthic flux across the SWI (Table 11).

Outflow CH_4 concentrations peak during mid-August 2000. Reservoir 2 and 3 outflow concentrations peak in mid-August and decline one-quarter to one-third thereafter (Figure 23). Reservoir 1 outflow sustains a greater CH_4 concentration than the other reservoirs (Figure 23). During 1999 (Joyce 2001) and 2000, outflow CH_4 concentration shows a general 1>2>3 trend.

Outflow $\delta^{13}C$-CH_4 values exhibit different trends in 1999 and 2000. In 1999, outflow $\delta^{13}C$-CH_4 values remain depleted (–89.3 to –65.9‰) throughout the flooded season (Boudreau 2000). In 2000, outflow $\delta^{13}C$-CH_4 values show an enrichment trend during the entire flooding season (-99.4 to –35.9‰). Outflow $\delta^{13}C$-CH_4 values are similar in 1999 and 2000, until approximately early August when outflow $\delta^{13}C$-CH_4 values from 2000 become more enriched. Reservoir 1 outflow $\delta^{13}C$-CH_4 values are more enriched than those of reservoir 2. Reservoir 3 outflow $\delta^{13}C$-CH_4 values enrich more than those of the other reservoirs (Figure 23).

The mass of CH_4 in the outflow of reservoirs 1, 2 and 3 is: 3.2, 2.3 and 1.1 kgC-CH_4, respectively (Table 11). The loss of CH_4 via outflow is less than 40% of the total CH_4 output (Table 11). The mass weighted stable isotope values indicate a different trend. The $\delta^{13}C$-CH_4 value of the reservoir 2 outflow is approximately 10‰ more depleted than that of reservoirs 1 and 3. Mass weighted $\delta^{13}C$-CH_4 values of outflow are –53.9, -64.8 and -56.2‰ for reservoirs 1, 2 and 3, respectively (Table 11).

Outflow CH_4 concentrations are more than one order of magnitude greater than that of the inflow indicating that CH_4 is produced in the reservoirs. The seasonal enrichment in outflow $\delta^{13}C$-CH_4 values indicates that there are multiple processes involving CH_4 in the reservoirs. Two processes, acetate fermentation and CO_2 reduction produce CH_4. Each process produces CH_4 with a distinct range of $\delta^{13}C$-CH_4 values. A third process, CH_4

oxidation, enriches the δ^{13}C-CH_4 value of the residual pool of CH_4. A combination of these processes can produce CH_4 with the range of outflow δ^{13}C-CH_4 values.

Benthic flux estimated from chambers

DIC flux from flooded soils is highly variable within and between reservoirs (Figure 24). Dark benthic DIC flux ranges from –95 to 2900 mgC-DIC·m^{-2}·d^{-1}. Light benthic DIC flux ranges from –320 to 2400 mgC-DIC·m^{-2}·d^{-1}. There is no seasonal change in benthic DIC flux in any of the reservoirs. The DIC flux across the SWI is immediate and is sustained during the flooded season. This input of DIC to the reservoirs is important because the range of per day flux values is of the same order of magnitude as the loss of DIC via the outflow.

Calculated ranges of δ^{13}C-DIC values of benthic flux, in dark chambers, enriches during the 2000 flood season from –31‰ to –25‰ before early July and –24‰ to –18‰ from mid July to end of flooding (Table 6 and Figure 15). Light benthic chamber δ^{13}C-DIC values added to the chamber range from –2 to –26‰ (Table 6 and Figure 15). The δ^{13}C-DIC values of dark chamber benthic flux are more depleted than the outflow. The δ^{13}C-DIC values of DIC added to light chamber is more enriched than that added to dark chambers. This indicates that the processes occurring in the chambers are different. Photosynthesis, which is light dependent, isotopically enriches the δ^{13}C-DIC values of the residual DIC pool. The magnitude of the DIC flux indicates that it is an important input of DIC to the reservoir water column and thus the δ^{13}C-DIC value of that flux is important for the isotope-mass budget. The variability of the benthic DIC flux and the δ^{13}C-DIC values added to chambers is evident in Figure 15 and Figure 24 so one value cannot be assigned to this flux.

The mass and mass weighted isotope value of DIC added to the reservoirs from the sediment to the water column is similar in reservoirs 1 and 2; 412 (-17.4‰) and 419 kgC-DIC (-16.8‰), respectively (Table 14). The mass added to reservoir 3 is smaller and more depleted than the other reservoirs, 287 kgC-DIC and more depleted, -19.2‰ (Table 14).

The range of benthic CH_4 flux rates increases from the beginning of flooding (1 to 29 mgC-CH_4·m^{-2}·d^{-1}) to the end of flooding (–61 to 190 mgC-CH_4·m^{-2}·d^{-1}). Calculated δ^{13}C-CH_4 values of the CH_4 flux into dark chambers ranges from -90 to -64‰, becoming

seasonally enriched. Calculated $\delta^{13}C\text{-}CH_4$ values of the CH_4 flux into light chambers exhibit a larger range, from –94 to –34‰. The $\delta^{13}C\text{-}CH_4$ of the benthic CH_4 flux is more enriched than –70‰ from the end of July to the end of flooding.

The mass of CH_4 added to reservoir 2 from the sediment to the water column is greatest and isotopically most enriched, 47.4 kgC-CH_4 and –40.8‰ (Table 12). Reservoirs 1 and 3 have similar mass and isotope values, 16.6 (-64.4‰) and 15.8 kgC-CH_4 (-54.2‰), respectively.

Unlike the DIC flux across the SWI, the CH_4 flux across the SWI begins small and grows during the flooded season. This input of CH_4 to the reservoirs is very important because the range of per day flux values is generally one order of magnitude greater than the loss of CH_4 via the outflow.

The $\delta^{13}C\text{-}CH_4$ values of benthic flux, though enriching with time, are neither generally more enriched nor generally more depleted than the $\delta^{13}C\text{-}CH_4$ values of reservoir outflow. The magnitude of the CH_4 flux indicates that it is a very important input of CH_4 to the reservoir water column and the range of the $\delta^{13}C\text{-}CH_4$ values added to the chambers indicate that the $\delta^{13}C\text{-}CH_4$ value of that flux controls the inputs for the isotope-mass budget. The variability of the benthic CH_4 flux and the $\delta^{13}C\text{-}CH_4$ values added to chambers is evident in Figure 16 and Figure 25 so one value cannot be assigned to this flux.

Gas exchange

Gas exchange from reservoirs 2 and 3 peaks mid- to end of July at 535 and 495 mgC-DIC$\cdot m^{-2}\cdot d^{-1}$ respectively, and drops thereafter. Gas exchange from reservoir 1 peaks in mid-August 2000 at 598 mgC-DIC$\cdot m^{-2}\cdot d^{-1}$, but remains higher than the other reservoirs thereafter because of higher DIC concentration and lower pH (RA Bodaly, unpubl. data) than the other reservoirs.

Isotope values of $\delta^{13}C\text{-}CO_2$ gas exchange with the surface of the reservoirs and the atmosphere depends on processes occurring in the reservoirs. The water column and surface $\delta^{13}C$-DIC values are controlled by input from inflow, overland flow and benthic flux and output from outflow, seepage and primary production. Calculating the $\delta^{13}C\text{-}CO_2$ value of the

gas exchange is a function of pH and temperature since the distribution of DIC species is controlled by pH and isotopic fractionation between species varies with temperature (Clark and Fritz 1998). When adjusted for pH and isotopic fractionation, surface $\delta^{13}C\text{-}CO_2$ values range from -27 to -15‰. Maximum flux from all reservoirs occurs with $\delta^{13}C\text{-}CO_2$ values of -23 to -18‰.

The mass of CO_2 lost via gas exchange is similar to the mass of DIC lost via the outflow, 300, 183 and 123 $kgC\text{-}CO_2$ for reservoirs 1, 2 and 3, respectively (Table 11). This is a very important loss from the reservoirs. However, the $\delta^{13}C\text{-}CO_2$ of the CO_2 lost was 3-4‰ depleted relative to the $\delta^{13}C$-DIC of the outflow: -17.9, -15.5 and –14.9‰ for reservoirs 1, 2 and 3, respectively (Table 11). The reservoirs lose CO_2 depleted relative to the bulk DIC in the water column of the reservoirs because of the isotopic fractionation between DIC species and from dissolved species to gaseous species. The $\delta^{13}C\text{-}CO_2$ value of the CO_2 lost via gas exchange enriches the $\delta^{13}C$-DIC value of remaining DIC. This is important for the isotope-mass budget.

CH_4 gas exchange from reservoir 2 rises and stabilizes in mid-August with maxima of 10 $mgC\text{-}CH_4 \cdot m^{-2} \cdot d^{-1}$. Reservoirs 1 and 3 gas exchange peaks in mid-August at 19 and 38 $mgC\text{-}CH_4 \cdot m^{-2} \cdot d^{-1}$ respectively, but declines to 11 and 4 $mgC\text{-}CH_4 \cdot m^{-2} \cdot d^{-1}$ respectively by the end of flooding season. Because water column $\delta^{13}C\text{-}CH_4$ values enrich, outflow $\delta^{13}C\text{-}CH_4$ values and gas exchange $\delta^{13}C\text{-}CH_4$ values enrich (approximately 60‰) over the flooding season.

The mass of CH_4 lost via gas exchange is greater than that lost via outflow, 6.0, 3.1 and 4.8 $kgC\text{-}CH_4$ (Table 12). The $\delta^{13}C\text{-}CH_4$ of the CH_4 lost via gas exchange is similar to that of the outflow in reservoirs 1 and 2, -52.8 and –66.3‰; but is 13‰ enriched relative to the outflow in reservoir 3, -43.1‰. This is a very important CH_4 loss from the reservoirs because the outflows will have less importance to the budget than the gas exchange. The $\delta^{13}C\text{-}CH_4$ values of the gas exchange will be related to the rate and time weighted CH_4 production and consumption processes. The enrichment of the $\delta^{13}C\text{-}CH_4$ values of the gas exchange is large and must be well characterized because the mass loss is so important to the budget.

Wall Seepage

Reservoir water seeped through and under the reservoir walls comprising 16-19% of the total water balance (Beaty 2001). The mass of DIC and CH_4 lost via wall seepage is 8-10% of total DIC output and 7% of total CH_4 output. The δ^{13}C-DIC values of mass weighted wall seepage are within 0.5‰ of outflow values and δ^{13}C-CH_4 values are within 3‰ of outflow values. Wall seepage is similar to outflow in δ^{13}C values and the mass loss is small compared to outflow and gas exchange.

Fracture Seepage

Reservoir 3 is the only reservoir that has fracture seepage. Forty percent of the water budget of reservoir 3 was lost through one or more bedrock fractures. The location of one fracture was discovered in Fall 2000. But after repairs, the egress, down slope and outside of the reservoir, continued to flow at a similar rate during the 2001 flooding season (K. Beaty, pers. comm.) The volume of underground storage is not known and concentration and isotope analyses show that water at the egress has significantly changed from reservoir water column water, bottom water and soil pore water (Venkiteswaran, unpubl. data; Boudreau 2000). The same concentration and stable isotope values applied to wall seepage water are applied to fracture seepage water—the average of the concentration and stable carbon isotope values of water 2 and 20 cm above the SWI.

The mass of DIC lost via fracture seepage is slightly greater than that lost via the outflow, 125 kgC-DIC. Similarly, a greater mass of CH_4 is estimated to be lost via fracture seepage than via the outflow, 1.4 kgC-CH_4. In reservoir 3, relative to wall seepage, the fracture seepage is much more important. The δ^{13}C values are similar to those of the outflow and have similar importance in the budgets and therefore a better understanding of the water lost via fracture seepage is needed so that masses and δ^{13}C values that better reflect the loss can be applied.

Storage

DIC and CH_4 accumulate in the reservoir during flooding. On 22-September-2000 (day 115 of flooding) one or two drain valves in each reservoir were opened to drain the reservoirs.

The DIC and CH_4 in the water column and below the bottom of the outflow V-notch weir is not part of the outflow measurement. The water column DIC and CH_4 added prior to and on 22-September-2000 are included as input via benthic flux and must be considered as an output. The storage of DIC is 6-10% of outflow (outflow plus fracture seepage in reservoir 3) and the storage of CH_4 is 9% of outflow in reservoirs 1 and 2. In reservoir 3 storage is 28% of outflow plus fracture seepage because bottom water concentrations of CH_4 are greater in reservoir 3 than the other reservoirs. The δ^{13}C-DIC of storage is within 3‰ of the outflow. Reservoirs 1 and 3 have δ^{13}C-CH_4 of storage approximately 3-4‰ enriched compared to outflow. Reservoir 2 has storage about 15‰ enriched relative to outflow. With the exception of reservoir 3 CH_4, the mass of DIC and CH_4 storage is similar to that of wall seepage and is small compared to outflow and gas exchange.

Periphyton

Attached algae, and associated communities formed a biofilm that covered much of the surface area of the reservoirs. This includes wall surfaces, trees and shrubs. Algae should exhibit δ^{13}C-bulk values depleted relative to DIC ($\varepsilon_{algae\text{-}CO2}$=-19‰) if the algae are not carbon-limited and a smaller enrichment factor if they are carbon-limited (Hecky & Hesslein 1995). It is unlikely that algae in areas where there is a lot water movement are carbon-limited, but algae in areas with less water movement may be carbon limited due to boundary-layer effects. The δ^{13}C-bulk values of carbon limited algae will be enriched relative to those δ^{13}C-bulk values of algae that are not carbon limited because the enrichment factor is smaller. Bacteria should exhibit a δ^{13}C-bulk approximately equal to δ^{13}C-DOC (≈-25‰) . Samples of biofilm on pine dowels harvested after one month indicate a signal that is a mixture of expected values for algae, bacteria and detritus.

Samples ranged from -32.2 to -31.0‰ on 17-August-2000 and from -37.3 to -29.0‰ on 12-September-2000 (Table 13). Periphyton in August and September should have a δ^{13}C-bulk value of approximately –39 to -34‰ if outflow and water column δ^{13}C-DIC values are corrected for the pH and temperature controlled fractionation factor between the DIC species and a –19‰ enrichment factor is applied to the $CO_{2(g)}$. The biofilm δ^{13}C analysis (Table 13) indicates that bacteria quickly colonize the biofilm and the biofilm accumulates detritus.

Post-flood biofilm is more depleted than that which grew on pine dowels (Table 13). A δ^{13}C-bulk value of –38‰ is applied to periphyton accumulation in the reservoirs. The periphyton accumulation rates for the reservoirs, the pH and temperature controlled DIC species isotope fractionation and photosynthetic fractionation were combined to produce the δ^{13}C-bulk value of -38‰.

Periphytic biomass was highly variable between sampling sites and between reservoirs. Total carbon accumulation was 61, 73 and 36 kgC in reservoirs 1, 2 and 3, respectively. This is 7-14% of the total output of DIC (equation 6, Table 10). This does not include benthic photoautotrophs. This is an underestimate because the total surface area available for growth does not include the formation of 'sheets' between branches and the sloughing of periphyton during sampling reduced the yield from the pine dowels. Some periphytic biomass is lost to sedimentation and decomposition.

The DIC flux from the light and dark benthic chambers includes the effects benthic algal growth, but algae attached surfaces other than the bottom must be assessed by a different method because it is another DIC loss from the water column. It is of the same order of magnitude as wall seepage and storage. Additionally, the algal biomass is depleted relative to the water column DIC and thus is also important in the isotope-mass balance.

Phytoplankton

The estimates of phytoplankton mass are time-weighted means for each reservoir. This is an estimate of the average daily standing stock of plankton over the period (e.g. in reservoir 1 there was an average 0.4 $g \cdot m^{-3} d^{-1}$ and 3.3 kg over the flooded season). The change in the standing stock is the net accumulation of carbon by phytoplankton. In reservoirs 2 and 3 2.3 and 5.2 kgC was accumulated, respectively. Some fraction of this accumulated biomass is lost to decomposition. The same δ^{13}C-bulk value applied to periphyton accumulation was applied to phytoplankton accumulation because phytoplankton are not likely to be carbon-limited because their constant movement through the water column reduces potential formation of a boundary layer. The δ^{13}C-bulk value is based on water column and outflow δ^{13}C-DIC values.

Ebullition

Ebullition is a reservoir effect and a source of GHGs to the atmosphere. It is included in the total mass budget of the reservoirs but not in the mass balance because ebullition bypasses the dissolved phase in the water column. Ebullition can, however, provide information about soil decomposition processes.

The mass of CO_2 lost via ebullition was <1% of outflow or gas exchange. $\delta^{13}C\text{-}CO_2$ values of ebullitive flux are 2-5‰ enriched relative to gas exchange $\delta^{13}C\text{-}CO_2$ values (Table 11). Ebullition of CO_2 is a very small GHG flux from the reservoir relative to other outputs.

Greater than 90% of the mass of ebullition occurred during the last four weeks of flooding. The mass of CH_4 lost via ebullition was of the same order of magnitude as outputs from the reservoirs: 1.8, 1.2 and 3.6 kgC·CH_4 for reservoirs 1, 2 and 3, respectively (Table 12). The $\delta^{13}C\text{-}CH_4$ values of the ebullitive flux of CH_4 was more enriched than the other outputs by 5-17‰ (Figure 29) but the ebullitive flux is heavily weighted by the flux during the last four weeks. The CH_4 that accumulates in the bubbles is from the residual CH_4 pool that has undergone some oxidation because the $\delta^{13}C\text{-}CH_4$ values are enriched.

5.5 Discussion

Mass Balances

Inflow concentration and intra-reservoir processes and the renewal rate of the water control outflow DIC and CH_4 concentrations. Because renewal rates are different for each reservoir directly comparing outflow concentrations does not give an accurate representation of reservoir processes. Similarly, outflow stable carbon isotope values are the combination of inflow and intra-reservoir processes. For examples, as inflow $\delta^{13}C$-DIC enriches there is a concomitant enrichment of outflow $\delta^{13}C$-DIC. However, only after considering renewal rate and mass-weighting the isotope values can the influence of changing inflow be removed. Stable carbon isotope values are combined with the mass values to determine which processes are not well characterized by the mass budget.

The budgets are comprised of inputs and outputs. Inputs are from Roddy Lake inflow, overland flow and benthic flux across the SWI. Outputs are outflow, gas exchange, wall and fracture seepage, storage, periphyton, phytoplankton and sedimentation from algae. The mass budgets do not balance because the inputs do not equal the outputs.

Inflow δ^{13}C-DIC values from Roddy Lake enrich (Figure 22) from depleted values mixing at vernal turnover. The ephemeral L114 inflow creek drains an approximately 25 year old second growth forest with no wetlands. Dissolved constituents in L114 inflow creek are from leaching, decomposition of vegetation and soils and root respiration. The average L114 inflow creek δ^{13}C-DIC value of -25.7‰ falls within the expected range of values since the early-stages of decomposition of litter (≈-28‰) and FH soil (≈-26‰) exhibits a 2-3‰ enrichment in the produced DIC (Baril 2001; Boudreau 2000; Venkiteswaran, unpubl. data).

Benthic chamber determined flux rates of DIC and CH_4 from the flooded soils into the water column vary within and between reservoirs. Most sites showed no seasonal change in benthic DIC flux or a decline in benthic DIC flux. Generally, benthic flux in light chambers, influenced by benthic photosynthesis, exhibit δ^{13}C-DIC values enriched relative to those of the dark chambers. There is an enrichment of benthic δ^{13}C-DIC values of DIC flux during the flooded season that may be from increased primary productivity (see Chapter 4:) or increased input of DIC from deeper soil layers diffusing upward through the flooded soil (Venkiteswaran, unpubl. data).

Benthic CH_4 flux determined by benthic chambers exhibits a wider variability than benthic DIC flux as flooding progressed. Some sites became larger sources and some sites became larger benthic sinks for CH_4. Analysis of side-by-side light and dark benthic chambers reveals an enriched δ^{13}C-CH_4 flux in the light chamber relative to the dark chamber (see Chapter 4:).

The decomposition of soil organic carbon to DIC and CH_4 is the majority of the mass of DIC and CH_4 added to the reservoirs. The flux across the SWI is the least well known portion of the isotope-mass budget for many reasons: the spatial heterogeneity of soils (Boudreau 2000) and fluxes (Joyce 2001); a small area is sampled to represent a large area (<0.5 m^2 sampled with benthic chambers versus ≥ 5000 m^2 in reservoir area); flux across the

SWI from part of the soil is not measurable with benthic chambers because of rocks and trees; and the action of sampling from benthic chambers may draw soil pore water or water column water into the chambers, skewing the estimated flux values. Benthic DIC flux estimated directly from benthic chamber data underestimates the DIC production required to balance the mass budget by approximately 25% in reservoirs 1 and 3 and overestimates the benthic CH_4 flux by approximately 50% in reservoirs 1 and 3. Reservoir 2 benthic DIC flux is overestimated by 5% and the benthic CH_4 flux is overestimated by eight times.

The δ^{13}C-DIC values of the benthic DIC flux are expected to be –27 to –21‰. Photosynthesis will cause further isotope enrichment of δ^{13}C-DIC values (see Chapter 4:). The δ^{13}C-DIC benthic flux values are more enriched than expected. The benthic chamber determined δ^{13}C-DIC values required to balance the DIC mass and isotope budgets are within the range of expected values but are too enriched to balance the isotope-mass budget (Table 11).

Values for the mass of DIC produced and δ^{13}C-DIC values can be determined in four ways: directly from benthic chambers; assuming the mass from benthic chambers is correct and calculating δ^{13}C-DIC from the isotope-mass balance; assuming the δ^{13}C-DIC values are correct and calculating the mass from the isotope-mass balance; and calculating the mass and δ^{13}C-DIC required to balance. The equations required are summarized in Table 10. Calculated DIC and δ^{13}C-DIC flux values are summarized in Table 14.

The masses of DIC and δ^{13}C-DIC values assigned to the benthic flux do not balance the mass budget or the isotope-mass budget. δ^{13}C-DIC values should be similar between reservoirs because of the common soil type in the reservoirs and the similarity of soil δ^{13}C-bulk values between reservoirs. The moist soil in reservoir 1 also produced δ^{13}C-DIC values within the expected range (-27 to –21‰) for all soils during laboratory incubations (see Chapter 4:). The δ^{13}C-DIC values determined by benthic chambers are too enriched to balance the isotope-mass budget and are more enriched than predicted. If the mass of DIC determined from benthic chambers is correct, the calculated δ^{13}C-DIC values for reservoirs are too varied (7‰) and are at the edge of the expected range (see 5.4) of values. By determining the total mass of DIC produced and δ^{13}C-DIC values from the mass balance and isotope-mass balance the mass

of DIC produced increased by 22%, decreased by 7% and increased by 30% for reservoirs 1, 2 and 3, respectively. The δ^{13}C-DIC values calculated are between –23 and –21‰. The range of these values is smaller than the range of expected values and falls within the expected range of values of DIC produced. The isotope-mass budget can constrain the mass budget by determining process-based values for DIC production that do not suffer from the problems associated with benthic chambers.

Outflow δ^{13}C-CH_4 values enrich more than 60‰ in 2000 (Figure 23). Since there is little CH_4 in the Roddy Lake inflow (<2% of outputs) the outflow δ^{13}C-CH_4 values can be interpreted as representing the CH_4 processes in the reservoirs during the previous 8-10 days, i.e. renewal time. CH_4 exchange with the atmosphere reduces the mass of CH_4 in the reservoir but does not affect the δ^{13}C-CH_4 value of dissolved reservoir CH_4 much. Enriched δ^{13}C-CH_4 values indicate that the CH_4 pool has undergone some CH_4 oxidation (Whiticar 1999). In 1999, Boudreau (2000) did not observe this oxidation and subsequent δ^{13}C-CH_4 enrichment.

The mass of CH_4 production and δ^{13}C-CH_4 values can be calculated in the same four ways as the mass of DIC production and δ^{13}C-DIC values. Calculated CH_4 and δ^{13}C-CH_4 flux values are summarized in Table 15. The benthic flux estimated from benthic chamber data indicates that reservoir 2 had approximately 30% greater benthic CH_4 flux than the other reservoirs. Water column, porewater concentration profiles (Venkiteswaran, unpubl. data) and outflow concentrations (Figure 23) do not indicate this large difference in flux. Further, using the benthic chamber mass to calculate δ^{13}C-CH_4 values produces very enriched δ^{13}C-CH_4 values; so enriched they cannot be balanced against the known outputs. The mass of CH_4 produced must be recalculated via the isotope-mass balance.

If the δ^{13}C-CH_4 values from benthic chambers are used to calculate CH_4 production, the predicted mass of CH_4 is much closer to that which is required to balance the CH_4 budgets. The calculated δ^{13}C-CH_4 values that balance the isotope-mass budgets are between those of the outflow and gas exchange, the two largest outputs of CH_4. So, of the four ways described, recalculating the CH_4 production to balance the isotope-mass budget yields values that fit into the budgets and have δ^{13}C-CH_4 values that fit observations of benthic CH_4 processes (see Chapter 4:).

Importance of CH_4 oxidation to the CH_4 isotope-mass budgets

The amount of CH_4 oxidation can be estimated if the fractionation factor associated with CH_4 oxidation in a given system is known. Whiticar (1999) reports a wide variety of fractionation factors ($\alpha_{CO2\text{-}CH4}$) in the literature; generally >0.990, but some as large as 0.970. Preliminary experiments yield similar fractionation factors for the FLUDEX reservoirs: 0.987±0.001 (mean ± standard deviation, n=8) (Venkiteswaran, unpubl. data). To estimate CH_4 oxidation the $\delta^{13}C\text{-}CH_4$ values of the source and residual (i.e. post-oxidation) CH_4 must be known. The $\delta^{13}C\text{-}CH_4$ values of the dark chamber CH_4 flux and $\delta^{13}C\text{-}CH_4$ values of pore water are the best source of $\delta^{13}C\text{-}CH_4$ values that are close to the source $\delta^{13}C\text{-}CH_4$ in value. Weighting the $\delta^{13}C\text{-}CH_4$ values by the dark chamber CH_4 flux produces unoxidized CH_4 production $\delta^{13}C\text{-}CH_4$ values; the source $\delta^{13}C\text{-}CH_4$ values are 5-10‰ depleted relative to the calculated $\delta^{13}C\text{-}CH_4$ values of CH_4 produced in the reservoirs (Table 15).

Using the outflow $\delta^{13}C\text{-}CH_4$ values and $\delta^{13}C\text{-}CH_4$ values of CH_4 added to light chambers as the oxidized $\delta^{13}C\text{-}CH_4$ values the Rayleigh equation is used to determine the fraction of CH_4 that has been oxidized (rearrangement of Equation 6, using $\delta^{13}C\text{-}CH_4$ values and α=0.987). Approximately half of the potential CH_4 production is oxidized: 43, 53 and 56% in reservoirs, 1, 2 and 3, respectively.

The ebullitive loss is a GHG flux from the reservoir to the atmosphere and for CH_4 it is of the same order of magnitude as the gas exchange of CH_4 from the reservoir to the atmosphere. The ebullitive flux of CH_4 enriches 30-40‰ during the flooded season indicating that bubble formation occurs where CH_4 is being oxidized. The potential ebullitive CH_4 flux to the atmosphere is much greater than the actual flux because the $\delta^{13}C\text{-}CH_4$ values are enriched, i.e. oxidized. Most likely, bubble formation occurs within the top few centimetres of soil since benthic photoautotrophs encourage CH_4 oxidation by O_2 production at the SWI (see Chapter 4:). The distance that O_2 can diffuse into the soil is balanced against O_2 consumption by heterotrophic respiration.

The soil porewater $\delta^{13}C\text{-}CH_4$ values enrich during the flooding season (Venkiteswaran, unpubl. data). This makes assigning a source $\delta^{13}C\text{-}CH_4$ value difficult however during the greatest period of pre-drawdown ebullitive flux (>90%) to the atmosphere, the soil porewater

$\delta^{13}C\text{-}CH_4$ values range –53 to –63‰ (one value at -70‰). The fraction of CH_4 oxidized is determined to be 25-75% of the potential ebullitive CH_4 flux via the Rayleigh equation, as above.

In other reservoirs, CH_4 oxidation is an important process that controls the flux of CH_4 from the reservoir surface to the atmosphere. CH_4 oxidation is a very important process in the GHG budget of ELARP. The decrease in importance of CH_4 oxidation relative to CH_4 production is exhibited by a depletion of $\delta^{13}C\text{-}CH_4$ values. The Rayleigh equation is used to determine the fraction of CH_4 that has been oxidized (rearrangement of Equation 6, using $\delta^{13}C\text{-}CH_4$ values and $\alpha=0.982\pm0.004$, mean ± standard deviation, n=8) (Venkiteswaran, unpubl. data). The pre-flood pore water $\delta^{13}C\text{-}CH_4$ values were as depleted at –70‰ (Kelly et al. 1997). Pre-flood $\delta^{13}C\text{-}CH_4$ values of CH_4 emitted from undisturbed peat (-28‰; Kelly et al. 1997) indicate that 91% of the CH_4 was oxidized. Post-flood, the CH_4 at the surface of flooded peat was less oxidized (-38‰; 85% oxidized). The floating peat islands show the greatest decline in the importance of CH_4 oxidation with $\delta^{13}C\text{-}CH_4$ values of –56‰. This indicates that only 56% of the CH_4 was being oxidized. The oxidation of CH_4 to CO_2 has significant implications for the GWP of the GHG flux from the FLUDEX and ELARP reservoirs since CH_4 has a GWP twenty-one times that of CO_2 (IPCC 1996).

Importance of primary production to the DIC isotope-mass budgets

Periphytic removal of carbon from the reservoirs is an important output of carbon in the mass and isotope-mass budget. However, estimating the total mass of carbon removed and the net mass of carbon removed from the water column is very difficult because of turnover of algal biomass, sloughing during collection and the accumulative growth of other biota and inclusion of detritus in the periphyton-based biofilm. Further, estimating the surface area on which algae can attach and the area between points of attachment where sheets form is very difficult. Composite samples collected from pine dowels yield $\delta^{13}C$-bulk values generally enriched relative to the expected range of -43 to –38‰. This estimate of algal growth applied to surface area within the reservoirs is an underestimate of carbon removed from the reservoirs but provides an estimate and allows the use of the isotope-mass budget to constrain better the other inputs and outputs, such as the benthic flux.

Two estimates of reservoir-scale primary production can be made. The first estimate uses the mass of DIC produced calculated in the Mass Balances section and the estimate of 15-33% DIC removed by benthic photoautotrophs determined by benthic chambers (see Chapter 4:). Using a conservative estimate of 15% this methods estimates that 66-89 kgC are removed by benthic photoautotrophs (Table 17). This estimate assumes that benthic photoautotrophy is the majority of total reservoir primary production.

The second method of estimating reservoir primary production uses the mass of DIC produced and δ^{13}C-DIC values calculated in the Mass Balances section. Because the net DIC production is the balance between total DIC production and primary production, the mass of DIC removed by primary production can be calculated with δ^{13}C-DIC values (see Table 16 for equation). This method estimates that 13-70 kgC are removed by total reservoir primary production. This is 3-19% of the net DIC added to the reservoirs.

Both methods of estimating total reservoir primary production are within the same order of magnitude as the pine dowel periphyton accumulation estimates. This confirms that primary production is an important process in the reservoirs because it reduces the DIC pool in the water column and enriches the remaining δ^{13}C-DIC values. However, it has not been possible to determine the total mass of DIC removed from the reservoirs with any more accuracy than order-of-magnitude estimates. Subsequently, estimating detrital production as the difference between potential primary production (pCO_2 laboratory experiments) and pine dowel periphyton accumulation estimates is impossible.

Storage and drawdown and isotope-mass budgets

Storage in the water column is included in the isotope-mass budget. During and after drawdown the benthic flux across the SWI, gas exchange and porewater are not included in the isotope-mass budgets. A better estimate of drawdown effects is needed because fluxes during this time are a part of the overall effects caused by reservoir creation and operation.

The water stored in the reservoirs at the end of flooding contributes to reservoir effects in two ways. First, there are GHG fluxes to the atmosphere from the surface of the reservoirs and downstream water bodies, outflow from the reservoirs and through seepage water.

Second, downstream effects of water level changes and water though not well studied are important (Nilsson and Berggen 2000; Nilsson et al. 1997).

Benthic flux into the water column continues while the water level is being lowered in the reservoirs and must be balanced against an output. The storage estimates based on water column concentration profiles are underestimates of GHG mass removed from the reservoir since leeching of GHG-rich porewater is not considered. The stable isotope estimates based on water column profiles also do not include porewater values, which are generally more depleted that the water column values. Since these reservoir effects are not considered in the isotope-mass budgets (Table 11 and Table 12) the budgets are underestimates of reservoir GHG effects.

5.6 Summary

Reservoir inflow from Roddy Lake exhibits an enrichment of δ^{13}C-DIC values from -13.5 to -5.5‰. This trend was not observed in 1999 (Boudreau 2000). It is suspected that the earlier flood season in 2000 than 1999 has captured the end of vernal turnover. Overland flow into the reservoirs, using L114 inflow creek as a proxy, has DIC concentrations approximately six times that of Roddy Lake inflow and is isotopically depleted (-25.3‰) relative to Roddy Lake inflow.

The reservoir outflow δ^{13}C-DIC values range from -21.0 to -10.3‰. This is a greater range than observed in 1999 (Boudreau 2000). Reservoir processes that add and remove DIC from the water column control these values. Reservoir 1 outflow is generally the most depleted (-21.0 to -16.5‰). Reservoirs 2 and 3 outflow δ^{13}C-DIC values are more enriched (-20.0 to -12.0‰ and -19.3 to -10.3‰, respectively) than those of reservoir 1. In 1999, outflow δ^{13}C-DIC values were not more enriched than -14‰.

Reservoir outflow δ^{13}C-CH_4 values enriched 45-60‰ during the flood season, from -100 to -80‰ in early July to -47 to -36‰ in mid-September. The enriched values indicate that the reservoir CH_4 pool has been highly oxidized. In 1999, outflow δ^{13}C-CH_4 values more enriched than -66‰ were not observed (Boudreau 2000).

The isotope-mass balances identify the importance of reservoir processes such as primary production and CH_4 oxidation to the over all budget. Estimates of total reservoir primary production indicate that 3-19% of the total DIC production is removed by photoautotrophs. This loss of DIC is an important part of the isotope-mass budgets of the reservoirs. The carbon cycling in biofilm and the importance of benthic versus epixylic (on dead wood) primary production needs to be better understood.

CH_4 oxidation in the soils reduces the potential flux of CH_4 across the SWI by approximately 50%. This is similar to the fraction of CH_4 oxidation in peat islands in ELARP. CH_4 oxidation reduces the water column CH_4 concentration and reduces the loss of CH_4 to the atmosphere via gas exchange. The ebullitive flux of CH_4, of the same important as gas exchange to the GHG flux from the reservoir is also oxidized. This indicates that bubble formation occurs near the surface of the soil because CH_4 oxidation occurs where there are low concentrations of O_2.

Table 10 Summary of isotope-mass budget equations and abbreviations.

Item	Equation	Equation number
Mass budget and mass balance	$m_{input} = m_{inf\ low} + m_{overland} + m_{bf}$ $m_{output} = m_{outflow} + m_{ge} + m_{wall} + m_{fracture} + m_{storage} + m_{peri} + m_{phyto}$ $m_{input} = m_{output}$	(6)
Isotope-mass budget and Isotope-mass balance	$\delta_{input} = \frac{(\delta \times m)_{inf\ low} + (\delta \times m)_{overland} + (\delta \times m)_{bf}}{m_{input}}$ $\delta_{output} = \frac{(\delta \times m)_{outflow} + (\delta \times m)_{ge} + (\delta \times m)_{wall} + (\delta \times m)_{fracture} + (\delta \times m)_{storage} + (\delta \times m)_{peri} + (\delta \times m)_{phyto}}{m_{output}}$ $\delta_{input} = \delta_{output}$	(7)
Net DIC production	$(m_{output}) - (m_{inf\ low} + m_{overland}) = m_{DIC\ prod}$ $((\delta \times m)_{output}) - ((\delta \times m)_{input} + (\delta \times m)_{overland}) = (\delta \times m)_{DIC\ prod}$	(8) (9)
CH_4 production	$(m_{output}) - (m_{inf\ low}) = m_{CH_4\ prod}$ $(\delta \times m)_{output} - (\delta \times m)_{input} = (\delta \times m)_{CH_4\ prod}$	(10) (11)

Abbreviation	Item	Notes
input	all inputs to the reservoirs	
inflow	inflow from Roddy Lake	
overland	overland flow	not applicable to CH_4 budgets
output	all output from the reservoirs	
outflow	outflow via the V-notch weir	
ge	gas exchange	
wall	wall seepage	
fracture	fracture seepage	only applies to reservoir 3
storage	storage in the reservoirs before drawdown	
peri	periphytic algae within non-benthic biofilm	not applicable to CH_4 budgets
phyto	phytoplankton	not applicable to CH_4 budgets
DIC prod	Net DIC production	net production of DIC in the reservoirs
CH_4 prod	Net CH_4 production	net production of CH_4 in the reservoirs

Table 11 DIC-CO_2 isotope-mass balance for FLUDEX reservoirs from 30-May to 22-September-2000. (Inflow, bottom flux, gas exchange and ebullition data C. Matthews, unpubl. data; periphyton and phytoplankton data M. Paterson & D. Findlay, unpubl. data).

	DIC (kgC)			δ^{13}C-DIC (‰vs. VPDB)		
	R1	**R2**	**R3**	**R1**	**R2**	**R3**
Inflow	143	108	168	-8.7	-8.7	-8.8
Overland Flow	102	15	1	-25.7	-25.7	-25.7
Bottom Flux (from chambers)	412	419	287	-17.4	-16.8	-19.2
Total Inputs[1]	**657**	**542**	**457**	**-16.8**	**-15.5**	**-15.4**
Outflow	300	183	123	-17.9	-15.5	-14.9
Gas Exchange	301	192	175	-21.3	-19.4	-17.5
Wall Seepage	62	51	55	-18.0	-16.0	-15.3
Fracture Seepage			125			-15.3
Storage (Drawdown)	24	11	26	-15.0	-16.7	-16.0
Periphyton	61	73	36	-38.0	-38.0	-38.0
Phytoplankton	3	2	5	-38.0	-38.0	-38.0
Total Outputs	**752**	**513**	**545**	**-20.9**	**-20.4**	**-17.7**
Net Gain (Out - In)	**94**	**-29**	**88**			
Missing (Net/Input)	14%	-5%	19%			
Ebullition (CO_2)	0.1	0.1	0.2	-16.0	-17.5	-14.6
DIC production (required to balance the isotope-mass budget)	506	390	375	-23.4	-23.4	-21.6

[1] DIC input from precipitation is <1% that of the inflow; pH of rain at ELA May-November-2001 was 5.48±0.57 (mean ± standard deviation, n=42, range 4.35-6.65) (SJ Paige & K Beaty, pers. comm..))

Table 12 CH_4 isotope mass-balance for FLUDEX reservoirs from 30-May to 22-September-2000. (Inflow, bottom flux, gas exchange and ebullition data C. Matthews, unpubl. data).

	CH_4 (kgC)			$\delta^{13}C$-CH_4 (‰vs. VPDB)		
	R1	**R2**	**R3**	**R1**	**R2**	**R3**
Inflow	0.1	0.1	0.1	-45.0	-45.0	-45.0
Bottom Flux (from chambers)	16.6	47.4	15.8	-64.4	-40.8	-56.2
Total Inputs	**16.7**	**47.5**	**15.9**	**-61.3**	**-40.8**	**-56.1**
Outflow	3.2	2.3	1.1	-53.9	-64.8	-56.2
Gas Exchange	6.0	3.1	4.8	-52.8	-66.3	-43.1
Wall Seepage	0.7	0.5	0.6	-55.1	-67.8	-53.5
Fracture Seepage			1.4			-53.5
Storage (Drawdown)	0.3	0.2	0.7	-50.0	-52.0	-60.0
Total Outputs	**10**	**6**	**9**	**-53.2**	**-65.4**	**-48.6**
Net Gain (Out - In)	**-6.6**	**-41.5**	**-7.3**			
Missing (Net/Input)	-39.5%	-87.3%	-45.6%			
Ebullition (CO_2)	1.75	1.18	3.59	-49.4	-47.9	-45.9
CH_4 production (required to balance the isotope-mass budget	10.0	5.9	8.5	-53.8	-66.3	-49.3

Table 13 Periphyton $\delta^{13}C$, $\delta^{15}N$ and C:N values. Periphyton sampled in August and September-2000 grew on pine dowels in FLUDEX reservoirs for approximately one month before being harvested. Periphyton sampled *post-flood* was collected from sheets hanging from trees in the reservoirs after the water had been removed from the reservoirs.

Location	Date	^{13}C (‰ vs. VPDB)	^{15}N (‰ vs. AIR)	C:N
Reservoir 1	17-Aug-00	-31.7	-4.9	22
Reservoir 1	17-Aug-00	-31.6	-0.2	18
Reservoir 1	12-Sep-00	-32.2	-0.3	13
Reservoir 1	12-Sep-00	-36.7	-1.3	20
Reservoir 1	12-Sep-00	-33.6	-0.6	13
Reservoir 1	12-Sep-00	-32.4	-0.4	10
Reservoir 2	17-Aug-00	-32.3	-0.6	16
Reservoir 2	17-Aug-00	-30.9	0.0	15
Reservoir 2	17-Aug-00	-32.0	-0.4	15
Reservoir 2	12-Sep-00	-31.7	-0.4	14
Reservoir 2	12-Sep-00	-31.3	0.6	10
Reservoir 2	12-Sep-00	-35.6	-0.5	21
Reservoir 3	17-Aug-00	-31.6	0.2	14
Reservoir 3	17-Aug-00	-31.3	-0.9	16
Reservoir 3	12-Sep-00	-29.8	0.7	13
Reservoir 3	12-Sep-00	-31.4	-0.2	14
Reservoir 3	12-Sep-00	-31.5	-0.7	15
Reservoir 3	12-Sep-00	-29.0	-0.8	15
Reservoir 1	post-flood	-38.6	-0.8	26
Reservoir 2	post-flood	-34.9	-0.5	22
Reservoir 3	post-flood	-36.2	-1.1	17

Table 14 DIC isotope-mass balance from 30-May to 22-September-2000 to determine DIC production via four methods.

	DIC (kgC)			DIC (‰ vs. VPDB)		
	R1	**R2**	**R3**	**R1**	**R2**	**R3**
DIC production (from chambers)	412	419	287	-17.4	-16.8	-19.2
DIC production (if chambers flux is correct, isotope required to balance)	412	419	287	-27.7	-20.6	-27.3
DIC production (required to balance mass budget)	506	390	375	-22.6	-22.1	-20.9
DIC production (if isotope is correct, chambers flux required to balance)	655	512	408	-17.4	-16.8	-19.2

Table 15 CH_4 isotope-mass balance from 30-May to 22-September-2000 to determine CH_4 production via four methods.

	CH_4 (kgC)			CH_4 (‰ vs. VPDB)		
	R1	**R2**	**R3**	**R1**	**R2**	**R3**
CH_4 production (from chambers)	16.6	47.4	15.8	-61.4	-40.8	-56.2
CH_4 production (if chambers flux is correct, isotope required to balance)	16.6	47.4	15.8	-32.4	-8.3	-26.6
CH_4 production (required to balance mass budget)	10.0	5.9	8.5	-53.8	-66.3	-49.3
CH_4 production (if isotope is correct, chambers flux required to balance)	8.8	9.6	7.5	-61.4	-40.8	-56.2

Table 16 Summary of equations and abbreviations of primary production estimates of DIC removed from FLUDEX reservoirs.

Item	Equation	Equation number
Mass of reservoir primary production	$m_{pp} = \frac{m_{net}(\delta_{net} - \delta_{total})}{\delta_{total} - \delta_{pp}}$	(12)

Abbreviation	Item	Notes
m_{pp}	mass of primary production	
m_{net}	mass of net DIC production	estimated in Mass Balances section
δ_{total}	δ^{13}C-DIC of total DIC production	estimated by mass weighted dark benthic chamber DIC flux and δ^{13}C-DIC values
δ_{pp}	δ^{13}C-DIC removed by primary production	estimated by periphyton (-38‰; Periphyton section); and estimated by δ_{total} with pH and temperature DIC species fractionation correction (-43.5‰)

Table 17 Primary production estimates of DIC removed from FLUDEX reservoirs 30-May to 22-September-2000.

	DIC (kgC)			DIC (‰ vs. VPDB)		
	R1	**R2**	**R3**	**R1**	**R2**	**R3**
Values required to balance the DIC isotope-mass budget, see Table 11	506	390	375	-23.4	-23.4	-21.6
Mass of DIC removed by primary production (periphyton δ^{13}C-bulk values)	**31**	**23**	**70**	-38.0	-38.0	-38.0
Mass of DIC removed by primary production (dark chamber δ^{13}C-DIC values)	**18**	**13**	**39**	-43.5	-43.5	-43.5
Mass of DIC removed by primary production (benthic chamber estimate of 15%, see Chapter 4:)	**89**	**69**	**66**			

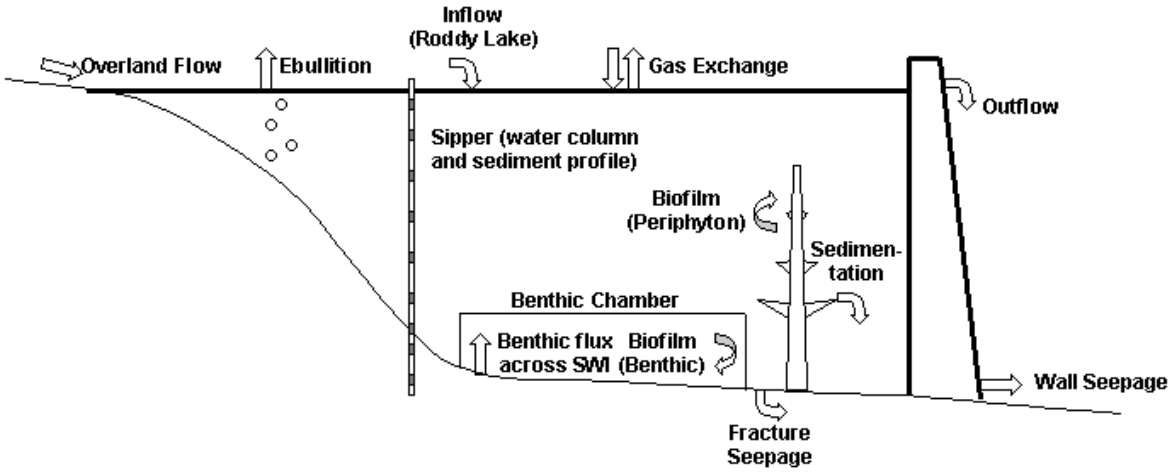

Figure 21 Schematic diagram of the components of FLUDEX reservoirs that are sampled.

Inflow is pumped from Roddy Lake. Overland flow is an important component only in reservoir 1. Outflows are through a V-notch weir and wall seepage. In reservoir 3 there is additional outflow via fracture seepage. Gas exchange with the atmosphere is measured at the surface of the reservoirs by SF_6 tracer experiments (C. Matthews unpubl. data). Benthic chambers are used to measure mass and stable isotope flux across the SWI and benthic biofilm activity. Attached biofilm is measured for carbon accumulation. Attached biofilm sloughing and sedimentation are not directly assessed. Water column and sediment concentration and stable isotope profiles are measured with sippers. Ebullition is measured with floating inverted funnels (not shown), bubble traps.

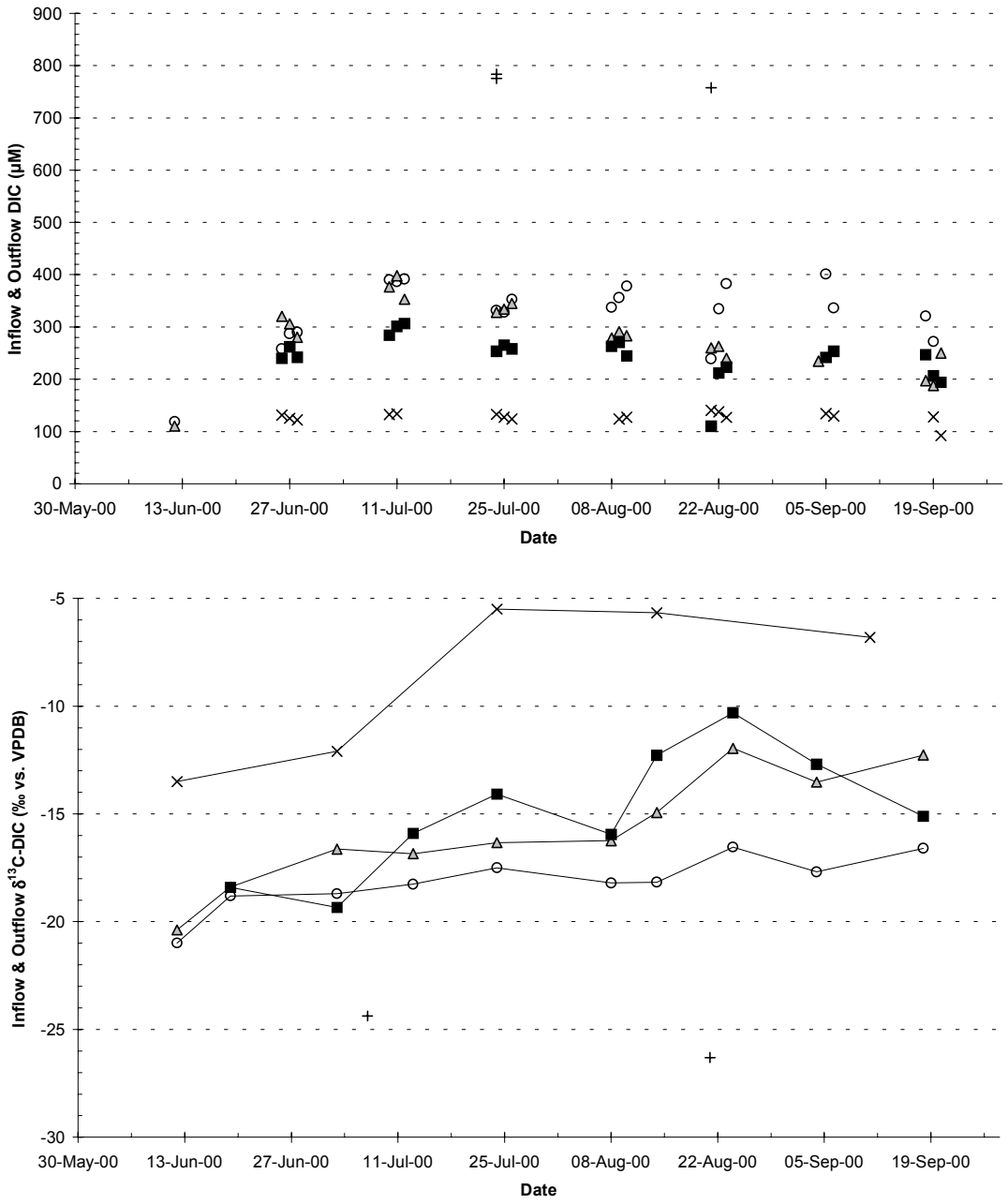

Figure 22: FLUDEX reservoir inflow and outflow δ^{13}C-DIC value and DIC concentration.

Concentration data from C. Matthews (unpubl. data). Reservoir inflow from Roddy Lake (×), overland flow into reservoirs estimated from L114 catchment inflow (diamond), reservoir 1 overland inflow (+) and reservoir 1 (circle) 2 (triangle) and 3 (square) outflow.

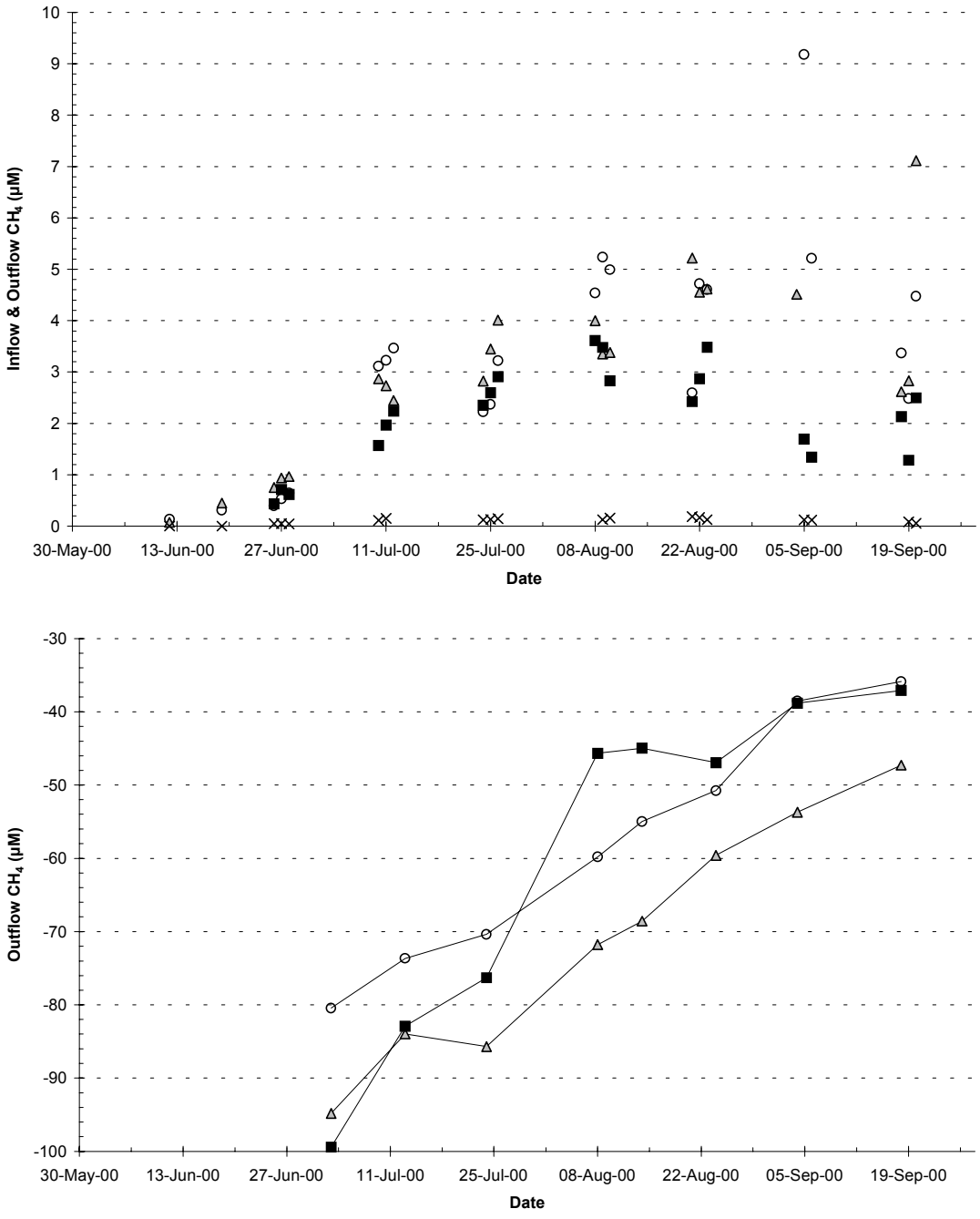

Figure 23: FLUDEX reservoir inflow and outflow $\delta^{13}C$-CH_4 value and CH_4 concentration.

Concentration data from C. Matthews (unpubl. data). Reservoir inflow from Roddy Lake (×) and reservoir 1 (circle) 2 (triangle) and 3 (square) outflow.

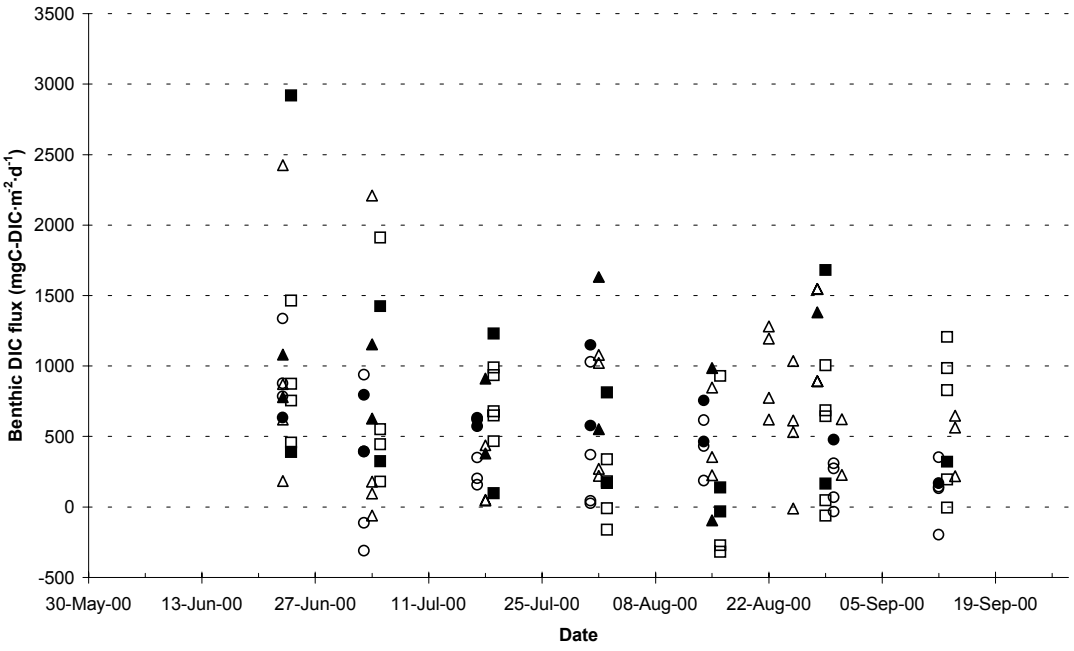

Figure 24: Benthic DIC flux from the soil to the water column estimated via light (open) and dark (closed) benthic chambers in reservoirs 1 (circle), 2 (triangle) and 3 (square).

Flux was estimated seven times during the flooded season (C. Matthews, unpubl. data).

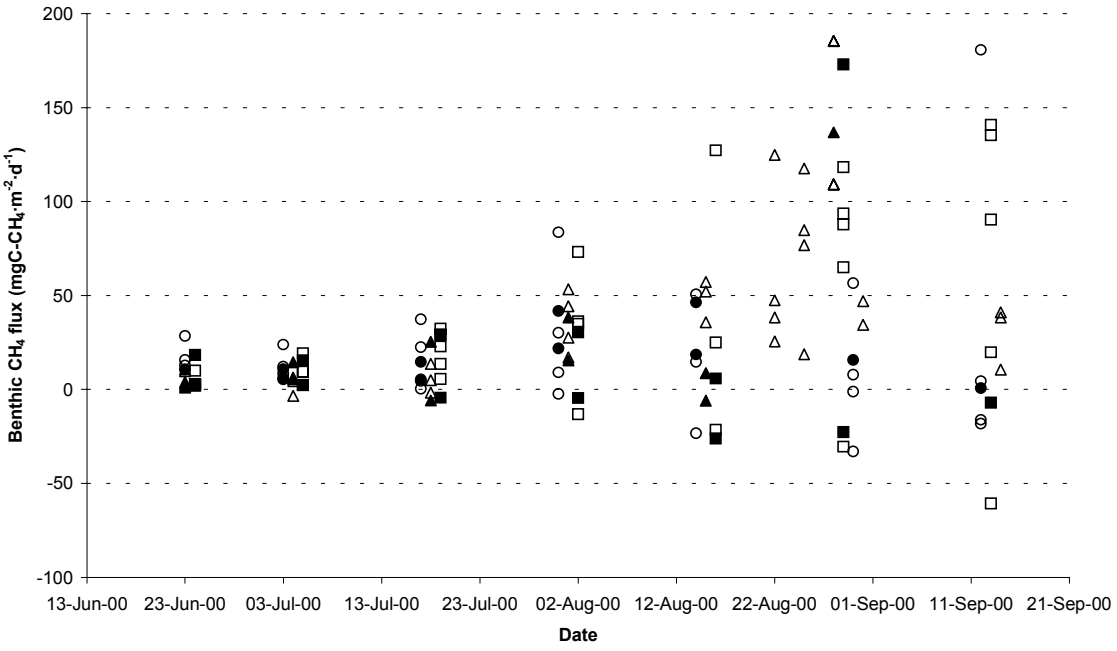

Figure 25: Benthic CH_4 flux from the soil to the water column estimated via light (open) and dark (closed) benthic chambers in reservoirs 1 (circle), 2 (triangle) and 3 (square).

Flux was estimated seven times during the flooded season (C. Matthews, unpubl. data).

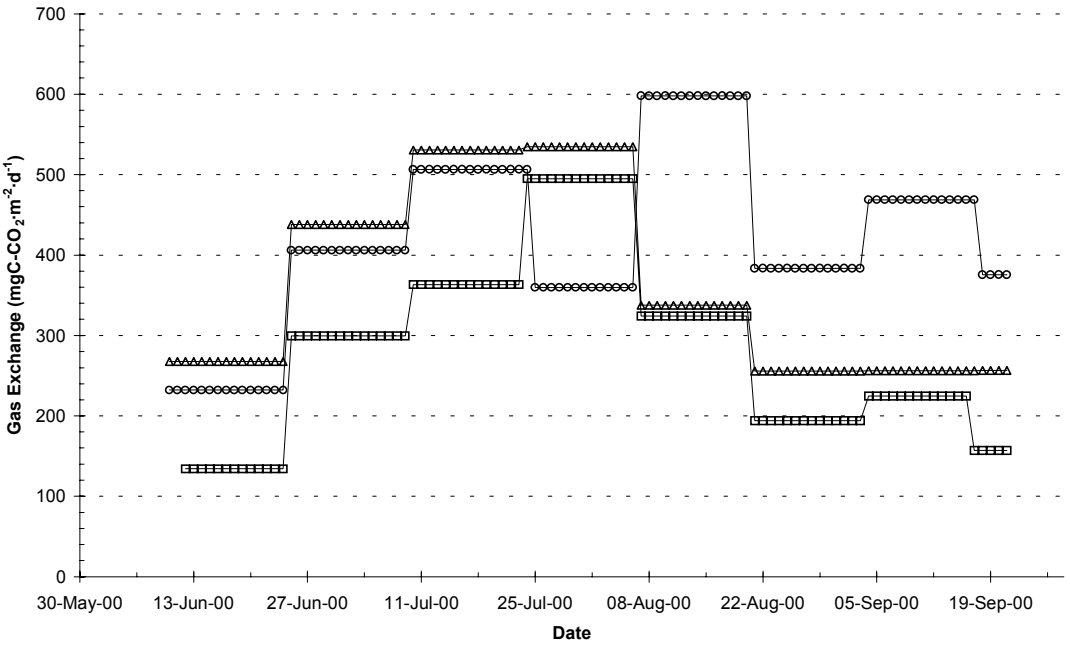

Figure 26: Reservoir surface CO_2 gas exchange of reservoirs 1 (circle), 2 (triangle) and 3 (square).

Gas exchange was calculated from CO_2 concentration and SF_6 tracer experiments eight times during the flooded season (C. Matthews, unpubl. data).

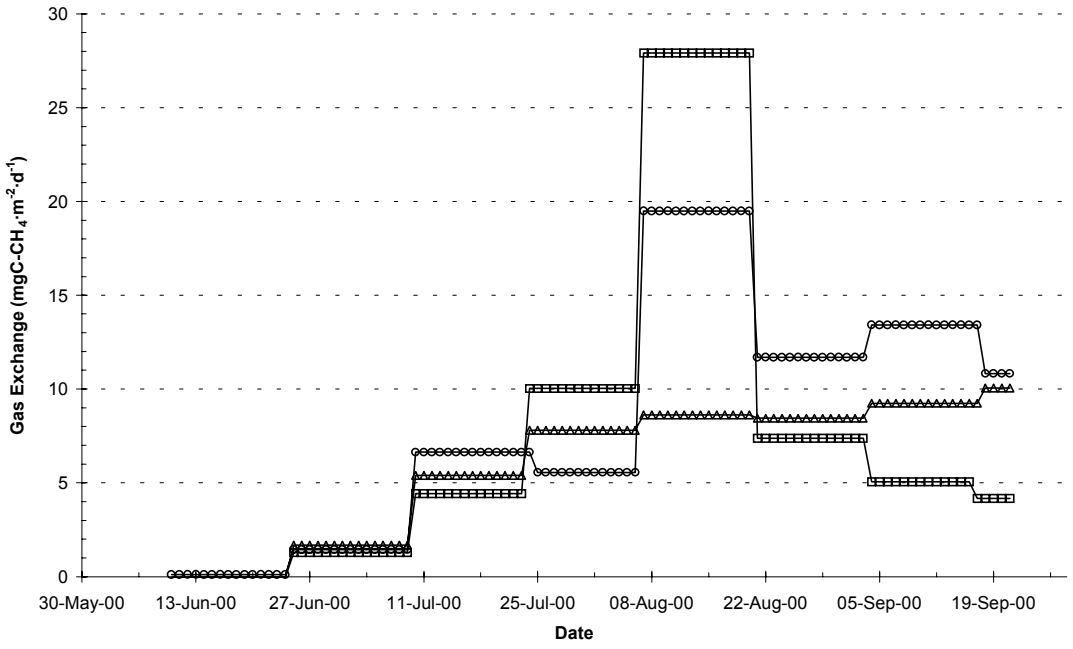

Figure 27: Reservoir surface CH_4 gas exchange of reservoirs 1 (circle), 2 (triangle) and 3 (square).

Gas exchange was calculated from CO_2 concentration and SF_6 tracer experiments eight times during the flooded season (C. Matthews, unpubl. data).

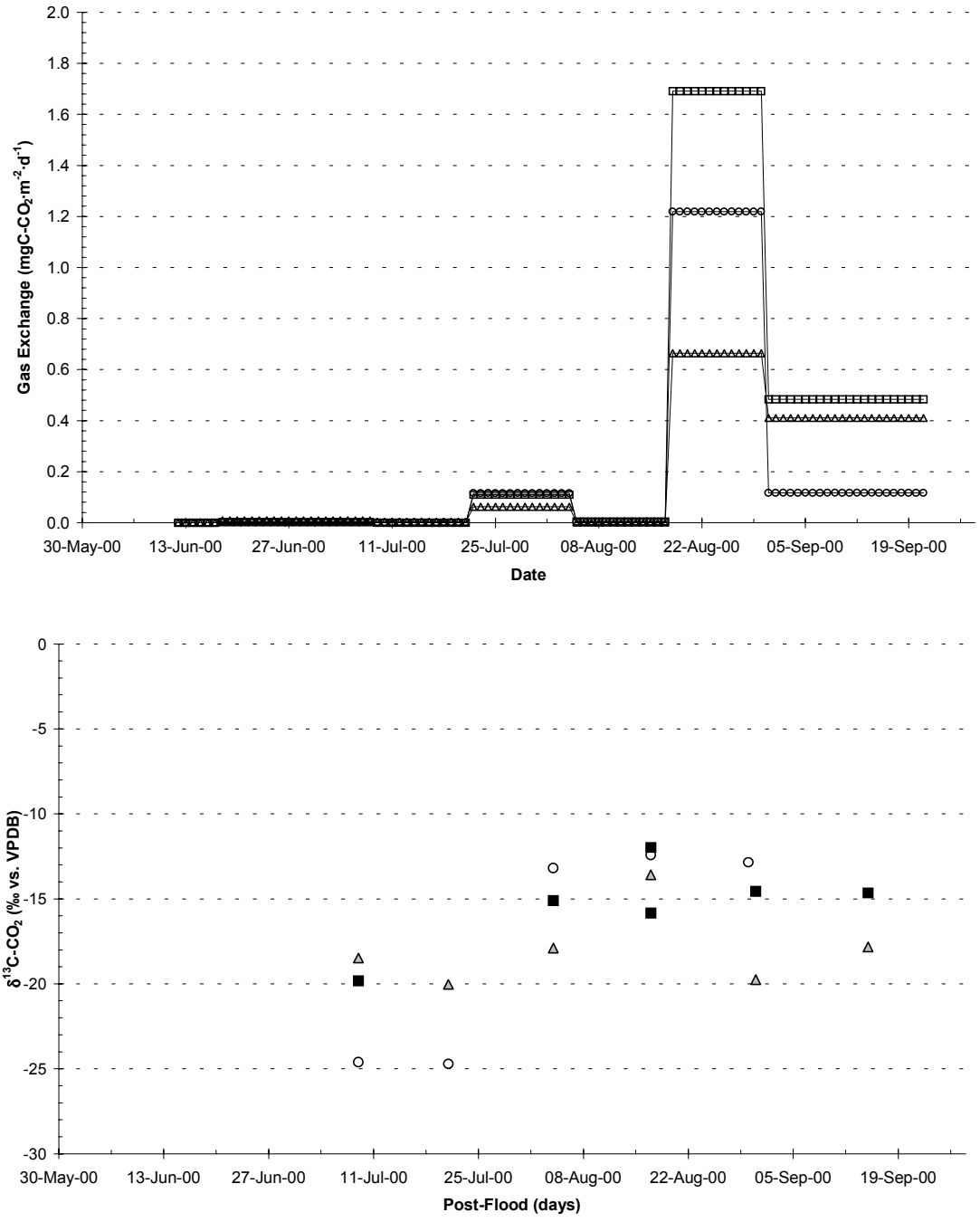

Figure 28 Reservoir CO_2 ebullition rates and $\delta^{13}C$-CO_2 values of bubbles from reservoirs 1 (circle), 2 (triangle) and 3 (square).

Flux was estimated seven times during the flooded season (C. Matthews, unpubl. data).

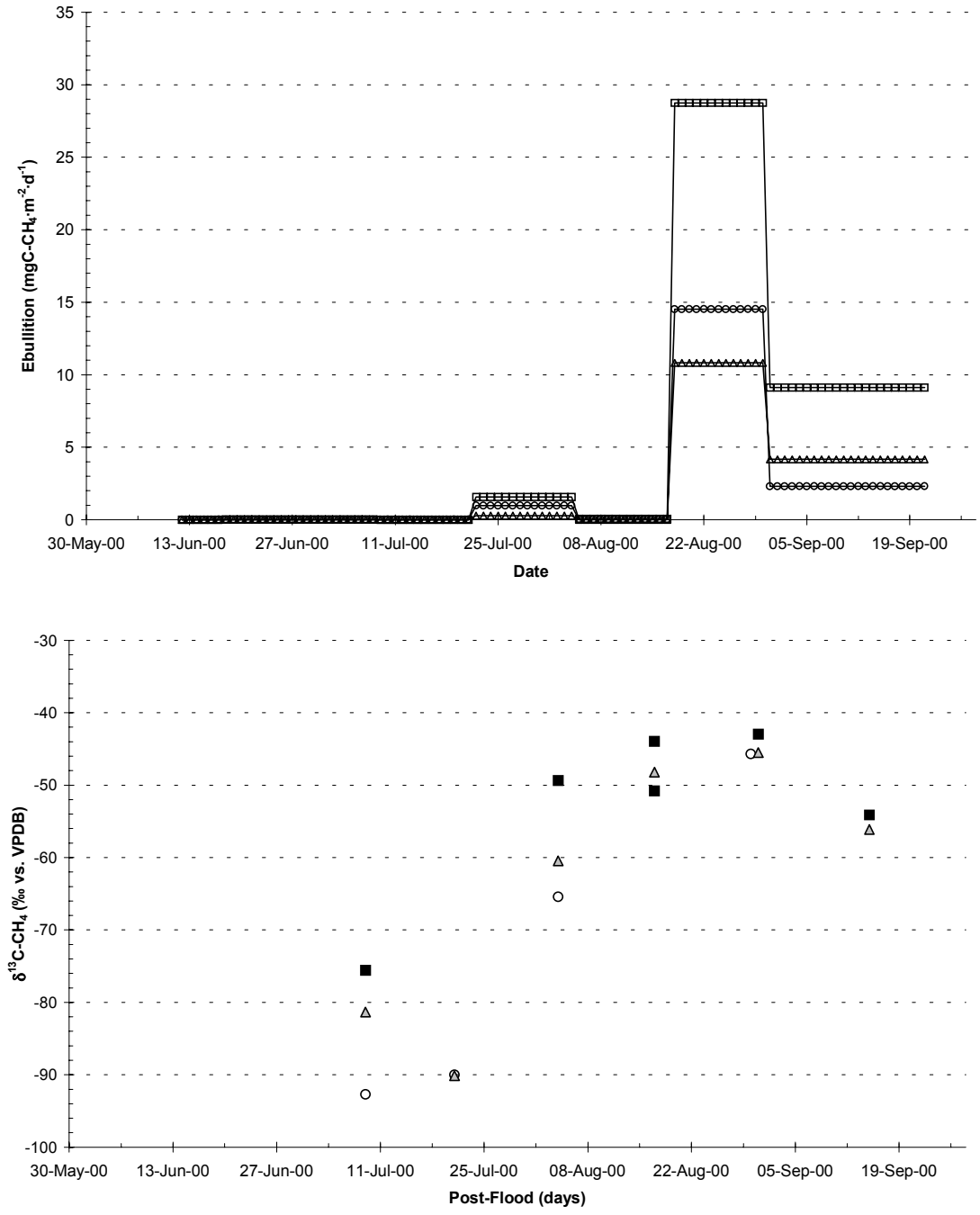

Figure 29 Reservoir CH_4 ebullition rates and $\delta^{13}C$-CH_4 values of bubbles from reservoirs 1 (circle), 2 (triangle) and 3 (square).

Flux was estimated seven times during the flooded season (C. Matthews, unpubl. data).

Chapter 6: Conclusions and Recommendations

Overall, this research was successful in using stable isotopes of carbon and oxygen to determine the importance of decomposition, CH_4 oxidation and photosynthesis in the FLUDEX reservoirs. The use of stable isotopes brings a process-based approach to GHG studies of reservoirs. Better predictive models can be constructed by using an isotope process-based approach instead of a mass-based approach because multiple processes affect GHG cycling in reservoirs. This chapter presents observations and general conclusions and identifies areas where further research should be conducted.

6.1 Benthic studies

Benthic chambers were used to determine rates of respiration and photosynthesis with respect to DIC and O_2. A new $\delta^{18}O$-O_2 technique was used to determine rates of gross photosynthesis. The ability to determine gross photosynthesis directly is advantageous because it removes the necessary assumptions made when combining light and dark benthic chambers. Also it is a direct measure of gross photosynthesis instead of using O_2 or DIC concentration as a proxy or performing laboratory ^{14}C-pCO_2 experiments with further simplifying assumptions. The benthic flux of DIC across the SWI and the $\delta^{13}C$-DIC value of that flux were investigated to better understand the $\delta^{13}C$-DIC contribution of soil decomposition to the reservoir DIC pool. Benthic photoautotrophs reduced the flux of DIC across the SWI into the water column by 15-33% and enriched the $\delta^{13}C$-DIC value of that flux relative to the flux without benthic photoautotrophs by several permil. Further, the benthic flux of CH_4 across the SWI and the importance of CH_4 oxidation on the benthic CH_4 flux were investigated using CH_4 concentration and $\delta^{13}C$-CH_4 analyses.

Benthic chamber determined DIC and CH_4 fluxes across the SWI are variable, by more than three orders of magnitude for DIC and more than two orders of magnitude for CH_4, site-to-site within reservoirs and between reservoirs. Soil decomposition needs to be better understood so that the flux variability can be better interpreted. Presently, the $\delta^{13}C$ dynamics during decomposition are not well known. Soil profiles show an enrichment of $\delta^{13}C$-bulk with depth implying that the CO_2 and DOC produced from soil decomposition are depleted relative

to the bulk source material (Nadelhoffer & Fry 1988; Boudreau 2000). However, laboratory incubations indicate that the oppose case is true for the 20 year old soils in the FLUDEX reservoirs (Baril 2001; Boudreau 2000; Ferguson 2000; Venkiteswaran, unpubl. data). Variability in soils may produce the variability in flux across the SWI, but the decomposition processes and hydrology of the site will also affect the flux of DIC and CH_4 across the SWI.

The movement of DIC and CH_4 rich soil porewater is unstudied in the FLUDEX reservoirs. The movement of DIC and CH_4 via hydrological flow paths, diffusion or simple soil porosity will influence which areas of the reservoirs exhibit a large or small flux across the SWI. So, the decomposition processes need to be better understood to predict the δ^{13}C-DIC and δ^{13}C-CH_4 values of the flux of DIC and CH_4 across the SWI and the role of hydrology in the stony and peaty soils needs to be better defined to interpret the variability of the flux of DIC and CH_4 across the SWI.

The area of activity for O_2 processes is the water column trapped by the benthic chamber and just above the SWI where the benthic photoautotrophs are located. Though the relative importance of water column O_2 processes relative to soil processes is expected to be small. The distance O_2 diffuses into the soil is controlled by the consumption of O_2 by respiration—O_2 does not diffuse more than a few centimetres (Venkiteswaran, unpubl. data). Soil porewater O_2 concentrations confirm this at several locations in the reservoirs during the flood season (Venkiteswaran, unpubl. data). The area of activity for DIC and CH_4 processes is in the underlying soil and around the SWI. CH_4 is oxidized in the upper few centimetres of the soil with O_2 from benthic photoautotrophs and DIC is removed just above the SWI by benthic photoautotrophs. The relationship between O_2 and carbon processes needs to be better understood so that predicting the flux of DIC and CH_4 away from the SWI involves all these processes. Figure 11 provides evidence that net photosynthesis increases with increasing community respiration (DIC flux across the SWI); at greater rates of net photosynthesis more O_2 evolved. More data is needed in order to better link the increased O_2 evolution with increased rates of CH_4 oxidation in light benthic chambers (see Figure 16). The role soil structure and hydrology plays in O_2 diffusion downward into the soil in unknown.

Photosynthesis becomes more important relative to respiration during the flood season. This is important for CH_4 oxidation and for maintaining adequate O_2 concentration for fish. The role of benthic photoautotrophy to the O_2 regime of the entire reservoir needs to be separated from water column and other attached photoautotrophy to determine which sources of O_2 are most important for fish. Constructing an O_2 and $\delta^{18}O$-O_2 budget will quantify the importance of photosynthetically derived O_2 and permit an estimate of whole reservoir gross primary production.

Algal photosynthesis is currently limited by light at depth in the water column; at 1 m depth light is approximately 10% that of the incident light and the light extinction coefficient is between 2 and 3 (M. Paterson, unpubl. data). Nitrogen may also be limiting the growth rate of algae since nitrate concentration is low (typically ≤ 4 $\mu g \cdot L^{-1}$, maximum 14, minimum below detection limit, n=258) (Bodaly RA, unpubl. data) and algal biomass C:N are elevated at 15±3 (mean ± standard deviation, n=18).

The total carbon accumulation by benthic photoautotrophs is not well known. Bacteria quickly colonize the biofilm (see Periphyton, in Chapter 5:) but the rate of turnover of recently fixed carbon is unknown. It is quite possible that benthic and epixylic photoautotrophs are important to the reservoir O_2 regime but do not accumulate a large quantity of carbon relative to the benthic flux of DIC across the SWI or gas exchange because of bacterial decomposition, animal grazing and sloughing of the biofilm.

6.2 Isotope-mass balance

An isotope-mass budget of DIC and CH_4 was completed for each reservoir. Because of the heterogeneity of processes at the SWI and the importance of photosynthesis the mass budgets do not balance, stable carbon isotopes can be used to determine the contribution of individual processes to the budget. The values assigned to the benthic flux of DIC and CH_4 across the SWI into the water column are the least certain and largest input term. Using stable carbon isotope analysis, primary production and the concomitant enrichment of $\delta^{13}C$-DIC values was identified as an important process that is not directly assessed by a mass only approach. The isotope-mass budget is able to constrain budget items in a different manner than a mass only budget because the isotope approach identifies processes directly.

During decomposition the degradation of the different components of soil organic matter is only described in general terms, e.g. carbohydrates, proteins, celluloses and hemicelluloses and lignin. The carbon isotope fractionation during the decomposition of different components of soil organic carbon is well determined but the contribution of different sources is not well understood. This uncertainty reduces the ability of using stable carbon isotopes to better constrain decomposition in the reservoirs and thus must be measured directly. The $\delta^{13}C$ dynamics of decomposition need to be investigated further.

The contribution of litterfall from inside and outside the reservoirs to the flooded forest floor is not directly quantified. Litterfall was determined to be an importance source of phosphorus to ELA reference lake L239 (McCullough 1998). Using McCullough's litterfall estimates for the forest regenerating after the 1980 fire, the contribution of litterfall from particulates outside of the reservoirs is many orders of magnitude smaller (0.1-10 $kgC \cdot a^{-1}$ from litterfall) than the carbon located in the forest floor of the reservoirs (approximately 10 000-20 000 kgC; Boudreau 2000). Potential litterfall from inside the reservoirs can be estimated with vegetation data collected before flooding (Heubert 1999). The fresh litter and shrub carbon that can become litterfall is two to three orders of magnitude smaller (200-1000 $kgC \cdot a^{-1}$) than the carbon located in the forest floor of the reservoirs. On an annual basis, this figure is even smaller. In late-September-2001, after three years of flooding, visual inspection of jack pine tree indicates that 10-20% of needles remain on the dead trees. In subsequent years, this input of carbon will become even smaller.

The CH_4 isotope-mass budgets indicate the importance of CH_4 oxidation to the overall CH_4 budget of each reservoir. The $\delta^{13}C$-CH_4 values of the benthic flux of CH_4 across the SWI indicate that oxidation is reducing the potential flux of CH_4 in to the water column. That the $\delta^{13}C$-CH_4 value of the ebullitive flux of CH_4 to the atmosphere is enriched indicates that the CH_4 is highly oxidized. This confirms the benthic chamber results that CH_4 oxidation is occurring and indicates that CH_4 oxidation and bubble formation occur in top few centimetres of the soil.

The $\delta^{13}C$-CH_4 values of the benthic flux of CH_4 across the SWI can only be determined when the concentration is adequate for analysis. The result is that the flux of CH_4 across the

SWI early in the flood season, though smaller in magnitude (Figure 25) is not well evaluated for $\delta^{13}C$-CH_4 values. The detection limit of GC-C-IRMS analysis of $\delta^{13}C$-CH_4 is currently approximately 4 μM dissolved CH_4 concentration. If the detection limit can be reduced, greater certainty can be placed on the CH_4 isotope-mass budget because the CH_4 processes in the soils that fuel the benthic CH_4 flux across the SWI can be better understood. Though a small contribution to the CH_4 isotope-mass budget, determining $\delta^{13}C$-CH_4 values of outflow and water column CH_4 at low concentrations provides information about CH_4 processes. Since CH_4 is produced by CO_2 reduction in highly reducing environments and when acetate and other small DOC molecules are not available (Whiticar 1999) the development of these conditions could be monitored with $\delta^{13}C$-CH_4 values at low CH_4 concentration. Similarly, the development of CH_4 oxidizing bacteria can be monitored with $\delta^{13}C$-CH_4 values at low CH_4 concentration. Water column concentration analysis alone cannot determine whether low CH_4 concentrations are a result of little CH_4 production and/or a result of CH_4 oxidation. Analysis of $\delta^{13}C$-CH_4 at low concentrations can provide valuable information about the processes that affect CH_4 concentration.

The carbon isotope fractionation during CH_4 oxidation varies between systems (Whiticar 1999). Thus, it must be determined for each system so that estimates of the degree of CH_4 oxidation can be made. Preliminary laboratory studies have determined the $\alpha_{CO2\text{-}CH4}$ value in two FLUDEX reservoirs and the ELARP reservoir at 21-23ºC. The influence of temperature and nutrients on the isotope fractionation factor has not been studied for these reservoirs.

References

Ågren GI, Bosatta E and Balesdent J (1996) Isotope discrimination during decomposition of organic matter: a theoretical analysis. Soil Sci. Soc. Am. J 60:1121:1126.

Baxter RM, Glaude P. (1980) Environmental effects of dams and impoundments in Canada: Experience and prospects. Canadian Bulletin of Fisheries and Aquatic Sciences 205:134.

Beaty KG (2001) Hydrology. In: Bodaly RA (ed) The Upland Flooding Experiment (FLUDEX) Summary Report for 2000. Department of Fisheries and Oceans, Winnipeg. Unpublished manuscript.

Beaty KG & Lyng ME (1989) Hydrometeorological data for the Experimental Lakes Area, northwestern Ontario, 1982-1987. Can. Data Rep. Fish. Aquat. Sci. 759: v + 280 p.

Bender ML (1990) $\delta^{18}O$ of dissolved O_2 in seawater: a unique tracer of circulation and respiration in the deep sea. J. Geophys. Res 95:22,243-22,252.

Bender ML & Grande K (1987) Production, respiration and the isotope geochemistry of O_2 in the upper water column. Global Biogeochem. Cycles 1:49-59.

Bender M, Grande K, Johnson K, Williams PJLeB, Marra J, Sieburth J, Pilson M, Langdon C, Hitchcock G, Orchardo J, Hunt C, Donaghay P & Heinemann K (1987) A comparison of four methods for determining planktonic community production. Limnol. Oceanogr. 32(5):1085-1098.

Blom CWPM & Voesenek LACJ (1996) Flooding: The survival strategies of plants. Trends Ecol. Evol. 11:290 295.

Bodaly, RA, St. Louis VL, Paterson MJ, Fudge RJP, Hall BD, Rosenberg DM & Rudd JWM (1997) Bioaccumulation of mercury in the aquatic food chain in newly flooded areas. In: Sigel A & Sigel H (eds) Mercury and its Effects on Environment and Biology. Vol. 34, Metal Ions in Biological Systems. Marcel Dekker, New York.

Boudreau NM (2000) Sources of CH_4, CO_2 and DOC in newly flooded boreal upland reservoirs. MSc thesis. University of Waterloo.

Bourassa R (1985) Power from the north. Prentice Hall, Scarborough.

Brunskill GJ and Schindler DW (1971) Geography and bathymetry of selected lake basins, Experimental Lakes Area, northwestern Ontario. J. Fish. Res. Board Can. 28(2):139-155.

Chanton JP, Whiting GJ, Blair NE, Lindau CW & Bollich PK (1997) Methane emission from rice: stable isotopes, diurnal variations, and CO2 exchange. Global Biogeochem. Cycles 11(1):15-27.

Chao BF (1991) Man, water and global sea level. EOS, Transactions of the American Geophysical Union 72:492.

_____ (1995) Anthropogenic impact on global geodynamics due to reservoir water impoundment. Geophys. Res. Let. 22:3529-3532.

Clark ID & Fritz P (1997) Environmental isotopes in hydrology. CRC Press, Boca Raton.

Cole JJ & Caraco NF (1998) Atmospheric exchange of carbon dioxide in a low-wind oligotrophic lake measured by the addition of SF_6. Limnol. Oceanogr. 43(4):647-656.

Craig H (1954) Carbon-13 in plants and the relationship between carbon-13 and carbon-14 variations in nature. J. Geol. 62:115-149.

Crill PM, Bartlett KB, Harriss RC, Gorham E, Verry ES, Sebacher DI, Madzar L & Sanner W (1988) Methane flux from Minnesota peatlands. Global Biogeochem. Cycles 2:371-384.

Davies, J.C., and A.P Pryslak. 1967. Ontario Department of Mines Map 2115, Kenora - Fort Frances Sheet, Geological Compilation Series, Kenora, Rainy River Districts.

Department of Agriculture, Canada (1978) The Canadian system of soil classification. Minister of Supply and Services, Hull.

Duchemin É, Lucotte M, Canuel R & Chamberland A (1995) Production of the greenhouse gases CH4 and CO2 by hydroelectric reservoirs of the boreal region. Global Biogeochem. Cycles 9(4):529-540.

Dyrness CT & Norum RA (1983) The effects of experimental fires on black spruce forest floors in interior Alaska. Can. J. For. Res. 12: 879-893.

Falkowski PG & Raven JA (1997) Aquatic Photosynthesis. Blackwell, Winnipeg.

Farrar JL (1995) Trees in Canada. Fitzhenry & Whiteside & The Canadian Forestry Service, Markham.

Ferguson GAG (2000) Sources of dissolved organic carbon in flooded uplands. BSc thesis. University of Waterloo.

Frenzel P & Karofeld E (2000) CH_4 emission from a hollow-ridge complex in a raised bog: the role of CH_4 production and oxidation. Biogeochem. 51:91-112.

Frockling S & Crill P (1994) Climate controls on temporal variability and methane flux from a poor fen in southeastern New Hampshire: measurement and modeling. Global Biogeochem. Cycles 8:385-397.

Gorham E (1991) Northern peatlands: role in the carbon cycle and probable responses to climatic warming. Ecol. Appl. 1:182-195.

Guy RD, Fogel ML & Berry JA (1993) Photosynthetic fractionation of the stable isotopes of oxygen and carbon. Plant Physiol. 101:37-47.

Natural Resources Canada (2001) National Atlas of Canada. Government of Canada.

Happell JD, Chanton JP, Whiting GJ & Showers WJ (1993) Stable isotopes as tracers of methane dynamics in Everglades marshes with and without active populations of methane oxidizing bacteria. J. Geophys. Res. 98(D8):14,771-14,782.

Hecky RE et al. (1991) Increased methylmercury contamination in fish in newly formed reservoirs. In: Suzuki T, Imura A & Clarkson TW (eds) Advances in Mercury Toxicology (pp 33-52). Plenum, New York.

Hecky RE & Hesslein RH (1995) Contributions of benthic algae to lake food webs as revealed by stable isotope analysis. J. North Am. Benthol. Soc. 14(4): 631-653.

Huebert D (1999) Experimental Lakes Area Upland Flooding Experiment: Vegetation Analysis. Second edition, revised and expanded. Winnipeg.

(ICOLD) International Commission on Large Dams (1998) World register of dams. International Committee on Large Dams, Paris.

Joyce EM (2001) The impact of experimental reservoir creation on greenhouse gas fluxes from forested uplands. MSc Thesis. University of Alberta.

Junk WJ & Piedade MTF (1997) Plant life in the floodplain with special reference to herbaceous plants. In Junk WJ (ed) The Central Amazon Floodplain (pp 147 185). Springer-Verlag, Berlin.

Kasischke ES, Christensen, Jr NL & Stocks BJ (1995) Fire, global warming, and the carbon balance of boreal forests. Ecol. Appl. 5(2): 437-451.

Kelly CA, Rudd JWM, Bodaly RA, Roulet NP, St Louis VL, Heyes A, Moore TR, Schiff SL, Aravena RO, Scott KJ, Dyck B, Harris R, Warner BG & Edwards G (1997) Increases in fluxes of greenhouse gases and methyl mercury following flooding of an experimental reservoir. Environ. Sci. Tech. 31:1334-1344.

Kelly CA, Rudd JWM, St. Louis SL & Moore T (1994) Turning attention to reservoir surfaces, a neglected area in greenhouse studies. Eos 75(29):332-333.

Kiddon J , Bender M, Orchardo J, Goldman J, Caron D & Dennett M (1993) Isotopic fractionation of oxygen by respiring organisms. Global Biogeochem. Cycles 7:679-694.

King GM (1990) Regulation by light of methane emissions from a wetland. Nature 345: 513-515.

Kroopnick PM (1975) Respiration, Photosynthesis, and oxygen isotope fractionation in oceanic surface water. Limnol. Oceanogr. 20: 988-992.

Kroopnick P & Craig H (1972) Atmospheric oxygen: isotopic composition and solubility fractionation. Science 175:54-55.

_____(1976) Oxygen isotope fractionation in dissolved oxygen in the deep sea. Earth Planet. Sci. Lett. 32:375-388.

McCullough GK (1998) The contribution of forest litterfall to phosphorus inputs into lake 239, Experimental Lakes Area, northwestern Ontario. In: Brewin MK & Monita DMA (tech coord) Land Management Practices Affecting Aquatic Ecosystems. Proc. Forest-Fish Conf., May 1-4, 1996, Calgary AB. (pp 159-168) Can. For. Serv. North For. Cent. Inf. Rep. NOR-X-356.

McCutcheon S (1991) Electric rivers: the story of the James Bay Project. Black Rose Books, Montréal.

Mewhinney EJ (1996) The importance of hydrology to carbon dynamics in a small boreal forest wetland. MSc thesis. University of Waterloo.

Moore TR & Knowles R (1989) The influence of water table levels on methane and carbon dioxide emissions from peatland soils. Can. J. Soil Sci. 69:33-38.

Nalder IA & Wein RW (1999) Long-term forest floor carbon dynamics after fire in an upland boreal forest of western Canada. Global Biogeochem. Cycles 13(4):951-968.

Nicolson JA (1975) Water quality and clearcutting in a boreal forest ecosystem. Proc. of Can. Hydrology Symposium - 75. NRCC No. 15195, Aug. 11-14, Winnipeg, MB. p. 734-738.

Nilsson C & Berggren K (2000) Alterations of Riparian Ecosystems Caused by River Regulation. BioScience 50(9):783-792.

Nilsson C, Jansson R & Zinko U (1997) Long-term responses of river-margin vegetation to water-level regulation. Science 276:798 800.

O'Leary MH (1993) Biochemical basis of carbon isotope fractionation. In: Ehleringer JR, Hall AE & Farquhar GD (eds) Stable isotopes and plant carbon—water relations (pp 19-28). Academic, San Diego.

Osmond CB, Austin MP, Berry JA Billings, WD, Boyer JS, Dacey JWH, Nobel PS, Smith SD, Winner WE (1987) Stress physiology and the distribution of plants. BioScience 37(1): 38-48.

Poschadel C (McKenzie) (1997) Floating Peat Island Formation at an Experimentally Flooded Wetland: Impacts on Methane and Carbon Dioxide Production and Flux Rates to the Atmosphere. MSc thesis. University of Waterloo.

Rapalee G, Trumbore SE, Davidson EA, Harden J & Veldhuis H (1998) Soil carbon stocks and their rates of accumulation and loss in a boreal forest landscape. Global Biogeochem. Cycles 12(4):687-701.

Richardson B (1991) Strangers devour the land: a chronicle of the assault upon the last coherent hunting culture in North America, the Cree Indians of northern Quebec, and their vast primeval homelands. Douglas & McIntyre, Toronto.

Rosenberg RM, Bodaly RA, Hecky RE & Newbury RW (1977) The environmental assessment of hydroelectric impoundments and diversions in Canada. *In* Canadian aquatic resources. Healey RC & Wallace RR, eds. Canadian Bulletin of Fisheries and Aquatic Sciences 215. Ottawa: Department of Fisheries and Oceans.

Rosenberg DM, Bodaly RA & Usher PJ (1995) Environmental and social impacts of large scale hydroelectric development: who is listening? Glob. Environ. Change 5(2):127-148.

Rozanski K, Araguás-Araguás L & Gonfiantini R (1993) Isotopic patterns in modern global precipitation. *In* Climate change in continental isotopic records. Swart PK, Lohmann KC McKenzie JA & Savin S, eds. American Geophysical Union Monograph 78. 36pp.

Roulet NT, Ash R & Moore TR (1992) Low boreal wetlands as a source of atmospheric methane. J. Geophys. Res. 97(D4):3739-3749.

Rudd JWM, Furutani A, Flett RJ & Hamilton RD (1976) Factors controlling methane oxidation in shield lakes: the role of nitrogen fixation and oxygen concentration. Limnol. Oceanogr. 21(3):357-364.

Rudd JWM, Hamilton RD & Campbell NER (1974) Measurement of microbial oxidation of methane in lake water. Limnol. Oceanogr. 19(3):519-524.

Rudd JWM, Harris R, Kelly CA & Hecky RE (1993) Are hydroelectric reservoirs significant sources of greenhouse gases? Ambio 22(4):246-248.

Sansone FJ & Martens CS (1978) Methane oxidation in Cape Lookout Bight, N.C. Limnol. Oceanogr. 23: 349-355.

Šantrůčková H, Bird MI, Frouz J, Sustr V & Tajovsky K (2000a) Natural abundance of ^{13}C in leaf litter as related to feeding activity of soil invertebrates and microbial mineralization. Soil Biol. Biochem. 32: 1793-1797.

Šantrůčková H, Bird MI & Lloyd J (2000b) Microbial processes and carbon-isotope fractionation in tropical and temperate grassland soils. Func. Ecol. 14: 108-114.

Schindler, DW (1980) Evolution of the Experimental Lakes project. Can. J. Fish. Aquat. Sci. 37:313-319.

Scott KJ, Kelly CA & Rudd JWM (1999) The importance of floating peat to methane fluxes from flooded

peatlands. Biogeochem. 47:187-202.

Schweizer M, Fear J & Cadisch G (1999) Isotopic (^{13}C) fractionation during plant residue decomposition and its implications for soil organic matter studies. Rapid. Commun. Mass Spectrom. 13: 1284-1290.

Shiklomanov IA (1993) World fresh water resources. In: Gleich PH (ed) Water in Crisis: A Guide to the World's Fresh Water Resources (pp 13-24). Oxford University, Oxford.

St. Louis VL, Kelly CA, Duchemin É, Rudd JWM & Rosenberg DM (2000) Reservoir surfaces as sources of greenhouse gases to the atmosphere: a global estimate. BioScience: 50(9):766-775.

Stainton MP, Capel MJ & Armstrong FAJ (1977) The chemical analysis of fresh water. 2nd edition. Can. Fish. Mar. Serv. Misc. Spec. Publ. 25: 180 pp.

Urey HC (1947) The thermodynamic properties of isotopic substances. J. Chem. Soc. (London) 297: 562-581.

Vogel JC (1993) Variability of carbon isotope fractionation during photosynthesis. In: Ehleringer JR, Hall AE & Farquhar GD (eds) Stable isotopes and plant carbon—water relations (pp. 29-38). Academic, San Diego.

Wake LV, Rickard P & Ralph BJ (1973) Isolation of methane utilizing micro-organisms: a review. J. Appl. Bact. 36:93-99.

Wanninkhof R, Ledwell JR & Broecker WS (1985) Gas exchange wind speed relationship measured with sulfur hexafluoride on a lake. Science 227:1224-1226.

Wedin DA; Tieszen LL; Dewey B & Pastor J (1995) Carbon isotope dynamics during grass decomposition and soil organic matter formation. Ecology 76(5):1383-1392.

Whiticar MJ (1999) Carbon and hydrogen isotope systematics of bacterial formation and oxidation of methane. Chem. Geol. 161(1-3):291-314.

Whittenbury R, Phillips KC & Wilkinson JF (1970) Enrichment, isolation and some properties of methane utilizing bacteria. J. Gen. Micro. 61:205-218.